Experimental Characterization of High-Pressure Natural Gas Scrubbers

Trond Austrheim

Dissertation for the degree philosophiae doctor (PhD)
at the University of Bergen

2006-09-28

Table of Contents

Scientific Environment

This work has been carried out at the Petroleum and Process Technology group at the Department of Physics and Technology under the Faculty of Mathematics and Natural Sciences

This study has been carried out as part of the larger research program, High-Pressure Gas Liquid Separation, HiPGaS. The HiPGaS programme is a joint Competence Program between the Norwegian University of Science and Technology (NTNU), the University of Bergen (UiB), the University of Stavanger (UiS), three major oil companies and three vendors supplying separation equipment. The program was started in 2001 is sponsored by the Norwegian Research Council (NFR) and the participating industrial partners. The participating industrial partners are: Statoil, Norsk Hydro, Conoco-Phillips, Vetco, Aker-Kværner Process Systems and FMC Energy Systems. More details about the HiPGaS-program can be found on the web-page of the project, http://www.hipgas.ntnu.no

The experimental part of this study has been carried out at Statoil's research centre in Trondheim, Norway and at Statoil's large scale multiphase laboratory, K-lab, at Kårstø natural gas processing plant nearby Haugesund, Norway.

Acknowledgements

This work has been carried out at the University of Bergen and at Statoil Research Centre in Trondheim. I want to thank my supervisor professor Alex C. Hoffmann for your thorough comments and advices along the way of this work. Your critical eyes have helped me a lot and forced me into structuring my work better than it would have been otherwise. I also wish to thank my co-supervisor Staff engineer Lars Henrik Gjertsen at Statoil for a lot of help on ensuring that this work focused on some very important topics concerning natural gas scrubber performance. Without your continuous feedback along the way, the applicability of this work would have been considerably less.

The extensive and challenging experimental part of this work could not be done without a lot of skilled people at the mechanical workshops at the Department of Physic and Technology, UiB and at Statoil. The numerous problems encountered in the lab have been solved one by one. A special thank goes to Kai Arne Kristiansen for the close collaboration on the development of the high-pressure droplet size measurement arrangement.

During this work I have had the pleasure of being closely connected with the Gas Separation project at Statoil R&T. Thank you all for your willingness to shear your knowledge and for giving me access to the unique portfolio of experimental test rigs. A special thank goes to Dr. Carl Birger Jenssen for the many discussions on fluid dynamics.

Abstract

Scrubber design practice today is largely based on experimental data generated at ambient conditions with model fluid system such as air-water. Though good efficiency is often measured in the lab, real natural gas scrubbers often fail to meet the requirements. Mal-functioning scrubbers can lead to a series of operational and mechanical problems further downstream such as compressor breakdown, fouling, breakdown of gas cleaning processes and off-spec gas quality. Therefore one of the most common scrubber configurations has been put to the test in three different test rigs –a low-pressure rig, a high-pressure rig and a large scale high-pressure rig at an onshore gas plant. The scrubber configuration consisting of a vane-type inlet, a mesh pad and a bank of axial flow cyclones, has been tested at wide range of operating conditions and fluid properties. For the first time scientific laboratory scrubber measurements have been reported for live hydrocarbon fluids at pressures up to 113 barg. The separation efficiencies and pressure drops have been measured and reported for all tests. In addition some few unique measurements of the droplet size distribution in a high pressure scrubber have been carried out.

The results show that the commonly used K-value (Souders-Brown equation) is a good design criterion for conditions where the mesh pad is below flooded condition, while it fails at more compact conditions i.e. $K > 0.15$ m/s. In most cases the largest droplets were larger than 400 microns and efficient droplet separation could therefore be expected. Though, droplets formed from condensation at high-pressure natural gas where found to be in the size range 1- 10 microns which is hard to separate under these conditions. The performance degradation of the axial flow cyclone used in this study was totally governed by a general re-entrainment process rather than insufficient separation of small droplets. A new approach to predict cyclone efficiency was therefore needed. By mathematically modelling cyclone geometry, flow and fluid properties a brand new relationship was derived that correlates extraordinary well with separation efficiency –the dimensionless re-entrainment number.

In general the results showed that the efficiency decreased with increasing pressure. Also, it was seen that the efficiency dropped considerably when a live hydrocarbon fluid system was used instead of a model fluid system where only minor amounts of the gas is dissolved in the liquid phase and vice versa. Also, differences where found between the large scale and the small scale scrubber due to the uneven distribution of the fluids in the scrubber cross section. This work has therefore revealed the importance of carrying out tests with “real fluids”, at relevant pressure and at large scale in order to predict the performance of real natural gas scrubbers.

List of Symbols and Abbreviations

Latin Letters

A	Area [m^2]
A_s	Specific area [m^2/m^3]
C_d	Drag force coefficient [-]
C_w	Coefficient for internal flow
C	Number concentration of droplets in gas [-]
c	Constant for the swirl pattern in a cyclone
D	Diameter [m]
D	Characteristic length [m]
d	Droplet size [m]
Eu	Euler number
g	Acceleration of gravity
H	Height [m]
K_{50}^3	Characteristic separation energy [J]
L_frac	The fraction of liquid drained from outer cyclones to inner [-]
$\dot{m}$	Mass rate [kg/hr]
N_μ	Dimensionless viscosity number
R ,r	Radius
Re	Reynolds number
Stk	Stokes number
T	Gas temperature
u	Velocity [m/s]

Greek Letters

α	Swirl vane angle relative to cyclone diameter
β	Swirl vane angle relative to axial axis (exit angle)
Δ	Differential (like differential pressure, height, etc)
δ	Uncertainty
δ	Liquid film thickness [m]
ε	Void fraction of free volume in mesh pad [-]
λ	Gas Load Factor (K-value)
η	Efficiency
μ	Viscosity
ρ	Density (general), [kg/m^3].
σ	Interfacial tension [mN/m]
ψ_A	Inertial separation parameter [-]

Superscript

a	Power of viscosity number
*	Dimensionless

Subscript

A	Inertial impaction parameter
b	Body
B	Bürkholz
CO	Carry-Over
cr	critical

Subscript

d	drag
d	droplet
dem	demister in the HP-rig
drain	drain tank for the cyclones
g	gas phase
g	grade
l	liquid phase
mix	mixed two-phase
r	relative
r	resistance
r	radial
s	superficial
set	terminal settling
v50	Median size based on the volumetric distribution of droplets
w	wire
0	initial
50	50% separation
95	95% separation
θ	tangential

Abbreviations

AFC	Axial Flow Cyclone
GC	Gas Chromatograph
CFD	Computational Fluid Dynamics
DSD	Droplet Size Distribution
EOS	Equation of State

Abbreviations

GLF	Gas Load Factor
GLCC	Gas-liquid-cylindrical-cyclone
GPSA	Gas Processors Suppliers Association
HAP	Hazardous Air Pollutants
HiPGaS	High-Pressure Gas Liquid Separation
HSE	Health, Safety, Environment
HP-rig	High-Pressure rig (at Statoil R&D)
I.D.	Internal Diameter
I-SEP	Involute Separator
IRIS	Inline Rotary Separator
K-lab	Kårstø control and metering laboratory
LNG	Liquefied Natural Gas
LP-rig	Low-Pressure rig (at Statoil R&D)
MEG	Mono Ethylene Glycol
NTNU	The Norwegian University of Science and Technology
PFD	Process Flow Diagram
PTV	Particle Tracking Velocimetry
PVT	Pressure, Volume, Temperature
SRK	Soave-Redlich-Kwong EOS (Soave, 1972)
TEG	Tri Ethylene Glycol
UiB	University of Bergen
UiS	University of Stavanger

CHAPTER 1

Introduction and Objectives

The petroleum sector is the largest industry in Norway and was responsible for 19.2 % of Norway's GNP in 2002, which corresponds to approximately three times the added value of all other industry (OED, 2003). Oil has been the far most important commodity, but the production of natural gas and gas-related products has increased and now covers more than 1/3 of the total production given in million standard cubic meter oil equivalents (Mill. scmoe) as shown in Figure 1.1. While oil production is expected to reach a plateau around 2004, the production of natural gas and associated products is expected to increase and become increasingly important as new gas fields are being developed and oil fields enter tail-end production.

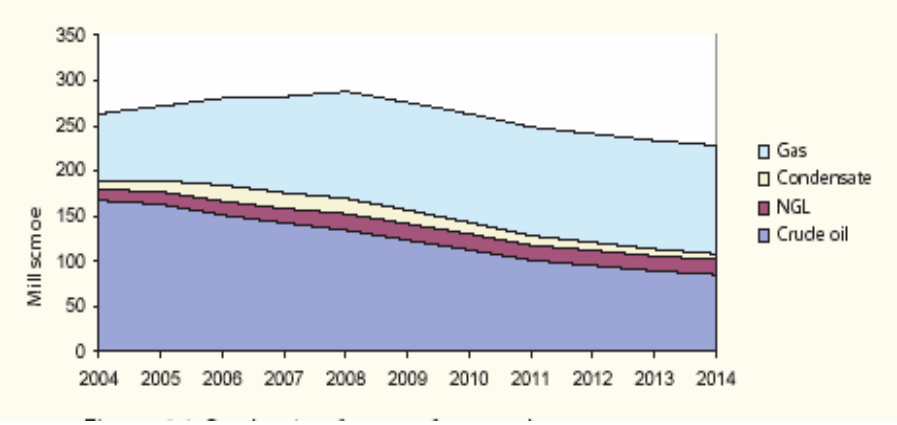

Figure 1.1 The expected production of oil & gas on the Norwegian Continental Shelf in the period from 2004 – 2014. The production is given as mill. scmoe (Figure from Ministry of Petroleum and Energy, 2003)

The development of oil and gas fields both on the Norwegian continental shelf and in other places of the world moves towards smaller and more remote fields where more cost effective solutions must be found. The vision is to do all offshore gas/liquid and liquid/liquid separation sub-sea, i.e. a total high-pressure separation concept. Arguments for such a shift are to avoid expensive topside facilities, to facilitate the separation processes themselves, to lower the amount of water and gas to be transported and/or discharged and to reclaim gas at a high pressure, making recompression before pipeline transport unnecessary or more efficient.

A total sub-sea solution requires much more rigorous design procedures for separators in general, as the expenses related to unsatisfactory design are very high compared with the situation today. For installation of sub-sea process equipment, large ships are required that can carry and submerge the equipment to its right location on the sea bed. Since there are clear limitations to the weight or size that these ships can handle, compact separation equipment might be required in many cases. Compact separation has shown to be more challenging than separation in traditional large scrubbers.

1.1 Gas Scrubbers in Natural Gas Production

Liquid is removed from the gas in all kinds of gas processing facilities for a number of reasons such as:

- Prevent breakdown of rotating equipment like expanders, compressors and turbines
- Prevent foaming in gas dryers or CO2 removal units
- Prevent hydrate formation or other forms of fouling in downstream equipment
- To keep water- or hydrocarbon dew point within sales gas- or transport specifications
- Prevent loss of expensive and/or destructive chemicals such as e.g. glycols or amines
- Protect burners, catalysts etc.
- Air pollution control

In the process of separating liquid and gas, two types of vessels typically exist -the horizontal oriented and the vertical oriented vessel. Horizontal vessels are most often used when the vessel must handle large amounts of liquids, e.g. inlet separators on platforms. The vertical vessels are used when the fluid has a large gas to liquid ratio. While horizontal vessels often are called separators, vertical vessels handling large gas to liquid ratios are often referred to as gas scrubbers (Arnold and Stewart, 1984). The majority of natural gas scrubbers in operation today handle less than 4 vol% liquid. The operating pressures ranges from atmospheric conditions up to several hundred bars, while the temperature might range from

-170 ^{0}C in Liquefied Natural Gas (LNG) plants up to more than +100 ^{0}C downstream of stripping columns.

Huge costs are associated with problems induced by mal-functioning scrubbers. These costs relate mainly to reduced income due to operational problems, but modifications and reconditioning of different process equipment can also be a significant item of expenditure. In addition, scrubber efficiency is often a bottleneck in the production and therefore efficiency improvements can increase the production capacity of processing facilities in many cases (Bjørnestad et al. 2001, Gjertsen et al., 2003).

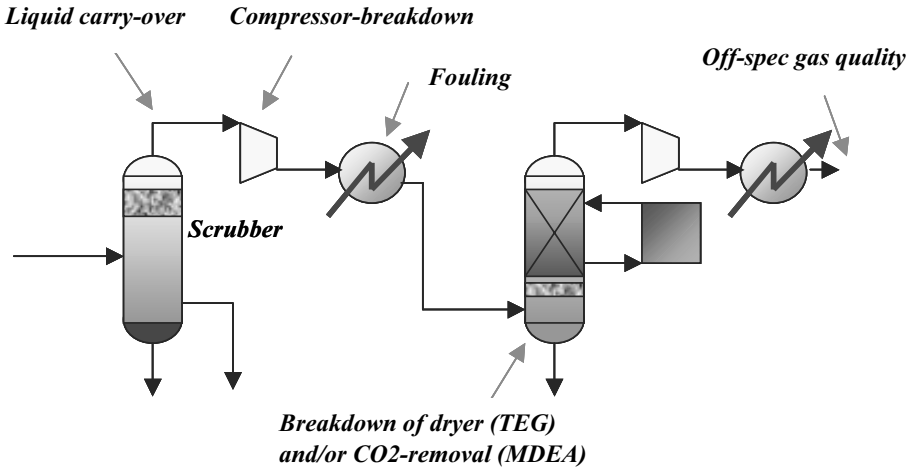

Figure 1.2 Typical problems related to liquid carry-over from scrubbers in a natural gas processing plant.

1.2 Selection of Gas/Liquid Scrubbers

Various types of gas/liquid separation equipment that range from equipment designed for bulk liquid separation to equipment designed for very fine mist removal are available on the market today. Often, two or several separation internals are combined to achieve the required gas quality. Since both the conditions for the gas/liquid stream and the required efficiency may vary widely, care must be taken when selecting a proper separator. For instance, slug-protection in front of a heat-exchanger where condensation occurs, requires only a bulk separation of the liquid, while scrubbers that is protecting rotating equipment, may require internals with very high demisting efficiency, also for very small droplets.

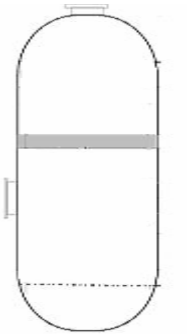

Figure 1.3 Sketch of a typical vessel configuration of low compactness where the gas flow needs to be kept low. The grey field illustrates a mesh pad

Gas/liquid scrubbers for the oil and gas industry has, during the latest decades, developed from large knock-out drums that may have been equipped with a single mesh pad as shown in Figure 1.3, to more and more compact solutions. This includes both compact vessel units like different cyclone-type scrubbers and sophisticated internals like advanced inlet vapour distributors, complex mesh pads, vane-packs and different cyclone solutions for traditional vessels. (Verlaan et al. 1989; Oranje 1990; Verlaan 1991; Diekmann et al. 1994; Swanborn et al. 1995; Gomez et al. 1999, 2000; Shoham and Kouba 1998; Stewart et al. 1998; Movafaghian et al. 2000; Sterner 2001; Chin et al.2002; Gjertsen et al. 2003).

1.2.1 Scrubber Internals

Scrubbers most often consist of a vertical vessel with different separation internals installed in series. The inlet pipe is mounted horizontally and at the inlet, arrangements are mounted in order to reduce the gas and liquid momentum, separate the bulk liquid, prevent liquid shattering, distribute the gas and liquid over the scrubber cross section and also break-down foam in some cases. An inlet arrangement used frequently in the past is the half pipe arrangement, which simply consists of a horizontally oriented cylinder where the lower, lengthwise half of the cylinder is removed. Today, the most commonly used inlet consists of a series of vanes that gradually releases the gas and liquid into the scrubber. The inlet vane arrangement has a rumour of distributing the gas and liquid evenly with low pressure drop. In applications where foaming occurs, an inlet cyclone arrangement is often used since the centrifugal force exerted in this type of equipment, can break-down the foam. The cyclones are normally of the cylinder-on-cone type with tangential inlet.

Above the inlet arrangement, a coalescing or agglomeration section often is installed. The most common types of equipment are either one or several mesh pads or vane packs. The mesh pad consists of layers of knitted wires. Originally knitted steel wires were used, but today also different types of composite materials are used to create complex mesh pads (Brunazzi et al. 2001). Vane packs consist of plates that are formed in a zigzag pattern, where the gas has to flow. When the

vessel is quite large compared to the gas volumes, the mesh or vane pack acts as a final demisting stage. However, when the volumetric gas rate increases, the liquid can not be drained efficiently by gravity against the gas flow. In these cases, the second stage acts as a pre-conditioner that agglomerates the liquid droplets so that they are more easily separated further downstream.

The final demisting stage in a relatively compact scrubber, most often consists of a bank of cyclones or a vane pack with channels that are shielded from the gas to allow unhindered drainage of the liquid. The liquid from the cyclone deck or vane pack are drained through drainpipes that extend down to the liquid sump in the bottom of the scrubber.

Cyclones used in a scrubber can be of a reverse flow type or axial flow cyclones (AFC). In the reverse flow cyclones the gas usually enters through a tangential inlet in the top of the cyclone. The gas spins downwards leaving the liquid at the wall. The liquid is then drained through a hole in the bottom while the gas reverses direction and leaves through a smaller pipe in the top of the cyclone –the vortex finder. In an AFC, on the other hand, the gas flow usually enters in an axial direction. The gas is set to spin by an arrangement of stationary swirl vanes. The upwards spinning gas forces the liquid to the wall where it is separated through slits or eventually through an annular gap between the wall and the vortex finder at the end of the cyclone. The liquid drainage through the slits at the wall is usually assisted by a small purge gas that flows through the slits and to the drain chamber. From here, the purge gas is either being routed back to the centre of the static swirl elements (recycling AFC), or it leaves through a secondary gas outlet in the top of the drain chamber (non-recycling AFC). The secondary gas may be cleaned by a mesh pad. The AFC is today more commonly used in scrubbers than reverse flow cyclones due to a lower pressure drop and relative compact design.

1.2.2 Compact Separation

The development of more compact equipment has almost solely focused on cyclonic type of equipment. Examples of such are the Gasunie cyclone (Oranje, 1990) and the gas-liquid-cylindrical-cyclone (GLCC)(Arpandi et al. 1995, Shoham and Kouba, 1998; Gomez et al. 1999, 2000; Wang et al. 2000a, 2000b), which both are a type of reverse flow cyclone. The motivation for this is to reduce the size, footprint and weight of the scrubber unit.

The latest stage of development in scrubber technology for the oil and gas industry is to remove the vessels and replace them with even more compact units. Typically these are of the inline-type which means that the scrubber unit is mounted directly in the existing pipes such that piping codes for the material and thickness can be used instead of the more rigid vessel codes. The new inline scrubbers are of axial flow cyclone-type. Examples of such are the inline Degasser and Deliquidiser (Chin et al. 2003; Barker and Schook, 2005), the Inline Rotary Separator (IRIS)

(Rawlins and Ting, 2002) and the Involute Separator (I-SEP) (Sarshar et al. 2005). However, the newest developments are not yet widely employed and the de-liquidiser for instance, is yet mostly used as a pre-separation stage upstream of existing scrubbers. Since more conventional designed scrubbers often fail at high pressures, there is a need for better understanding of the basic separation mechanisms before the later developments will be widely employed.

1.3 High Pressure Gas-Liquid Separation

Even though there has been a lot of focus on geometry of different scrubber internals, details on the variations with operating conditions (gas and liquid rates) and physical fluid properties like densities, viscosities and interfacial tension are less known. When the gas to liquid density ratio decreases, it will make gas-liquid separation more challenging. Likewise will a low interfacial tension possibly result in smaller droplets that are more difficult to separate, and it may also lead to break-up of liquid films formed in a scrubber. The importance of viscosity is less obvious, but gas and liquid viscosity are important parameters when describing the gas and liquid flow and may therefore also affect gas liquid separation.

Tests are usually carried out under low pressure, and often with a mixture of air-water at ambient conditions. SF_6-gas has been utilized in order to simulate high-pressure conditions. SF_6 is a very dense gas which is approximately 10 times as dense as air or natural gas, hence, the gas density of SF6 in a lab rig operating at 10 bara is approximately the same as the density of natural gas at 100 bara. However, even though the gas density changes in such a rig the liquid density, the viscosities and the interfacial tension remains unchanged.

Data at high-pressure and with hydrocarbon fluids are scarce. To the author's knowledge, no scientific studies at high-pressure conditions are reported in the public domain for conventional scrubber internals. For compact separation equipment, some few results are found. The Gasunie scrubber (Oranje, 1990) where tested with processed natural gas at operating pressures up to 40 bara, but no information was given for the liquid phase. More recently, some few efficiency measurements have been published for the inline Degasser (Chin et al. 2003) and the IRIS (Rawlins and Ting, 2002). Chin et al. used a mixture of methane and diesel up to 40 bara, but no information was given on the physical fluid properties. In a sense the fluid is "live" since some diesel will evaporate and some methane will dissolve in the liquid. This system, however, only covers a small part of the gas-liquid properties relevant for real scrubbers.

Rawlins and Ting reported results for a long-term field test of an IRIS-unit at 77 bara pressure. The IRIS was mounted in a well stream consisting of natural gas, condensate and associated water from the well. Up till now, this is the tests of a natural gas separator with the most challenging conditions found in literature. In

addition Rawlins and Ting also did some more systematically testing in a large scale lab where processed natural gas and decane was used as the fluid system.

Even though some few measurements have been made at high pressure and with hydrocarbon fluids, the results have never been analysed in light of the physical fluid properties. Further, there is a lack of information about the high-pressure performance of the most commonly used scrubber internals like inlet arrangements, coalescers and cyclones. This lack of information is limiting the knowledge on how to design natural gas scrubbers for high-pressure service.

1.4 Objectives

The objectives of this study are to investigate the difference between low-pressure and high-pressure scrubber performance. Different fluids will have different separation characteristics, and the characteristics will change with different operating conditions such as gas and liquid loads, pressure and temperature. The aim is to investigate how relevant low-pressure and small scale lab testing is for the design of real scrubbers. Mechanisms that govern liquid carry-over at high-pressure conditions should be identified and if possible, quantified

Further, the performance of a large scale scrubber compared to a small scale scrubber, may relay on differences in how the gas and liquid are distributed within the scrubber. Differences in gas and liquid distribution in the rigs might affect the separation efficiency. The aim of this project is therefore also to identify and possibly explain important differences between small scale and large scale scrubbers.

Many different types of equipment for gas-liquid separation have been developed during the years, but the objectives of this study do not include any focus on optimal design of scrubber internals.

1.5 Scope

In order to investigate high-pressure scrubber performance, a suitable design for a typical scrubber must be defined. A very commonly used scrubber configuration today includes an inlet vane with a coalescing mesh pad and a bank of axial flow cyclones. This configuration that can be seen in Figure 1.4 is therefore the scope of this study. In order to avoid conflicts related to the confidentiality of geometrical details and other commercial aspects, only generic equipment will be used. Details of the selected internals are given later in Section 3.4

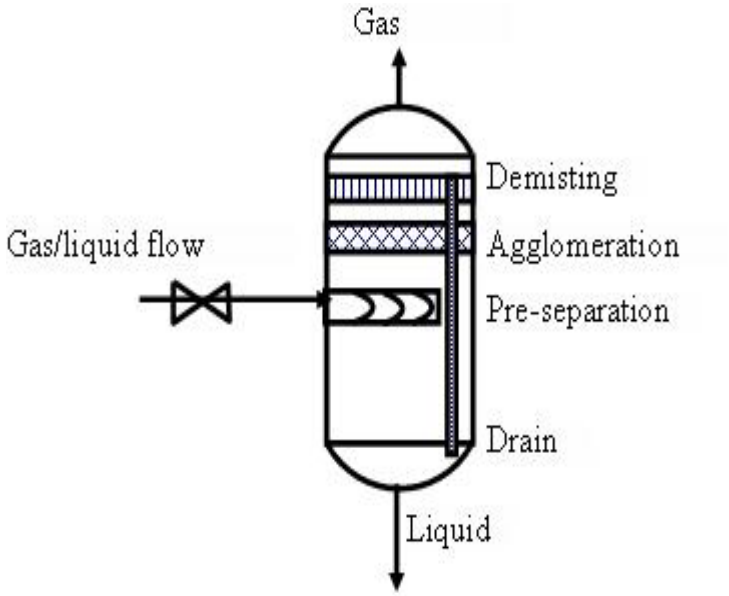

Figure 1.4 The standard scrubber configuration used as a basis in this study. The pre-separation consists of an inlet vane, the next stage consists of a mesh pad that acts as a separator at low gas loadings and as agglomeration/pre-conditioner at higher loadings, while the last stage is a bank of axial flow cyclones (AFC) mounted in parallel.

CHAPTER 2

Relevant Theory for Gas Scrubbers

Design of gas scrubbers is often based on empirical correlations and the different suppliers might also have different criteria. Often, the criteria are based on test results for tests carried out under low-pressure conditions and also –in many cases- air/water tests. There are some standards that have listed criteria for scrubber design such as the NORSOK P-100 standard (2001) that is widely used on the Norwegian continental shelf. Also, the Gas Processing Suppliers Association (GPSA, 1998) has published an engineering data book with theory and design guide rules for gas processing facilities. In this chapter some theory from the mentioned sources is presented and analysed. In addition, theories from other fields of research with relevance for high-pressure gas scrubbing are also presented. Some of this theory has been used to analyse the experimental results in Chapter 5.

In a design phase the available parameters are usually the fluid properties and the maximum and minimum gas and liquid rates. In multiphase science a whole range of parameters are often defined and used to describe the multiphase behaviour, but if the correlations/expressions should be applied in scrubber design, one must be able to relate them to the available design parameters in combination with the geometrical parameters. For instance, the droplet size is often used in several expressions, but if these expressions should be used in the process of designing a scrubber, one most also have expressions that can calculate the droplet size based on the available design parameters. The lack of connection between much of the published research and the available design parameters is limiting the applicability in scrubber design. This chapter is focused on theory that can or might be applied in scrubber design.

2.1 Vessel Diameter

In many processes practical limitations such as available 'footprint', weight, layout or production limitations determine the size of a scrubber. When the size of the vessel is not determined by some of the listed factors, the K-value is the most common design parameter. The K-value dawns from the so-called Souders-Brown Equation.

2.1.1 Souders-Brown Equation

The most used expression for sizing of gas scrubbers is the expression developed by Souders and Brown (1934) for sizing of fractionating columns. This expressions involves an empirical factor know as the Souders Brown value, K-value, C-factor, λ or Gas Load Factor (GLF). In this publication, the term K-value will be used. The basis of the expression is the force balance on a droplet in an upwards-flowing gas field as shown in Figure 2.1. The gravitation force on the droplet adjusted for buoyancy when resolved in vertical direction is:

$$G_d = \frac{\pi}{6} d^3 g \left(\rho_l - \rho_g \right) \tag{2.1}$$

The resistance of a droplet in a moving fluid resolved in the vertical direction can be expressed as:

$$F_r = K \mu_g \frac{\sqrt{\pi}}{2} d \cdot u_g + C_d * A_d \frac{1}{2} \rho_g u_g^2 \tag{2.2}$$

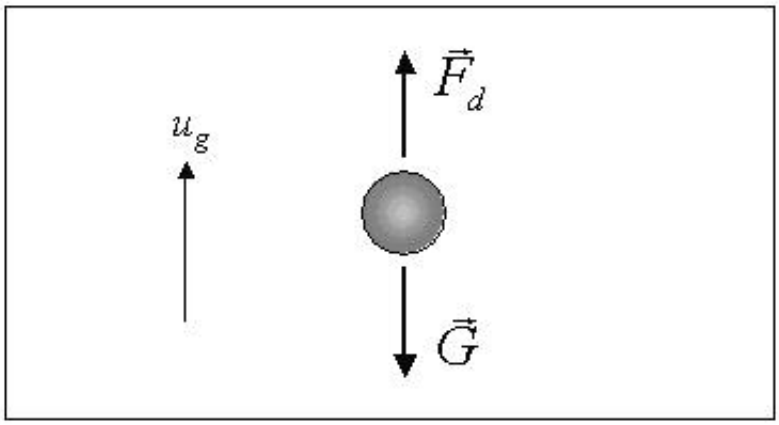

Figure 2.1 The relevant forces acting on a droplet in an upwards-flowing gas field

Souders and Brown argued that the viscosity of the gas phase was very small so that the viscous term could be neglected. The vapour velocity they sketched for a fractionating column was in the range 0.01 to 0.001 cP. This is also a relevant estimation for a typical natural gas in a gas scrubber. This leaves us only with the drag force F_d as the relevant force acting upwards as sketched in Figure 2.1. Assuming that the droplet has the shape of a sphere, the drag force therefore can be expressed as:

$$F_d = C_d * A_d \frac{1}{2}\rho_g u_g^2 = C_d * \frac{\pi}{4} d^2 \frac{1}{2}\rho_g u_g^2 \tag{2.3}$$

The terminal settling velocity is found when the drag force equals the gravitation so by equating the right-hand-sides of Equation (2.1) and (2.3) the settling velocity becomes:

$$u_{g,set}\sqrt{\frac{\rho_g}{\rho_l - \rho_g}} = \sqrt{\frac{4gd}{3C_d}} \tag{2.4}$$

If the droplet size and drag force coefficient is constant the right hand side of the expression also is a constant and this is the definition of the K-value:

$$\lambda = K = \sqrt{\frac{4gd}{3C_d}} \tag{2.5}$$

C_d is the drag coefficient which is dependent on the Reynolds number for the droplet. The classical result of Stoke is that that the drag coefficient is related to the Reynolds number as:

$$C_d = \frac{24}{Re_r} \tag{2.6}$$

where Re_r is the Reynolds number based on the relative velocity. This result, however, is only valid for Stokes flow i.e. $Re_r < 1$. In the settling section of a scrubber the Reynolds number is generally larger than this (except for very small droplets that have very low relative velocity to the gas flow). Putnam (1961) came up with the correlation:

$$C_d = \frac{24}{Re_r}\left(1 + \frac{Re_r^{2/3}}{6}\right) \tag{2.7}$$

This correlation is valid for $Re_r < 1000$, which is sufficient for most cases of droplets in a settling section of a scrubber.

2.1.2 Physical Meaning of Constant K-value

The use of K-value as a design parameter means that one has to reduce the gas velocity when pressure (and thereby gas density) is increased. The work by Souders and Brown (1934) is focused on the terminal settling but the K-value has a physical meaning beyond the point of equal drag and gravitational forces. The acceleration of a droplet in a gas stream can be expressed as:

$$\frac{d\overrightarrow{u_d}}{dt} = \frac{3}{4}\frac{C_d}{d}\left(\frac{\rho_g}{\rho_l - \rho_g}\right)\cdot\left(\overrightarrow{u_d} - \overrightarrow{u_g}\right)\cdot\left|\left(\overrightarrow{u_d} - \overrightarrow{u_g}\right)\right| \tag{2.8}$$

If a droplet is placed in a gas flow field such that the initial droplet velocity u_d is zero, the relative velocity becomes identical to the gas velocity and Equation (2.8) reduces to:

$$\frac{du_d}{dt} = \frac{3}{4}\frac{C_d}{d}\left(\frac{\rho_g}{\rho_l - \rho_g}\right)\cdot u_g^2 \tag{2.9}$$

Keeping the K-value constant therefore means:

$$\frac{du_d}{dt} = \frac{3}{4}\frac{C_d}{d}K^2 \tag{2.10}$$

If the Reynolds number is very high or very similar at two different pressures, the drag force coefficient is approximately the same and the physical meaning of constant K-value means: Equal sized droplets with zero initial velocity will have the same acceleration if K-value is kept the same at two different pressures.

2.1.3 Calculation of Vessel Diameter

The "critical" K-value is usually determined experimentally. "Critical" in this sense, means the value of K where the gas velocity equals the terminal velocity of the mean droplet size. The K-value is proportional to the superficial gas velocity from which the size of the vessel is determined by the following procedure. First the maximum velocity is calculated based on the critical K-value:

$$u_{s,g} = K\sqrt{\frac{\rho_l - \rho_g}{\rho_g}} \tag{2.11}$$

The calculated maximum velocity is then used to calculate the necessary diameter D of the vessel for the actual gas volume rate:

$$u_{s,g} = \frac{\dot{Q}_g}{A} = \frac{\dot{Q}_g}{\pi\left(\frac{D}{2}\right)^2} \Rightarrow D = \sqrt{\frac{4\dot{Q}_g}{\pi u_{s,g}}} = \sqrt{\frac{4\dot{Q}_g}{\pi K\sqrt{\frac{\rho_l - \rho_s}{\rho_l}}}} \tag{2.12}$$

The choice of which K-value to use (and thereby vessel size) can be chosen on basis of operating experience with other vessels that have very similar fluid properties or it can be calculated on basis of expected/required droplet size that is to be removed. However, since the expression uses the superficial velocity and not the actual velocity, it will not work well for increasing liquid concentrations. When an increased liquid amount is present in a vertical vessel, the available cross-section for the gas to flow decreases and thereby the mean gas velocity increases. This phenomenon is not accounted for in the expression for the K-value that uses the superficial velocity.

For low-pressure applications, the recommended K-value is $K < 0.1$ m/s and often a safety margin of 50 % is added if it is used for an otherwise empty vessel (flash tank). For increasing pressures the critical K-value has been seen to decline. This is not surprising since increasing pressure in oil/gas applications is often accompanied by a decrease in interfacial tension and thereby a decrease in the

droplet sizes and also increased risk of re-entrainment of separated liquid. GPSA, NORSOK P100 and Svrcek and Monnery (1993) recommend decreasing the K-value with 25 % for 85 bara pressure. This is of course a very harsh simplification since it does not account for the actual fluid properties at the given pressure. It should be noted that this advice is meant for separators with a mesh pad.

The K-value is not just used to ensure no liquid carry-over from the inlet section/mesh pad, but is also used as a benchmark parameter to describe the compactness of a scrubber. NORSOK recommends that scrubbers with demisting internals should operate below K = 0.15 m/s, but in practice some scrubbers operate at K-values close to 0.3 m/s (Gjertsen et al., 2003) and maybe even further. K-value of a scrubber larger than 0.1 m/s therefore means that another type of internals is needed further downstream in the scrubber e.g. cyclones, vane packs etc. to separate the liquid that has not been separated in the inlet/mesh section.

2.2 Inertial Separation

For droplets to separate out of a gas stream, the dominating way of achieving this is to utilize the inertia of the droplet. When the direction of a gas stream shifts, the droplets will no longer follow the path of the gas stream due to inertial forces. This may lead the droplet to hit a solid wall, wire or fibre and coalesce onto the surface. The principle of inertial separation is utilized in all demisting equipment used in a scrubber.

2.2.1 Scaling by use of Stokes number

In order to predict the performance of equipment in scrubbers that utilizes inertial separation, a scaling rule has to be established so that lab results can serve as a basis for demisting equipment in real scrubbers. The separation efficiency as function of droplet size is often referred to as the fractional efficiency or grade efficiency η_g i.e.

$$\eta_g = f\left(d\right) \tag{2.13}$$

Hoffmann and Stein (2002) use dimensional analysis to investigate how η_g for cyclones depends on a series of physical and operational parameters. During the deduction they make the following simplifications and assumptions:

- They ignore the effect of particle agglomeration or droplet-droplet coalescence.
- Geometrical similarity between model and prototype.

- The droplets are either perfectly spheres or that the Stokesian diameter is used. The Stokesian diameter is the equivalent diameter of a sphere with the same terminal velocity.
- The droplets have reached their terminal velocity.
- Gravity is assumed to be much smaller than centrifugal forces and is therefore neglected.
- Electrostatic forces are neglected
- Low solid (or liquid) loading are assumed and thereby no significant influence from the liquid on the gas stream.
- Wall roughness is ignored

Through this assumptions Hoffmann and Stein found that the grade efficiency could be expressed as:

$$\eta_g = f\left(Re_{g,} Stk, \frac{\Delta\rho}{\rho_g} \right) \tag{2.14}$$

Where Re_g is the gas Reynolds number and defined as:

$$Re_g \equiv \frac{\rho_g u_g D}{\mu_g} \tag{2.15}$$

Stk, is the Stokes number and defined as:

$$Stk \equiv \frac{\left(\rho_l - \rho_g\right) d^2 u_g}{18 \mu_g D} \tag{2.16}$$

The gas velocity u_g refers to a characteristic velocity e.g. the superficial velocity while D refers to a characteristic length e.g. the diameter of the cyclone body. With this definition the Stokes number accounts for the density differences and by investigating the equations of motion for the particles/droplets, they concluded that the density term in Equation (2.14) did not need to appear explicitly if the added mass and Basset term are neglected. Hence, the expression in Equation (2.14) was simplified to:

$$\eta_g = f\left(Re_{g,} Stk \right) \tag{2.17}$$

The cut size d_{50} of a cyclone is by definition the droplet size that will be separated with 50% efficiency. The notation for the corresponding Stokes number for the cut size is hence, Stk_{50}. The cut size of a cyclone that has been tested in a lab can be predicted for a real application by use of the Stokes number. Equation (2.17) shows that this is true if the Re_g is kept approximately the same as it was under test conditions. However, Overcamp and Scarlet (1993) showed that the Stk_{50} is

approximately constant for a wide range of Re_g. In practice the cut size of a cyclone therefore can be predicted by use of the Stokes number solely. Different cyclones will have different dependence on the Stokes number, and lab tests are therefore required in order to characterize a specific cyclone.

2.2.2 Pressure drop and cut size

The fact that there is a connection between pressure drop and grade efficiency has long been known. The required "energy cost" in terms of pressure drop are larger when small droplets must be separated compared to larger particles/droplets. Hoffmann and Stein gives an overview over some correlations developed for cyclones over the years. The relationship between pressure drop and grade efficiency is expressed with Stk_{50} and pressure drop coefficient i.e. the Euler number:

$$Eu \equiv \frac{\Delta P}{1/2\,\rho_g u_g^2} \tag{2.18}$$

In common for them all is that the Stk_{50} is inversely proportional with Eu or its square, meaning that the cut size of a cyclone decreases with increasing pressure drop. This result is not surprising if one investigate the cause of the pressure drop. The pressure drop in a cyclone is mainly related to the transition of static pressure P into dynamic pressure $1/2\,\rho_g u_g^2$. Therefore increased pressure drop implies higher gas velocities in the separator and, hence, stronger forces for droplet separation.

In the same way as there exists a relation between the pressure drop (or Euler Number) and the cut size (or Stk_{50}) for a cyclone, Bürkholz found through experiments a similar relationship. For wire filters of different sizes and thicknesses he found that the cut size was inversely proportional with the pressure drop in the power of 1/3, i.e.

$$d_{50} = K_{50}\frac{1}{\sqrt[3]{\Delta P}} \tag{2.19}$$

K_{50} is a proportional constant that has to be determined experimentally. Bürkholz offered a physical interpretation of K_{50}. If Equation (2.19) is rearrange so that the pressure drop appear at the left hand.

$$\Delta P = K_{50}^3 d_{50}^3 \tag{2.20}$$

K_{50}^3 has got the dimension of energy [J] and can be regarded as the characteristic separation energy needed in order to achieve the cut size d_{50} for a given separation unit. This is an important result, since it shows that better grade efficiency is

always accompanied by increasing pressure drop for a given demisting unit. Bürkholz has discovered this relation between pressure drop and cut size for a series of equipment designed for inertial separation, including cyclones, packed beds, wire filters, wire mesh and fibre filters.

Another important discovery was that smaller characteristic diameter, led to lower characteristic separation energy e.g. a small cyclone would separate droplets more energy efficiently, that is to say with less pressure drop, than a larger cyclone. Thus, in terms of grade efficiency it would for instance be wiser to install many small cyclone units working in parallel rather than some few large units. Equivalently, a mesh with wires of small diameter will separate liquid more energy efficiently than a mesh with larger wires.

Be aware that the numerical value of the characteristic separation energy is dependent on the experimental conditions and the units employed. Hence, in order to compare the characteristic separation energy of two different types of equipment, they must be tested with the same fluid under the same operating conditions so that the physical properties, i.e. densities and gas viscosity are identical.

2.2.3 Inertial Separation Parameter

Even though the scaling rule involving the Stokes number in Hoffmann and Stein was deducted for cyclones, many of the principles could and also have been used for other types of equipment that is designed for inertial separation. Bürkholz (1989) have used the same principles but with a more general approach.

Bürkholz made a dimensional analysis for the grade efficiency of a filter consisting of wires in a similar way that the analysis Hoffmann and Stein did for cyclones. However, Bürkholz also included the pressure drop as one of the parameters that the grade efficiency depended upon. In addition, the geometrical parameters did only include the wire diameter D and the thickness of the filter H. Hoffmann and Stein, on the other hand, assumed geometrical similarities between the prototype and a full scale model for the scaling rule to be valid. Assuming that the droplets are at their terminal velocity when they enter the filter, and neglecting the mutual influence of the flow pattern around the single wires, the grade efficiency was assumed to be a function of 9 parameters:

$$\eta_g = f\left(D, d, H, u_g, \Delta P, \rho_l, \rho_g, \mu_g, g\right) \tag{2.21}$$

In order to reduce the number of parameters, all the assumptions made in the analysis of Hoffmann and Stein were also made for this analysis. In addition, the filter thickness H was removed since the pressure drop is proportional with H for a

given velocity u_g. The validity of Stokes law was assumed and hence, the liquid density and drop size could be combined $\rho_l d_g^2$. Note that Bürkholz used the liquid density instead of the density difference in the expression for the Stokes number (Equation (2.16)). The Stokes number by Bürkholz' definition is hence denoted Stk_B. The difference will be discussed later.

This reduced the number of parameters to six and through dimensional analysis they were organised into three dimensionless groups and the expression in Equation (2.21) where reduced to:

$$\eta_g = f\left(D, \rho_l d_g^2, u_g, \Delta P, \rho_g, \mu_g\right) \Rightarrow \eta_g = f\left(Eu, Re_g, Stk_B\right) \tag{2.22}$$

By means of dimensional analysis alone, no further reduction of in the number of parameters was possible. However, Bürkholz combined the Stokes term, $\rho_l d_g^2$ with the relation between pressure drop and droplet size $\Delta P d_{50}^3$ (see Equation (2.20)) into one parameter $\rho_l d_g^2 \cdot \Delta P^2 d^3$. This made it possible to reduce the number of independent variables by one. In addition, the gas velocity did not need to appear explicitly in the expression since it was being reflected in the pressure drop

This reduced the list of variables from six to four. By use of matrix-mechanical rearrangement Bürkholz was able to arrange the parameters into one dimensionless group ψ_A the inertial separation parameter.

$$\eta_g = f\left(D, \rho_l d_g^2 \Delta P^2 d^6, \rho_g, \mu_g\right) \Rightarrow \eta_g = f\left(\psi_A\right) \tag{2.23}$$

Bürkholz showed that the inertial separation parameter could be written

$$\psi_A = Stk_B \cdot Re_g^{1/3} \cdot \left(\frac{Eu}{2}\right)^{2/3} \tag{2.24}$$

The expression could also be expressed with the basic parameters as:

$$\psi_A = \frac{1}{4}\left(\rho_l \rho_g^{-1/3} \mu_g^{-4/3}\right)\left(\Delta P^{2/3} D^{-2/3} d^2\right) \tag{2.25}$$

Even though the inertial impaction parameter was deduced for a wire mesh, the deduction is also valid for all types of separation equipment that work by the principle of inertial separation e.g. cyclones, fibre separators, vane pack and packed beds. The diameter D then represents a characteristic diameter of the impact body, typically the body diameter of a cyclone and the wire diameter of a mesh. Bürkholz has verified the validity of the inertial impaction parameter for all the mentioned types of equipment.

2.2.4 Scaling at high pressure

In the two presented scaling rules for grade efficiency two different definitions of the Stokes number has been used. Hoffmann and Stein (2002) used the following definition

$$Stk \equiv \frac{\Delta\rho d^2 u_g}{18\mu_g D} \tag{2.26}$$

While Bürkholz (1989) used a different definition:

$$Stk_B \equiv \frac{\rho_l d^2 u_g}{\mu_g D} \tag{2.27}$$

The subscript B denotes that it is the Stokes number the way it is defined in Bürkholz. The biggest difference is the use of the density difference $\Delta\rho$ versus the use of the liquid density solely. If the equation of motion for a droplet in a centrifugal field is investigated the relevance of the Stokes number becomes clear. The motion in the radial direction is

$$\left(\frac{\pi d^3}{6}\right)\rho_l \frac{\partial u_r}{\partial t} = -3\pi d\,\mu_g u_r + \left(\frac{\pi d^3}{6}\right)\Delta\rho \frac{u_\theta^2}{r} \tag{2.28}$$

If it is assumed that the droplet has reached its terminal velocity, the acceleration term on the left hand disappear and the expression becomes

$$u_r = \left(\frac{\Delta\rho d^2}{18\mu_g}\right)\frac{u_\theta^2}{r} \tag{2.29}$$

By making the Equation dimensionless, Equation (2.29) can be written (for details, see Hoffmann and Stein):

$$u_r^* = \left(\frac{\Delta\rho d^2 u_{g,s}}{18\mu_g}\right)\frac{u_\theta^{*2}}{r} = Stk\,\frac{u_\theta^{*2}}{r} \tag{2.30}$$

From the equation of motion, which in the current form is relevant for all kind of inertial separation equipment, it is seen that the relevant form of the Stokes number is the version that involves the density difference rather than just the liquid density. However, Bürkholz performed all experiments with air/water at ambient conditions where the liquid density is much larger than the gas density i.e.

$$\Delta\rho \approx \rho_l \tag{2.31}$$

The Stokes number by Bürkholz' definition is therefore correct for low pressure applications. However, if the described methods for scaling of droplet cut size are also to be used for high pressure natural gas where the ratio of gas to liquid density can become very small, the density difference rather than the liquid density should be used. Hence, the inertial separation parameter for high pressure applications becomes

$$\psi_{A,HP} = \frac{\Delta\rho}{\rho_l} Stk_B \cdot Re_g^{1/3} \cdot \left(\frac{Eu}{2}\right)^{2/3} = 18 Stk \cdot Re_g^{1/3} \cdot \left(\frac{Eu}{2}\right)^{2/3} \tag{2.32}$$

or

$$\psi_{A,HP} = \frac{1}{4}\left(\Delta\rho \cdot \rho_g^{-1/3} \mu_g^{-4/3}\right)\left(\Delta P^{2/3} D^{-2/3} d^2\right) \tag{2.33}$$

2.2.5 Advantages of the Inertial Separation Parameter

While scaling by use of the Stokes number offers a very simple expression, the inertial separation parameter has got some advantages over the Stokes number since its deduction includes the pressure drop. The Stokesian scaling requires geometrically similarities between the model and the prototype cyclone that the scaling procedure is being used for. If not, this procedure can be used if it is used in together with an appropriate Stk_{50} –Eu relation. The inertial separation parameter has shown to be applicable for equipment of varying pressure drop characteristics. However, it requires a pressure drop measurement of the equipment it is being used for.

In Figure 2.2 the advantages of using the Stokes number Stk and the inertial separation parameter ψ_A instead of the droplet size is shown. The figure shows how the grade efficiency could vary for two different demisters under three different process conditions. The curves are based on typical behaviour but not on actual measurements.

If the grade efficiency of a demister is plotted against the droplet size, an infinite number of curves exist for varying process conditions. If the grade efficiency is plotted against the square root of the Stokes number $\sqrt{Stk}$ (which is proportional to the droplet size) there will be one grade efficiency curve for each type of cyclone, mesh pad, filter or vane. However, the inertial separation parameter can account for e.g. differences in wire diameter in a mesh pad, sizes of cyclones and other geometrically variations since these differences are being reflected in the pressure drop characteristics. Hence, if the grade efficiency is plotted against the square root of the inertial separation parameter $\sqrt{\psi_A}$ (which is also proportional to the droplet size), cyclones with different pressure drop characteristics caused by e.g. different size or aspects ratios, will share the same characteristic efficiency curve. Likewise will mesh pads constructed with wires of different diameter, share

a common characteristic grade efficiency curve. However, experiments carried out by Bürkholz show that different types of equipment do not share the same characteristic separation curve. Hence, will the characteristic separation curve of cyclones be different than the characteristic separation curve of mesh pads.

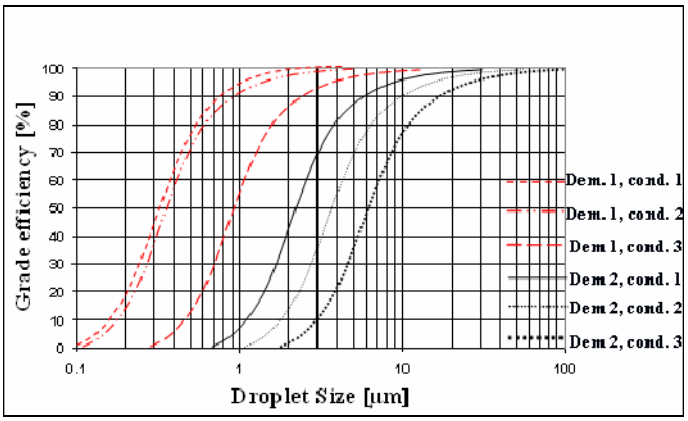

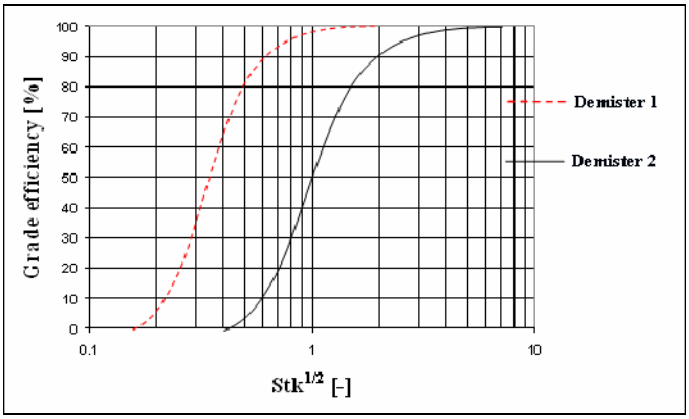

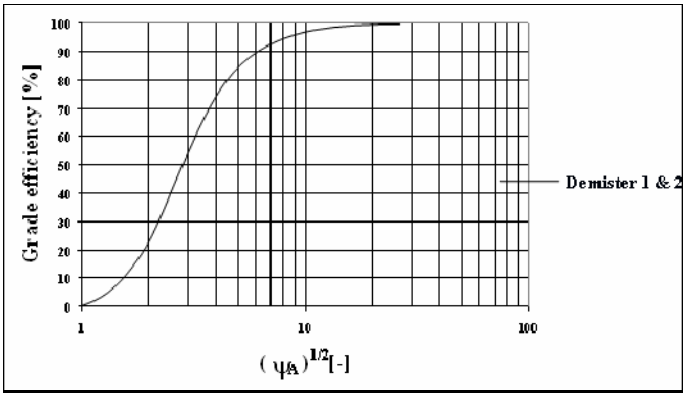

Figure 2.2 The figures shows the principles of how the efficiency of demisting equipment can vary with the droplet size, Stokes number and the inertial separation parameter. While the plot against droplet size requires one curve per process conditions for each type of demister, the Stokes number eliminates the process variations. The inertial separation parameter can in addition eliminate the variations in geometry for one type of demister e.g. cyclone or mesh pad.

2.3 Liquid Entrainment

Liquid entrainment in conjunction with a con-current gas-liquid film occurs when the relative velocity between the gas and liquid phase exceeds a critical limit. This limit is highly dependent on the physical properties of the liquid. Different mechanisms of entrainment that relates to different flow regimes in the film have been identified in literature but for entrainment to occur an interfacial instability must occur. In the case of a con-current gas liquid flow it is called the Kelvin-Helmholtz (K-H) instability (Chandrasekhar, 1961).

2.3.1 Entrainment Mechanisms

A wavy liquid film can be entrained into a gas flow in a number of different ways. Ishii and Grolmes (1975) summarize four different basic mechanisms for entrainment in con-current gas liquid flow. These mechanisms are shown in Figure 2.3. The work of Ishii and Grolmes were carried out on an angled plate containing a liquid film with gas blowing over.

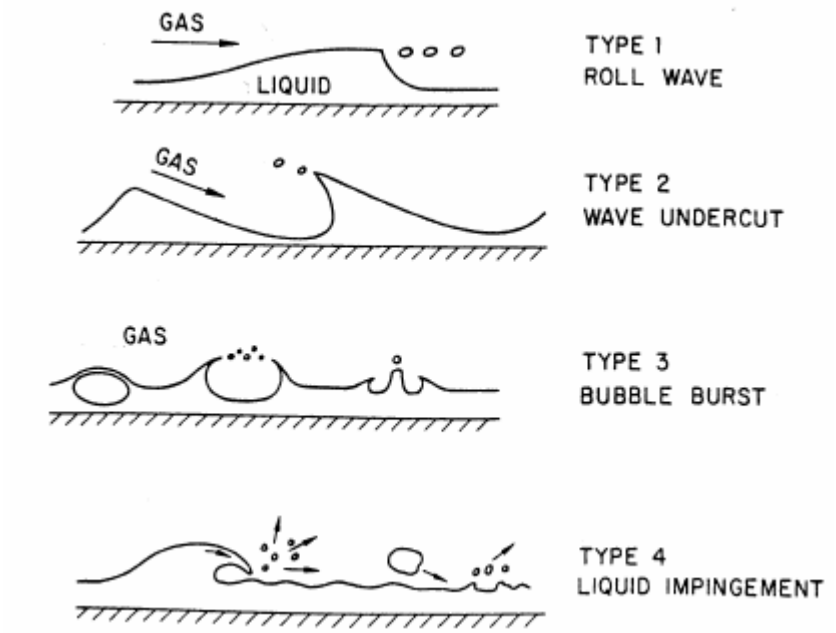

Figure 2.3 Different entrainment mechanisms for concurrent gas liquid flow. Reprinted with permission from the AIChE Journal, March 1975. Copyright © 1975 AIChE

The first mechanism is associated with droplets that are sheared of a roll-wave crest and is the dominant mechanism in a relatively high film Reynolds number regime. The second mechanism is undercutting of a wave crest and is most relevant in a lower film Reynolds number regime. The two last mechanisms are associated with either bubbles that burst or liquid that impinges on the liquid film surface and produce small droplets.

2.3.2 Flow Regimes and Inception of Droplet Entrainment

The different mechanisms of entrainment are dominant in different flow regimes. In order to differ between the different regimes, it is necessary to consider the Reynolds number for the liquid film

$$\mathrm{Re}_l = \frac{\rho_l v_l \delta_l}{\mu_l} \tag{2.34}$$

Ishii and Grolmes argued that the inception of entrainment was dependent on Re_l up to a certain level. They also pointed out that there exists a lower limit for Re_l. Below this limit entrainment does not happen except for some very high gas velocities. When the film Reynolds number was low and the gas velocity was high, a liquid film Weber-number correlation could be used to correlate the inception of entrainment (van Rossum, 1959). The different entrainment regimes are shown in Figure 2.4. The line represents the inception of entrainment represented by a dimensionless gas velocity as function of varying Re_l

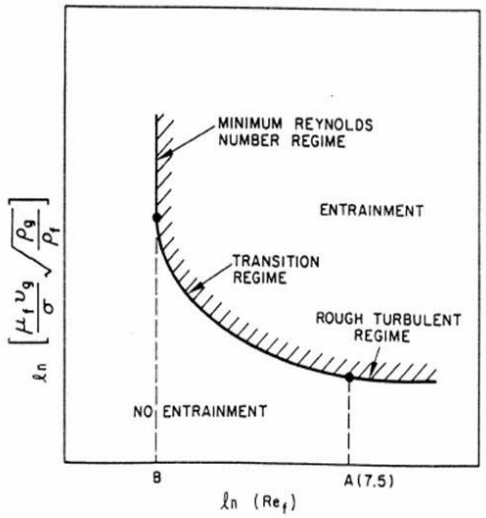

Figure 2.4 Different entrainment regimes occur at different regions of the liquid film Reynolds number Reprinted with permission from the AIChE Journal, March 1975. Copyright ©1975 AIChE

The boundaries for the limit between no-entrainment regime and transition regime were not firmly established but were given to be 2 for vertical down flow and 160 for horizontal or vertical up flow. The limit between the transition and rough turbulent regime was given to be in the range 1500 – 1750.

Roll Wave Entrainment

Ishii and Grolmes derived a criterion for the onset of re-entrainment by considering the force balance between the drag force F_d from the high shear flow of gas acting on the liquid wave crest, and the retaining force of the surface tension F_σ. They assumed that roll wave entrainment was possible when the drag forces exceeded the retaining force of the surface tension:

$$F_d \geq F_\sigma \tag{2.35}$$

By using the entrainment model shown in Figure 2.5 they derived one criterion for the inception of entrainment in the transition regime, and one criterion for the rough turbulent regime.

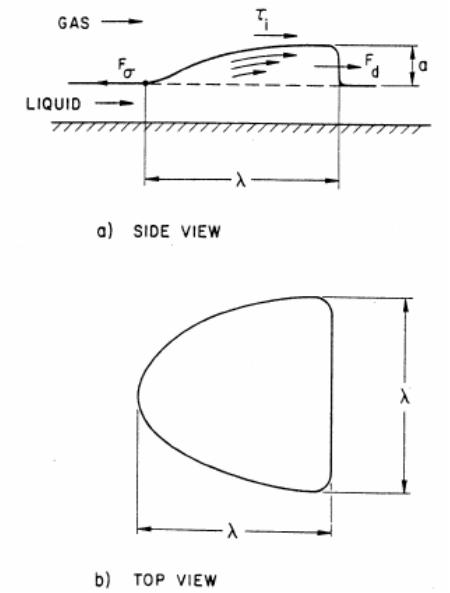

Figure 2.5 The model for entrainment based on roll-wave break-up. Reprinted with permission from the AIChE Journal, March 1975. Copyright ©1975 AIChE

For the transition regime the criteria were

$$\frac{\mu_l u_{g,s}}{\sigma}\sqrt{\frac{\rho_g}{\rho_l}} \geq 11.78 N_\mu^{0.8}\,\mathrm{Re}_l^{-1/3} \quad \text{for} \quad N_\mu \leq \frac{1}{15} \tag{2.36}$$

and

$$\geq 1.35\,\mathrm{Re}_l^{-1/3} \quad \text{for} \quad N_\mu \geq \frac{1}{15} \tag{2.37}$$

Ishii and Grolmes' entrainment criterion was the same at intermediate and high Re_l, but at high Re_l it can be written simpler

$$\frac{\mu_l u_{g,s}}{\sigma}\sqrt{\frac{\rho_g}{\rho_l}} \geq N_\mu^{0.8} \qquad \text{for} \quad N_\mu \leq \frac{1}{15} \tag{2.38}$$

$$\text{and} \qquad \geq 0.1146 \qquad \text{for} \quad N_\mu \geq \frac{1}{15} \tag{2.39}$$

N_μ is the viscosity number which originally was used by Hinze (1955) to analyze the problem of droplet disintegration in a gas flow. The group measures the viscous force induced by an internal flow to the surface tension force and when it is used for droplet entrainment it is defined as:

$$N_\mu = \frac{\mu_l}{\sqrt{\rho_l \sigma \sqrt{\frac{\sigma}{g\Delta\rho}}}} \tag{2.40}$$

The expression $\sqrt{\sigma/g\Delta\rho}$ has the dimension of length and it is proportional to the critical wavelength of a Taylor instability. The dependence on the acceleration of gravity g is explained by the stabilising effect of the gravity force on the wavy interface.

Low Reynolds Number Entrainment

Below the lower limit for entrainment shown in Figure 2.4, liquid entrainment is still possible if the gas velocity is sufficiently high. Van Rossum (1959) carried out entrainment experiments for nine different fluids with interfacial tension ranging from 30 to 78 mN/m. In his study, van Rossum analyzed the onset of entrainment in terms of two dimensionless numbers, the film Weber number with the liquid film thickness as length scale,

$$We = \frac{\rho_g u_g^2 \delta}{\sigma} \tag{2.41}$$

and a correlation parameter S,

$$S = \frac{u_g \mu_l}{\sigma} \tag{2.42}$$

It was discovered that the critical Weber number, for which the inception of entrainment occurred, was practically constant when $S > 5$, while it became dependent on S for lower values.

2.4 Inlet Arrangement

Ideally, a good inlet device shall reduce the inlet momentum, separate bulk liquid with minimum creation or shattering of droplets, and create an even gas and liquid distribution further downstream. The NORSOK standard (2001) sets a limitation to the allowable inlet gas dynamic pressure defined as:

$$\rho u^2 \tag{2.43}$$

The reason for limiting the inlet gas dynamic pressure is to avoid high shear forces in the inlet that potentially could produce small droplets that are more difficult to separate. The NORSOK standard recommends that where an inlet vane is installed, the dynamic pressure based on the superficial gas velocity in the inlet nozzle, should be kept below 6000 Pa.

Note, that the NORSOK standard does not specify what density that should be used. In the present study the gas density has been used, but it is also common to us a calculated two-phase density defined as:

$$\rho_{mix} = \frac{\dot{Q}_l \rho_l + \dot{Q}_g \rho_g}{\dot{Q}_g + \dot{Q}_l} \tag{2.44}$$

At small liquid rates the mixed density and the gas density are approximately the same.

The idea of the inlet vane is to reduce the gas momentum, separate the bulk liquid and produce an even flow pattern further downstream before the gas and remaining liquid enters the mesh pad or whatever is installed downstream of the inlet. However, the gas stream pattern downstream of an inlet vane is highly uneven. The flow pattern above an inlet vane in a 150 mm diameter column was experimentally investigated in a master thesis at the University of Bergen (Kvinnesland, 2004). The details of this inlet vane geometry will be discussed in more detail in Section 3.4.1. Experimental liquid separation efficiency results with this geometry are reported in Section 4.2.

By use of a novel technique with injected neutrally buoyant helium soap bubbles in the gas, the flow was recorded with a high-speed video camera. The high-speed video was then analyzed by use of a Particle Tracking Velocimetry (PTV) software in order to get a quantitative representation of the gas velocity. In addition the velocity was simulated by use of the commercial CFD package Fluent.

In Figure 2.6 an example of the measured and simulated gas flow pattern above an inlet vane placed in a 150 mm vessel is shown. The flow pattern that represents the horizontal components of the gas velocity shows that the gas is far from even

distributed. Two distinct axis-symmetric swirls are seen and two zones of strong velocity gradients at the wall.

In Figure 2.7 the vertical components of the gas velocity is shown in a side view of the vessel. The simulation shows that the gas velocity along the wall is much higher than the gas velocity in the centre of the vessel.

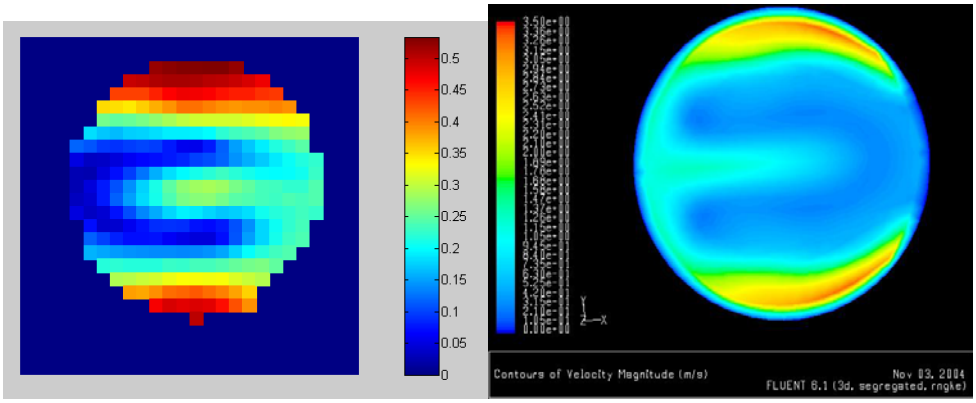

Figure 2.6 The horizontal velocity distribution 80 mm above an inlet vane. The left picture is the measured velocity distribution while the right picture is a CFD simulation of the same geometry rotated 180^0 around the centre axis. The gas inlet is to the left in the left picture.

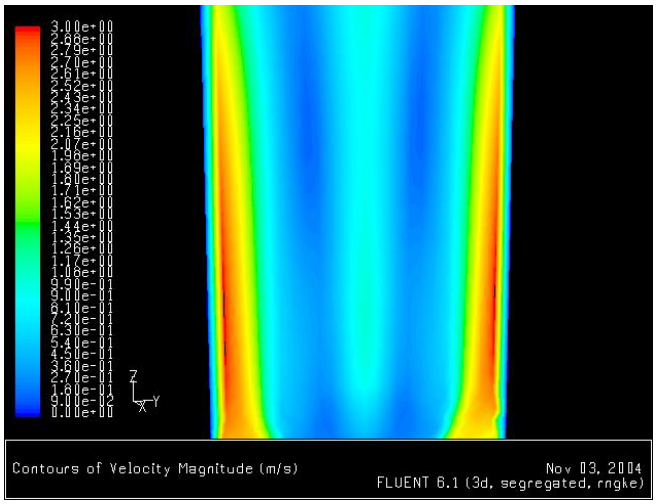

Figure 2.7 A CFD simulation of the vertical velocity distribution 70 – 170 mm above an inlet vane. The picture represents a plane in the middle of the vessel seen from the angle where the gas enters.

Due to the strongly uneven gas flow pattern, it is reasonable to assume that also liquid in the gas will be unevenly distributed. Uneven gas and liquid distribution above the inlet vane may have a bad impact on the performance of separation equipment further downstream in the scrubber.

2.5 Mesh Pad

The mesh pad is either installed in a scrubber in order to catch small droplets that coalesce to larger droplets that can settle out, or it is being used as a pre-conditioner in order to increase the average droplet sizes before the liquid enters a final demisting separation stage. The majority of mesh pads are made from wires of stainless steel but there also exists a lot of mesh pads made from different plastic substances like multifilament (Brunazzi and Paglianti, 2000).

2.5.1 Size

The diameter of a mesh pad is usually designed on basis of the K-value (York, 1954; Holmes and Chen, 1984; Bürkholz, 1989; Talavera, 1990; Svrek and Monnery, 1993; Feord et al. 1993; Brunazzi and Paglianti, 1998, 2001). The procedure is the same as described in Section 2.1.3. In order for the K-value to function as a demister, the vendors state that the K-value should typically be kept below 0.107 m/s. Some vendors also recommend a lower value for e.g. high liquid loading or high pressure services. The NORSOK–standard (NORSOK, 2001) recommends that the K-value is kept below 0.1 m/s for low-pressure applications, and for pressures above 20, 40 and 80 barg it is recommended that the K-value is reduced by 10, 20 and 25 % respectively.

2.5.2 Flood Point

If the gas velocity upstream of a mesh pad exceeds a certain limit, the droplets that have coalesced in the mesh pad, can no longer be drained efficiently by gravity and liquid therefore start to build up in the mesh. The point where this happens is called the flood point and is accompanied by a sudden increase in pressure drop over the mesh (Bürkholz, 1989; El-Dessouky et al. 2000). The theory behind the K-value is derived on basis of the maximum gas velocity in order for a droplet to settle out by gravity. By keeping the K-value constant the effect of e.g. droplet size and liquid load is ignored. Hence, it is not a consistent way of designing a mesh pad, but in practice the requirement assures that the mesh is being operated in a non-flooded condition. El-Dessouky et al. suggested a simple empirical expression for the flooding velocity that correlated well for experiments they carried out with water steam at 2 bara:

$$u_{g,f} = 128.358356 \cdot \rho_l^{-0.287031} \cdot D_w^{1.220656} \tag{2.45}$$

Expressing the flooding velocity solely as a function of the liquid density ρ_l and the wire diameter D_w of the mesh pad obviously must have a very limited range of applicability. The influence of e.g. gas density, liquid loading and droplet size is ignored.

Sherwood et al. (1938) investigated the flooding velocities in packed columns for a wide range of fluids. The diameter of the transparent column was 5.1 cm and it was filled with Raschig rings. The physical properties of the fluids varied from 26 – 73 mN/m for the interfacial tension, 0.91 – 96 cP for the liquid viscosity, 800 – 1187 kg/m^3 for the liquid density and 0.08 – 1.8 kg/m^3 for the gas density. The result showed that the flooding velocity was very little dependent on the interfacial tension within the tested range, but more dependent on the other physical properties mentioned here. In addition, the flooding velocity also varied with varying liquid load, surface area of the mesh pad and the void fraction of the mesh. Sherwood et al. showed that the flooding point could be correlated by use of two dimensionless groups. The first group is a kind of dimensionless gas dynamic pressure:

$$\frac{A_s u_{g,s}^2}{g\varepsilon^3}\left(\frac{\rho_g}{\rho_l}\right) \tag{2.46}$$

Where A_s is the specific area of the mesh i.e. the ratio of the surface area of the wires to the total volume of the mesh pad while ε is the void fraction of the wires. The second group was a dimensionless liquid concentration given as:

$$\frac{\dot{m}_l}{\dot{m}_g}\sqrt{\frac{\rho_g}{\rho_l}} \tag{2.47}$$

Here, $\dot{m}$ is the mass rate.

This method of determining the flooding point worked well for different gases in combination with water, but when other liquids with very different viscosities were used, the results deviated and they therefore recommended including the liquid viscosity in the expression in Equation (2.46), thereby making the expression dimensional. Hence they found the relationship:

$$\frac{A_s u_{g,s}^2}{g\varepsilon^3}\left(\frac{\rho_g}{\rho_l}\right)\mu_l^{0.2} = f\left(\frac{\dot{m}_l}{\dot{m}_g}\sqrt{\frac{\rho_g}{\rho_l}}\right) \tag{2.48}$$

Even though Sherwood et al. studied flooding in packed columns, the principles of flooding are the same as for a mesh pad. Bürkholz analyzed the flood point for two different mesh pads and found a good correlation with the expression in Equation (2.48). The correlation found by Bürkholz can be seen in Figure 2.8.

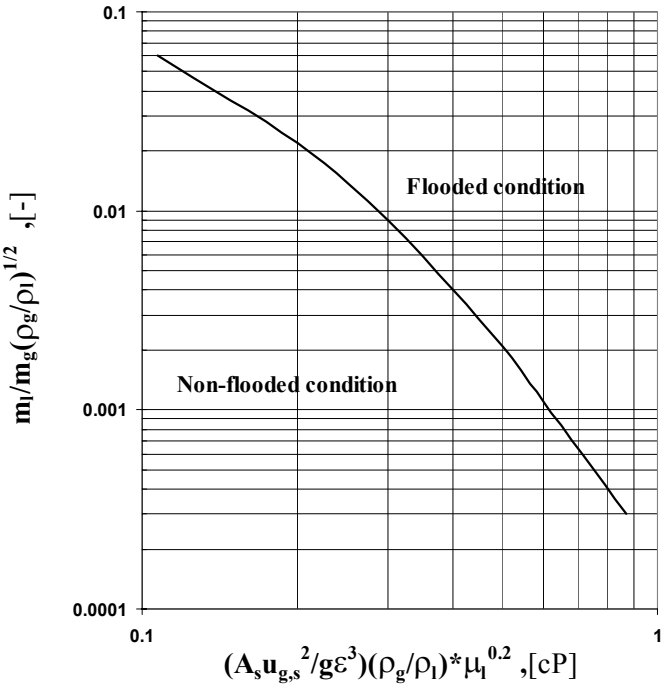

Figure 2.8 The figure shows the correlation Bürkholz found for the flooding point of two different mesh pads.

From the plot in Figure 2.8 in can be seen that the flooding velocities decreases with increasing liquid load. Also, if the pressure increases the density ratio, ρ_g / ρ_l increases and flooding will, hence, occur at a lower superficial gas velocity.

2.5.3 Grade Efficiency

Three different separation mechanisms are widely recognized to be relevant for a mesh pad. These three mechanisms are inertial impaction, direct interception and Brownian diffusion (Langmuir and Blodgett, 1946; Carpenter and Othmer, 1955; Davies, 1966; Holmes and Chen, 1984; Brunazzi and Paglianti, 1998; Ziebold, 2000). The principles of the three mechanisms are shown in Figure 2.9.

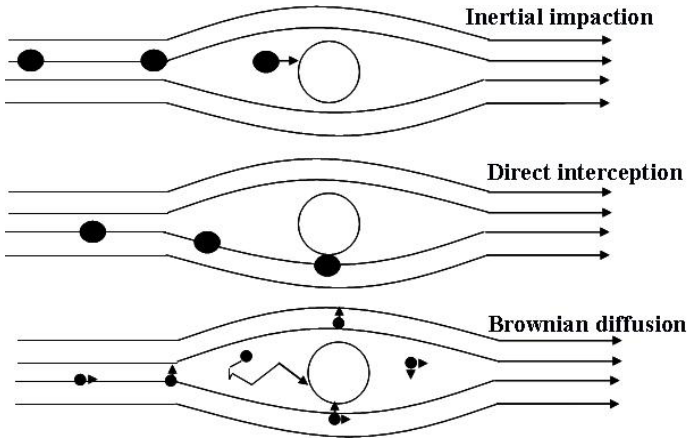

Figure 2.9 The figure shows the three separation mechanisms relevant for a wire in a mesh pad

Brownian diffusion is only relevant for very small droplets in the sub-micron range and its contribution to the total carry-over from a mesh pad can be neglected for all practical purposes. This leaves us with two separation mechanisms, inertial impaction and direct interception. However, most publications recognize inertial separation as the main contributor to the overall efficiency (Holmes and Chen, 1984; Brunazzi and Paglianti, 1998, 2000). The principle of inertial separation is described in more detail in Section 2.2. Carpenter and Othmer (1955) derived an analytical grade efficiency model based on the capture efficiency of a single wire. Later Brunazzi and Paglianti derived similar models for both metal and complex wire mesh pads, while Feord et al. (1993) used a stochastic model that also was based on the capture efficiency of a single wire. In common for them all was that they assumed that the capture efficiency of a single target was a function of the Stokes number, -or a similar expression, also referred to as Sells number (Feord et al.) or the inertial parameter (Chen, 1955). Brunazzi and Paglianti showed that in their experiments at ambient conditions, the efficiency of both metal and complex mesh pads was close to 100 % when Stk > 1. They also investigated the connection between pressure drop and d_{95} i.e. the droplet size that will be separated with 95% efficiency, as pointed out by Bürkholz (1989). In their experiments they found a good correlation with the findings of Bürkholz as explained in Section 2.2.2. Both Bürkholz and Brunazzi and Paglianti carried out experiments with air/water at ambient conditions**.** However, the correlation between the pressure drop and d_{95} is dependent on the experimental conditions. Therefore, in order to predict d_{95} or d_{50}, for other fluids, temperatures and pressures, the inertial separation parameter, ψ_A should be used. Bürkholz found that for all experiments with mesh pads the following was true:

$$d_{50} \Rightarrow 4 < \psi_A^2 < 5 \tag{2.49}$$

$$d_{95} \Rightarrow 7 < \psi_A^2 < 8 \tag{2.50}$$

If the fluid properties of a typical light live natural fluid[1] are used as a basis, the droplet size that will be separated with 95 % efficiency becomes larger when the system pressure is increased and the *K*-value is kept constant. In Figure 2.10 it is shown how d_{95} increases when the relationships Stk = 1 and $\psi_A^{1/2} = 8$ are used as scaling parameters for the mesh pad used in this study[2]. The main reason for the increasing d_{95} is that the velocity decreases with pressure when the *K*-value is kept constant.

The figure shows that the predictions of the two different scaling rules for d_{95} coincide. As discussed earlier, Stk_{95} may vary for different types of mesh pads, while the inertial separation parameter is more general and can be used for all kinds of mesh pads since the variations will be reflected in the pressure drop.

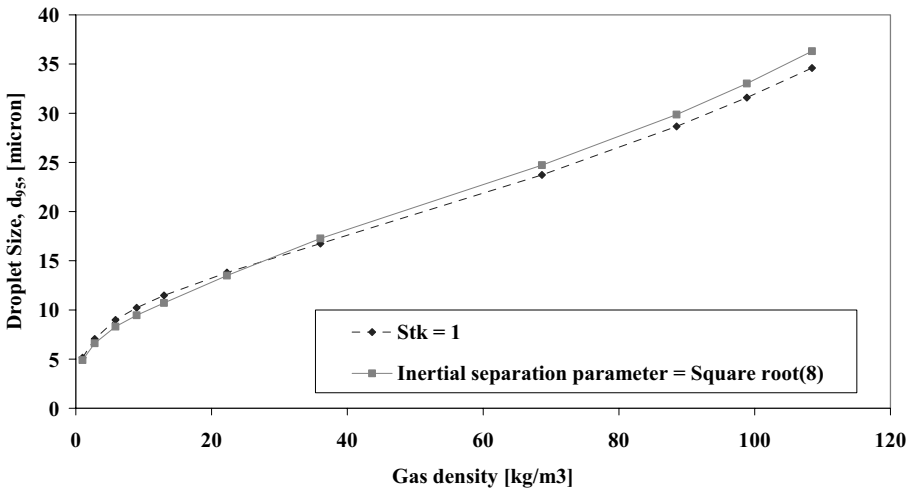

Figure 2.10 The figure shows how d_{95} changes with increasing gas density (i.e. pressure) for a live natural gas system and *K* = 0.1 m/s.

In order to calculate d_{95} by use of the inertial separation parameter, the pressure drop over the mesh pad must be known. The pressure drop over the mesh pad used in the standard setup in this study was shown to have an Euler Number at approximately 14. However, the Euler Number that has been used to calculate the pressure drop for the mesh pad is not constant but depends on the Reynolds number. Bürkholz showed how *Eu* was decreasing with increasing Re_g for a mesh

[1] This fluid system will be described in detail later. Se Section 3.2.4

[2] The details of the mesh pad are described later in Section 3.4.2

pad. The calculated pressure drop used in the calculation of $\psi_A^{1/2}$ in Figure 2.10 has therefore been corrected in accordance with the curve given by Bürkholz.

2.6 Axial Flow Cyclones

In literature there is a lot of work published on design and operation of reverse flow cyclones, but the amount of work carried out on axial flow cyclones (AFC) also referred to as once-through cyclones, uniflow cyclones or swirl flow separators, is less. The axial flow cyclones were first utilized in dust removal applications e.g. as engine intake filtration. Stenhouse and Trow (1979) gave a brief summary of their use and suggest a grade efficiency model based on results from dust experiments in the lab. Later Bürkholz (1989) also investigated axial flow cyclones that had very large length to diameter ratios in the range from 10 to 20. The axial flow cyclones gained increasing popularity in the oil and gas industry in the 90's, and they where often used when scrubbers were subjected to revamping. Several papers describe applications where axial flow cyclones have increased in popularity (Diekmann et al. 1992; Swanborn et al. 1995; Stewart et al. 1998; Sterner, 2001; Chin et al. 2002).

2.6.1 Grade Efficiency Models

The grade efficiency of cyclones has been studied widely in literature, but most of the work has focused on reverse flow cyclones and in particular cylinder-on-cone cyclones with tangential inlet. The grade efficiency models are in principal based on two different approaches, the equilibrium-orbit models and the time-of-flight models (Hoffmann and Stein, 2002). The equilibrium-orbit models try to predict the efficiency by consider whether a droplet of a certain size placed at the interface between the outer and inner vortex in a cyclone would be thrown to the wall or caught by the inner vortex and escape through the vortex finder. Since the flow pattern in an AFC does not comprise an inner part of the vortex with upward flow the second approach i.e. time-of-flight models have been used for these cyclones.

The time-of-flight models try to determine whether a droplet of a certain size has enough time to reach the cyclone wall before the carrier gas flows through the outlet of the cyclone. To determine this it is usually assumed that the droplets have reached their terminal velocity and that the Stokes drag for the droplets is valid i.e. the radial velocity of the droplet can be expressed:

$$u_{l,r} = \frac{\partial r}{\partial t} = \frac{\Delta \rho d^2}{18\mu} \frac{u_{g,tg}^2}{r} \tag{2.51}$$

Here, $u_{g,tg}$ is the tangential gas velocity at the position r in the cyclone. This requires a model for the tangential velocity in the cyclone. The tangential velocity distribution in a cyclone can be regarded as a combination of a 'forced vortex' flow

and a 'loss free vortex' flow as discussed by Hoffmann and Stein. The tangential velocity increases with increasing radius from the centre of the cyclone like a solid body rotation. However, since the gas viscosity is relatively low, the form of the vortex is more 'loss-free vortex'-like towards the wall. The resulting flow pattern is a modified Rankine vortex. The two different ideal flow profiles are sketched in Figure 2.11 together with the modified Rankine vortex.

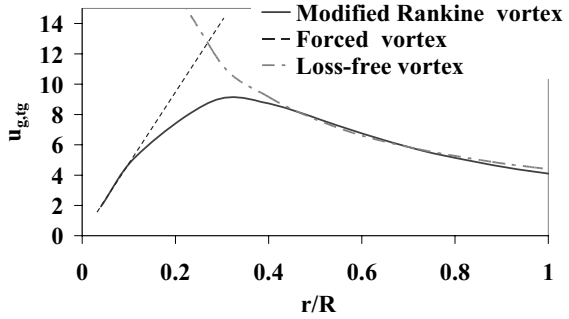

Figure 2.11 A typical tangential gas velocity distribution in the cyclone body (Rankine vortex), an approximate velocity distribution in the swirl vanes (forced vortex) and a "loss free vortex"

Several models for axial flow cyclones use a forced vortex flow as an assumption for the gas distribution in the cyclone (Stenhouse and Trow 1979; Verlaan 1991; Ramachandran et al. 1994, Nieuwstadt and Dirkzwager 1995; Maynard 2000). A forced vortex means that the angular velocity ω is constant and the tangential velocity $u_{g,tg}$ can be expressed as:

$$u_{g,tg} = \omega r \tag{2.52}$$

Another approach is to use an n-type model for the tangential gas velocity i.e.

$$u_{g,tg} = \frac{c}{r^n} \tag{2.53}$$

c is a constant for a specific cyclone at a certain volumetric gas rate and n can be taken as 0.7 - 0.8 for most centrifugal separators. This type of model produces a loss-free vortex profile as seen in Figure 2.11. The latter approach was used by Brunazzi et al. 2003 which used an expression for n that depended on the radius r and the temperature T of the gas as suggested by Licht (1980).

The axial flow cyclones described in literature can be divided into two main groups. The first consists of a tube with a swirl element at the inlet that induces the swirling motion of the gas and liquid, while the other type consists of a pipe with helical ducts inside. Recently, also an AFC with a set of tangential inlet vanes was investigated (Ng, 2005). For the helix-type of cyclones the forced vortex flow

pattern is a good assumption. For the cyclone body downstream of the swirl vanes this is a more inaccurate assumption as the flow pattern will develop into a flow pattern similar to a Rankine vortex. Stenhouse and Trow measured the gas flow pattern and concluded that the flow field was close to that of a forced vortex. Verlaan, on the other side, measured a velocity profile that was close to the forced vortex only from the centre and to r/R = 0.2. From this point and to the wall the tangential velocity decreased more like a loss free vortex. This flow pattern resembles a modified Rankine vortex.

No Radial Mixing of droplets

For the axial flow cyclones, two different approaches have been used as basis for the grade efficiency models. The first approach is to assume that there is no radial mixing of the droplets i.e. the droplets move in deterministic paths from their initial radial position and outwards to the wall. If a droplet reaches the wall before the carrier gas leaves the cyclone, the droplet is separated. This model assumption implies that there exists a critical initial radial position r_{cr} for a droplet at the inlet that determines whether it will be captured or not. A droplet with an initial position within the inner cross section of Figure 2.12 will be lost. The grade efficiency of a cyclone can, hence, be defined as:

$$\eta_g = \frac{R^2 - r_{cr}^2}{R^2} = 1 - \frac{r_{cr}^2}{R^2} \tag{2.54}$$

If the separation takes place in an annulus with an inner body of radius r_b the expression becomes

$$\eta_g = \frac{R^2 - r_{cr}^2}{R^2 - r_b^2} \tag{2.55}$$

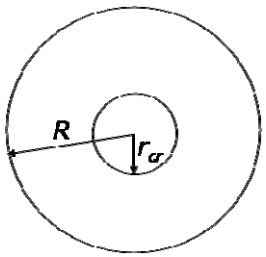

Figure 2.12 When no radial mixing of droplets are assumed, the droplet with an initial radial position less than the critical radius will not be separated. The critical radius depends on the droplet size the process conditions and the geometry of the cyclone.

The critical radius can be found by integrating Equation (2.51) from 0 to the residence time t_{res}. This requires a model for the tangential gas velocity. If a solid body rotation is assumed (Equation (2.52)), the following expression for the ratio of the critical radius to the body radius can be derived:

$$\left(\frac{r_{cr}}{R}\right)^2 = e^{-\frac{d^2\Delta\rho\omega^2 t_{res}}{9\mu_g}} \tag{2.56}$$

The residence time can be found from the volumetric gas flow and the total volume of the cyclone. If the volume is a cylinder the residence time is

$$t_{res} = \frac{\pi R^2 L}{\dot{Q}_g} = \frac{L}{u_{g,s}} \tag{2.57}$$

For an AFC with inlet swirl vanes the angular velocity, ω can be derived from the superficial gas velocity and the angle of the vanes relative to the horizontal direction. The tangential velocity at the wall is

$$u_{g,\theta}\,|_{r=R} = \omega R \Rightarrow \omega = \frac{u_{g,\theta}\,|_{r=R}}{R} = \frac{u_{g,s}}{R \cdot tan\alpha} \tag{2.58}$$

If we now combine Equation (2.56), (2.57) and (2.58) with Equation (2.54) we arrive at

$$\eta_g = 1 - e^{-\frac{d^2\Delta\rho\omega^2 t_{res}}{9\mu_g}} = 1 - e^{-\frac{d^2\Delta\rho u_{g,s}}{9\mu_g}\frac{L}{R^2 tan^2\alpha}} = 1 - e^{-8Stk\frac{L}{D\cdot tan^2\alpha}} \tag{2.59}$$

This procedure was the one used by Stenhouse and Trow. In addition they also derived the efficiency without making the assumption that the particles were always at their terminal velocity. They therefore started with Newton's second law solved in the radial direction for a particle in a centrifugal field.

$$m_d \frac{\partial^2 r}{\partial^2 t} = m_d r\omega^2 - 3\pi\mu_g d\frac{\partial r}{\partial t} \tag{2.60}$$

If the acceleration term on the left hand is neglected Equation (2.60) can be rearranged into Equation (2.51). For the derivation of the grade efficiency without the simplifying assumption that droplets are at their terminal velocity, it is referred to Stenhouse and Trow. Also Verlaan has derived the expression that included the acceleration term. The difference of including and excluding the acceleration term is illustrated in Figure 2.13. By ignoring the acceleration term, the water cut size, d_{50}, is lowered from 5.5 to 4 micron for the simplified assumption of a swirling flow in a 220 mm long pipe of 50 mm diameter at ambient conditions.

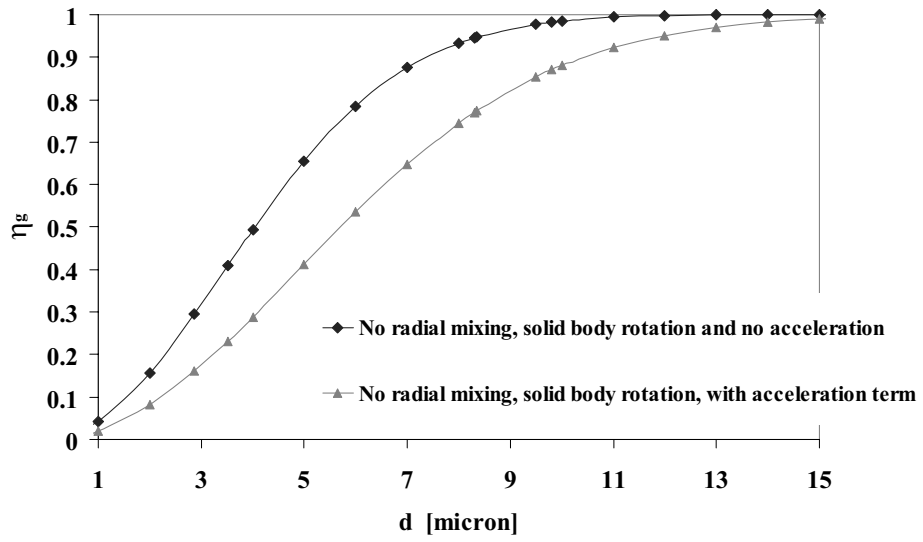

Figure 2.13 The calculated grade efficiency of a swirling gas with water droplets in a swirling pipe of 220 mm. Ambient conditions and 10 m/s superficial gas velocity with a swirl angle of 45^0 relative to the horizontal direction.

Equation (2.59) was derived under the assumption that the gas flow pattern was equal to a solid body rotation. If an n-type model is used instead, Equation (2.51) can be written:

$$u_{l,r} = \frac{\partial r}{\partial t} = \frac{\Delta\rho d^2}{18\mu}\frac{c^2}{r^{2n+1}} \tag{2.61}$$

Integrating the expression from $t = 0$ to t_{res} results after some rearrangement, in an expression for the critical radius:

$$r_{cr} = \left(R_2^{2n+2} - \frac{\Delta\rho d^2}{18\mu_g} c^2 \cdot t_{res}(2n+2) \right)^{1/(2n+2)} \tag{2.62}$$

The grade efficiency is now found by substituting the expression for r_{cr} in Equation (2.54) or (2.55) with Equation (2.62). This grade efficiency model is very sensitive to the calculation of the cyclone constant c since the critical radius is proportional to c^2.

The no radial mixing approach has been used by Nieuwstadt and Dirkzwager, Maynard, Stenhouse and Trow, and Verlaan. Brunazzi et al. also used this method but in addition, they derived a model for complete radial mixing as will be discussed.

Complete Radial Mixing

The second approach is to assume that there is a complete radial mixing of droplets that is to say that the droplet concentration C is uniform over any cross-section but decreases with the axial position. The efficiency then becomes a function of the concentration difference in the inlet C_0 and outlet C.

$$\eta_g = \frac{C_0 - C}{C_0} = 1 - \frac{C}{C_0} \tag{2.63}$$

To find an expression for how the droplet concentration decreases with the axial position, the droplets radial migration velocity at the wall must be found. This is done by replacing the variable radius, r, with the radius at the wall, R, in Equation (2.51)

$$u_{l,R} = \frac{\partial r}{\partial t} = \frac{\Delta\rho d^2}{18\mu}\frac{u_{g,\theta}^2}{R} \tag{2.64}$$

The rate of droplets that leave an infinitesimal thick ∂z cross section is equal to the amount of droplets that leave the volume of the cross section i.e.

$$\frac{\partial}{\partial t}\left(\pi R^2 C \partial z\right) = -2\pi R C u_{l,R}\partial z \tag{2.65}$$

By combining Equation (2.64) and (2.65), and rearranging, an expression for the concentration is found

$$\frac{\partial ln(c)}{\partial t} = -\frac{\Delta\rho d^2 u_{g,tg}}{9\mu_g R^2} \tag{2.66}$$

By integrating the expression over the residence time the grade efficiency is found:

$$\eta_g = 1 - e^{-\frac{\Delta\rho d^2 u_{g,tg}^2}{9\mu_g R^2} t_{res}} \tag{2.67}$$

The principle of complete radial mixing was used by Ramachandran et al. and Brunazzi et al. However, the latter failed to use the droplets radial migration velocity at the wall but instead they integrated the radial path of a particle starting in the middle of the cyclone at $t = 0$ to t_{res}. This procedure is inconsistent with the assumption of complete radial mixing since it implies that the radial positions of the droplets are random due to turbulence. Brunazzi et al. based their work on the model proposed by Leith and Licht (1972) which also suffered from the same inconsistency as pointed out in a later publication by Clift et al. (1991).

Comparison of Different Grade Efficiency Models

As discussed above, there are two main principles that grade efficiency models are based on, complete or no radial mixing of droplets. In addition, some assumptions must be made regarding the gas flow pattern. The average tangential gas velocity is often derived from the superficial gas velocity and the angle of the swirl vanes i.e.

$$\overline{u_{g,tg}} = \frac{u_{g,s}}{\tan(\alpha)} \tag{2.68}$$

For an n-type model, the tangential gas velocity depends on the prediction of c For reverse flow swirl tubes with an central swirl vane body of radius r_b Peng et al. (2004) suggested the following expression for c:

$$c = \frac{3-n}{3\pi} \cdot \dot{Q}_g \cdot \frac{R^3 - r_b^3}{\left(R^2 - r_b^2\right)\left(R^{3-n} - r_b^{3-n}\right)\tan\alpha} \tag{2.69}$$

This expression was derived under the assumption that the angular momentum of the gas in the swirl vanes is preserved in the downstream body. Brunazzi et al. derived c in a similar way from the mass balance and arrived at:

$$c = \overline{u_{g,tg}}\left(1-n\right)\frac{\left(R - r_b\right)}{\left(R^{1-n} - r_b^{1-n}\right)} \tag{2.70}$$

The calculation of the mean tangential gas velocity was based on the number of revolutions that the gas made within the cyclone, but no expression for how the number of revolutions should be calculated was given.

In the work of Stenhouse and Trow the expression in Equation (2.68) was used as an estimation of the tangential velocity at the wall, instead of the mean axial velocity. Combined with the assumption of solid body rotation it results in a mean tangential velocity that is half the velocity calculated by Equation (2.68), which will obviously affect the grade efficiency calculations. When the gas flow is assumed to follow a solid body rotation pattern in this study, the velocity calculated from Equation (2.68) is taken as the velocity at the wall.

In order to compare the influence of the different model assumptions, the grade efficiency models have been plotted for the cyclone geometry given by Verlaan. The 50 mm I.D. cyclone body downstream of the swirl vanes is 220 mm and the separation in the swirl vanes itself is neglected as a simplification. The swirl vanes have an exit angle of 45^0, which means that the mean tangential velocity is equal to the superficial velocity as can be seen from Equation (2.68). The comparison is shown in Figure 2.14, and the different models predict cut sizes d_{50} in the range 3-6 microns for a superficial velocity of 10 m/s at ambient conditions. The predicted grade efficiency curve is much sharper for the "No radial mixing and n-type

velocity"-model than for the other three models that approach the 100% efficiency limit asymptotically -more similar to most experimental investigations. For the n-type tangential velocity models n can be taken as 0.7-0.8 for most centrifugal separators and in Figure 2.14, $n = 0.8$ was used.

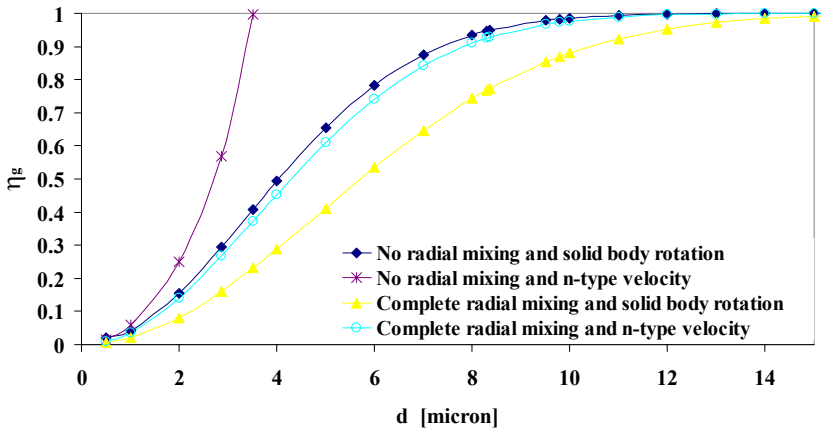

Figure 2.14 The grade efficiency models for the Verlaan cyclone at ambient conditions and 10 m/s superficial gas velocity

Comparison with experimental results in literature

In order to compare the different models with measurements reported in the literature, only results from AFC's with an open cyclone body downstream of a swirl element have been considered here. A selection of measurements is taken from Stenhouse and Trow, Bürkholz, Brunazzi et al. and Ng. Unlike the model approaches used by e.g. Maynard or Brunazzi et al., the efficiency of the swirl vanes or the vortex finder are ignored in order to make a rough benchmark of the suitability of the different model approaches.

Bürkholz carried out experiments with air/water at ambient conditions on cyclones with relatively large diameter and length. In Figure 2.15 the published results of one of the test with 10 m/s superficial gas velocity is shown. The AFC was 2 meter long and had a diameter of 190 mm with swirl vanes angle of 60^0. The "No radial mixing" models seem to predict the cut size fairly well. This cyclone had a very small vortex finder that can be ignored for all practical considerations. Still some separation may have taken place in the swirl element so that the efficiency of the cyclone body itself might have been slightly less.

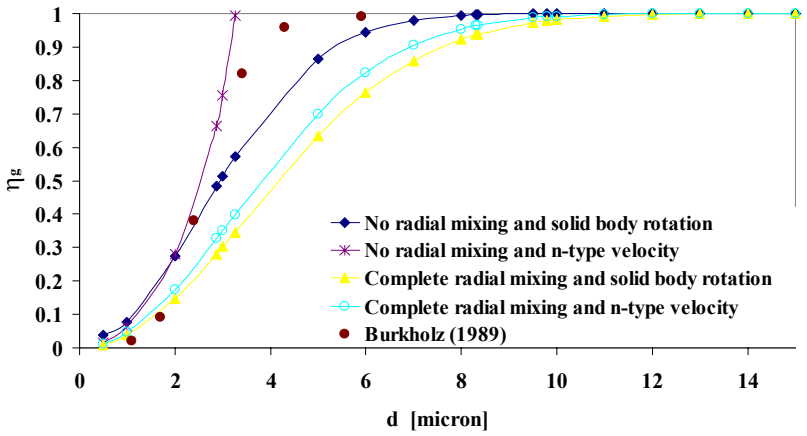

Figure 2.15 The figure shows a comparison between the experimental data of Bürkholz (1989) and four different model approaches at ambient conditions and 10 m/s superficial gas velocity

Stenhouse and Trow carried out experiments with dried feldspar dust in the size range 2-20 microns. In their experiments they used a small 37 mm diameter AFC that was only 70 mm long and a swirl angle of 60^0 at the wall. The results for a data set measured at 6.2 m/s is shown and compared to the different model approaches in Figure 2.16. Once again the "No radial mixing and n-type velocity"-model seem to predict the cut size well. However, the best representation in this case is achieved with the "complete radial mixing and solid body rotation" model.

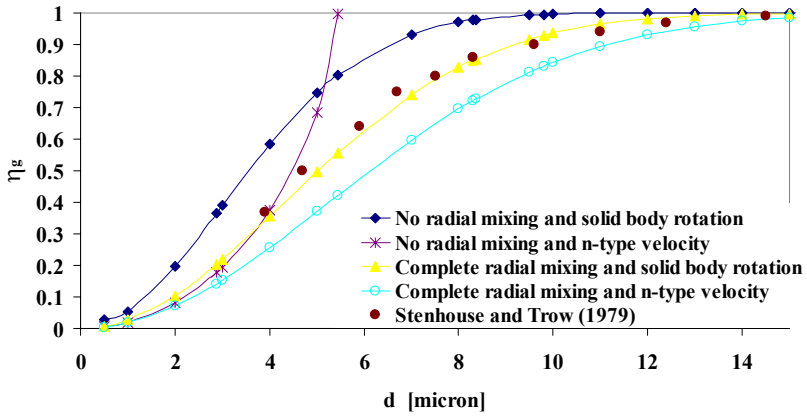

Figure 2.16 The figure shows a comparison between the experimental data of Stenhouse and Trow (1979) and four different model approaches at ambient conditions and 6.2 m/s superficial gas velocity

Brunazzi et al. measured the grade efficiency for air/water at ambient conditions for three different AFC's. Two of the AFC's where cyclones that consisted of pipes with helical ducts, while the third cyclone which was referred to as "type A" was an AFC with swirl vanes at the inlet, a cyclone body and a vortex finder in the top. This AFC had a diameter of 110 mm and was 500 mm long. The vortex finder in the top was quite narrow –only 54 mm in diameter, hence causing a considerable increase in gas velocity leaving the AFC. In Figure 2.17, a comparison of the experimental grade efficiency and the different model approaches at 10 m/s superficial gas velocity is shown. The efficiency is generally higher than predicted by the models. The relatively narrow vortex finder will lead to an inward drift of the gas which will reduce the outward migration velocity of the droplets. However, the reduced diameter of the vortex finder will also increase the tangential velocity which in turn will increase the efficiency. It is possible that the latter effect is the more dominant of the two, and since it is not accounted for in the models, this might by one of the reasons for the discrepancy in Figure 2.17.

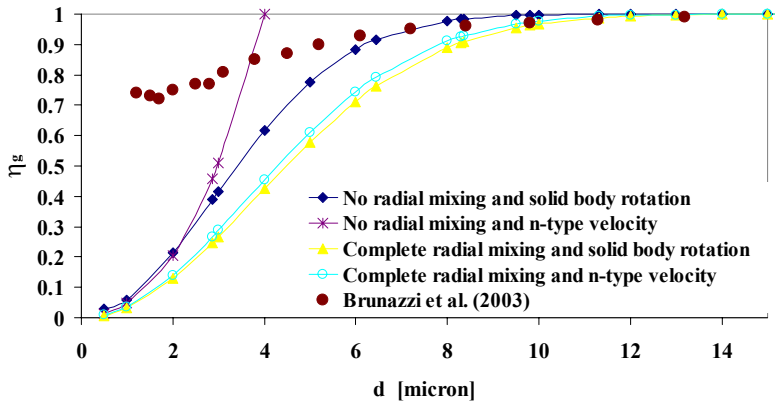

Figure 2.17 The figure shows a comparison between the experimental data of Brunazzi et al. (2003) and four different model approaches at ambient conditions and 10 m/s superficial gas velocity

Ng tested series of modifications to a standard AFC consisting of a 52 mm diameter and 384 mm long pipe section. During the development the swirl vanes that were mounted on a central body was replaced by tangential inlet vanes. The final geometry was then subjected to a grade efficiency study with air and water under ambient conditions. Since the gas enters the cyclone tangential, the exit angle of swirl vanes is 90^0 to the axial axis. However, the swirl within the cyclone must obviously follow a path with a smaller angle in order to flow upwards. In order to calculate the tangential gas velocity by use of Equation (2.68) or (2.69), a swirl angle must be specified. Since this information is not available, the experimental

grade efficiency is compared with the different model approaches when a swirl angle of 45^0 and 60^0 was assumed in Figure 2.18 and Figure 2.19, respectively.

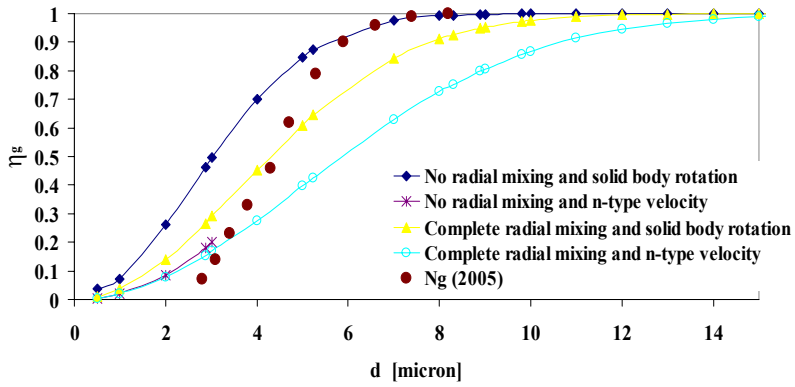

Figure 2.18 The figure shows a comparison between the experimental data of Ng (2005) and four different model approaches at ambient conditions and 11 m/s superficial gas velocity. The swirl angle was assumed to be 45^0 in this case.

The models seem to predict the efficiency well when a swirl angle of 45^0 is assumed, while it generally overestimates the grade efficiency when a swirl angle of 60^0 is used instead since this result in a larger calculated tangential gas velocity.

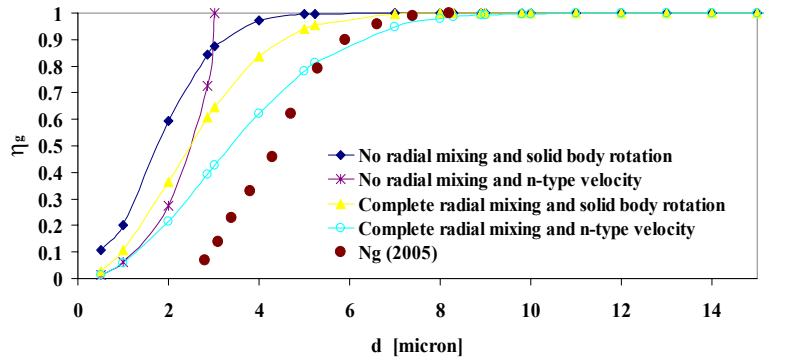

Figure 2.19 The figure shows a comparison between the experimental data of Ng (2005) and four different model approaches at ambient conditions and 11 m/s superficial gas velocity. The swirl angle was assumed to be 60^0 in this case.

In general, the grade efficiency models predict cut sizes of the different cyclones that deviate by ± 2 microns from the experimental results except for the AFC with the narrow vortex finder investigated by Brunazzi et al. The shape of the grade efficiency curve, however, varies with the different geometries and none of the model approaches seems to reflect the variations found experimentally. In general the models seem to be more influenced by the assumptions made for the tangential gas velocities than whether complete or no radial mixing is chosen as model assumption. This is clearly shown in Figure 2.18 and Figure 2.19, where the calculated grade efficiency heavily depends on the assumptions made about the swirl angle. More information is needed about the swirl flow pattern in order to check the performance of AFC's with tangential inlet vanes.

Maynard (2000) studied an AFC with helicoidally swirl vanes and derived one grade efficiency model for the swirl vanes and one model for the cyclone body. He then included both models in an overall grade efficiency model that combined the efficiency of the two sub models. This approach might also be used for AFC with swirl vanes at the inlet that have a central body of a certain radius i.e. one grade efficiency model for the swirl vanes and one model for the cyclone body. Brunazzi et al. also combined grade efficiency models for the inlet section, the cyclone body and the vortex finder in their study and the results were in agreement with the experiments. However, since the deduction of the 'complete radial mixing'-model was inconsistent the agreement might have been a coincidence.

The effect of liquid loading

In general the grade efficiency improves with increasing solids loading. This positive effect of solids loading on the grade efficiency has long been known for tangential inlet reverse flow cyclones, but the effect on cyclones with swirl vanes is less known. In principle, the nature of solids and liquids are the same when the phase is dispersed as particles and droplets. The effect of increased liquid loading on grade efficiency should is therefore expected to be the same as for increased solid loading.

The reasons for improved efficiency are not determined with certainty, but different explanations exist. Hoffmann and Stein give an overview over explanations and models given in literature. Some explanations are

- The turbulence in the gas can support only a certain critical load against the force of gravity, and the rest will fall out essentially unclassified.
- Particle agglomeration or droplet coalescence. The larger droplets/particles in a high concentration will "sweep up" smaller particles/droplets when they are transported to the cyclone wall.
- Particles shield one another from the drag force of the swirling gas that they would have experienced as single particles. This is equivalent to the

principles used by e.g. birds or bicycles that travels in formation in order to reduce the drag.

2.7 Comparison of Different Scaling Rules

In design of scrubbers, the efficiency of internals is often established through tests in low-pressure systems with model fluids that deviate from a live fluid in terms of the physical properties i.e. densities, viscosities and interfacial tension. A problem rises when test results carried out under low-pressure conditions are used as a basis for designing high-pressure scrubbers. In most cases vendors of scrubber internals try to take into account the effect of one or more of the changing physical properties. For instance, it is very common to decrease the superficial gas velocities with increasing pressure. One common way of doing the scaling is to keep the gas dynamic pressure constant i.e.

$$\rho_g u_{g,s}^2 = const. \tag{2.71}$$

Perry et al. (1997) and Brunazzi et al. (2003) have applied this criterion to balance the gas velocity with increasing gas densities in cyclones. Also, it is recommended in NORSOK (2001) that the gas dynamic pressure should be kept below 6000 Pa for scrubbers that have an inlet vane. The physical meaning of it appears when the gas shear force is investigated. The shear force τ_i from a gas stream on a liquid film can be expressed in terms of the gas density and the relative velocity between the two phases:

$$\tau_{i,tg} = f_{gi} \frac{\rho_g u_{r,tg}^2}{2} \tag{2.72}$$

Provided that the cyclone is operated within conditions where the friction coefficient is approximately constant and the gas velocity is much larger than the liquid film velocity the physical meaning of Equation (2.72) becomes:

$$\rho_g u_g^2 = const. \Rightarrow \tau_i = f_{i,g} \frac{\rho_g u_r^2}{2} \approx f_{i,g} \frac{\rho_g u_g^2}{2} = const. \tag{2.73}$$

Hence, scaling by use of constant gas dynamic pressure assures that the shear force from the gas on a liquid film remains constant. However, the properties of the liquid film are completely ignored when this scaling rule is used.

Another approach often used is to scale the superficial gas velocity by use of the *K*-value as shown in Equation (2.11). *K*-value has got no direct physical relevance in terms of separation efficiency for a cyclone. However, since the size of a scrubber is most often designed on basis of the *K*-value, keeping the *K*-value in the cyclone constant simply means that the ratio of the total cyclone area to vessel cross sectional area is kept constant.

Some vendors of cyclonic equipment focus on keeping the gas velocity constant regardless of operating pressure. If the velocity is kept constant, the centrifugal force of a defined particle will be approximately the same at different pressures. However, if the goal is to keep the cut size d_{50} (or d_{95}) of the cyclone constant, also the gas density, liquid density and the gas viscosity should be taken into account. In order to scale droplet separation in cyclones the Stokes number should be held constant i.e.

$$Stk \equiv \frac{\left(\rho_l - \rho_g\right) d^2 u_g}{18 \mu_g D} = constant \tag{2.74}$$

In the case of axial flow cyclones D refers to the diameter of the cyclone.

The different scaling rules focus on different mechanisms. If the aim is to avoid high shear forces, the gas velocity should be reduced as the operating pressure increases. If the aim is to keep the cut size unchanged with increasing pressures, the gas velocity must increase.

For instance, a cyclone has been tested in a laboratory at ambient conditions and was found to perform at its optimum when the superficial gas velocity was 10 m/s. How should the gas velocity be scaled with increasing pressure? Or said with others words: How many cyclones are required to operate in parallel in order to handle a certain gas volume at a certain pressure? In Figure 2.20 the superficial gas velocity is plotted as function of the gas density for all the mentioned scaling rules. As can be seen, the different scaling rules result in very different superficial velocities. Scaling by keeping the gas dynamic pressure constant compared to keeping the K-value constant results in approximately the same velocity. While if it is desirable to keep the cut size the same as under laboratory conditions when the gas density reaches 100 kg/m^3 (approximately 100 bara operating pressure), the superficial gas velocity should be 3 times higher than in the lab. Choosing Stokesian scaling over one of the other scaling rules may result in 60 times as high required gas velocity compared to if constant gas dynamic pressure or K-value are used as scaling rule instead. In other words, choosing constant dynamic pressure as scaling rule rather than Stokes number means that 60 times as many cyclones are required to handle a gas stream at 100 bara (~100 kg/m^3 gas density).

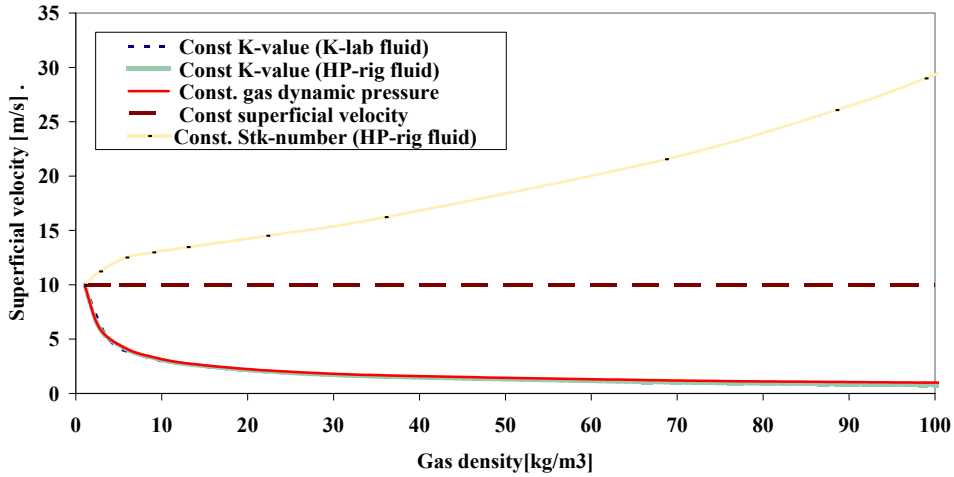

Figure 2.20 The figure shows how the superficial gas velocity changes with changing gas density when the different scaling methods are used. The bases for all the curves are a superficial gas velocity of 10 m/s at 1 kg/m^3 gas density.

Figure 2.20 illustrates the dilemma one is faced upon when low-pressure lab results for demisting equipment are used as a basis for use in a high-pressure environment where the fluid properties are different from those in the lab. The fluid properties used for the calculations in Figure 2.20 are discussed in details later in Section 3.2.4.

Clearly, the design at high pressure must either be a trade off between the different scaling rules, or it must ignore some basic differences between high-pressure and low pressure conditions.

CHAPTER 3

Experimental Setup and Analysis

Three different test rigs have been used in this project. The rigs are different with respect to size, operating pressures and fluids. Two of the rigs are placed at the laboratory at Statoil R&D, while the latter and largest are placed at the Kårstø gas processing plant –one of the largest processing facilities for natural gas in Europe. At Statoil R&D, one rig for low-pressure and one rig for high-pressure service has been built, while the rig at K-lab at Kårstø, is a unique large scale facility that use gas and condensate from the process plant.

3.1 Low-Pressure Rig

The "Low-pressure rig" (LP-rig) is used for measurements of the removal efficiency of different scrubber-internals like inlet arrangements, mist mats, vane-packs and demisting cyclones. The scrubber section is equipped with several windows and droplet phenomena, flow-directions and other flow-phenomena can therefore be studied. As liquids, both water and Exxsol D60^{TM} have been used. Exxsol D60^{TM} is a de-aromatized aliphatic hydrocarbon, where the major components are normal paraffin's, iso-paraffin's and cyclo-paraffin's. The liquid contain very low levels of hazardous air pollutants (HAP's), and has in addition a relatively low vapour-pressure, which makes it more suitable for indoor use from a Health-Safety-and-Environment (HSE) point of view. More information about the fluids used in the Low-pressure rig can be found in Table 3.1.

Table 3.1 Fluid properties in the LP-rig at 20 °C and 1 bara

	Density [kg/m^3]	Viscosity [cP]	Air/liquid interfacial tension [mN/m]
Air	1.19	0.0184	
Exxsol D60^{TM}	785	1.40	24.3
Water	1000	0.89	72.8

In Figure 3.1, a sketch of the most important features of the rig is given. The gas enters the rig through an 80 mm pipe and is distributed over the cross-section of a 389 mm I.D. scrubber cross-section by inlet vanes. The air is supplied from two compressors that deliver in sum a constant mass-rate of 0.88 kg/s at approximately 7 bara. The pressure in the scrubber, and, hence, the volumetric gas-flow, is controlled by a manually operated throttle valve in the piping upstream the scrubber inlet. This means that the volumetric gas flow and gas density cannot be controlled independently. The rig can operate at pressures down to approximately 2 bara. Since the mass rate of gas is constant, the volume rate in the test scrubber increases as the pressure is reduced and the gas is becoming less dense.

The liquid is fed through a nozzle in either the upstream piping or in the vessel itself (optional). Liquid that is separated in the inlet arrangement or other internals without internal drain pipes is collected in the bottom of the vessel and is fed back to the liquid reservoir. The liquid collected in the demisting equipment equipped with an internal drain system, is collected in a scale below the vessel while the liquid carry-over from the scrubber is separated in a large-capacity filter-coalescer and then collected in a separate scale. These two scales offer the opportunity of calculating the liquid mass-balance, and they have drains connected to the liquid reservoir to empty the scale-vessels when filled. All the monitored parameters from the rig, like flow rates, pressures, differential pressures, temperatures and accumulated liquid in the scales, are logged on a PC that monitors and controls parts of the rig. The system logs all parameters with an interval of two seconds, and when logging is finished, the average of all parameters are automatically written to a file and stored on the hard drive.

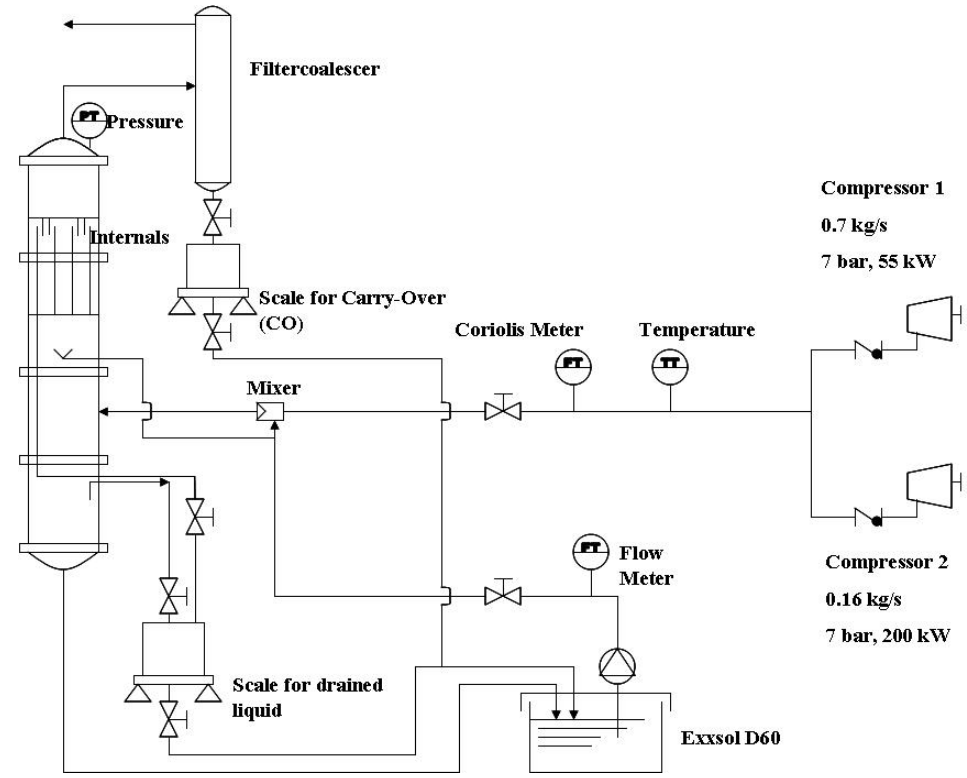

Figure 3.1 A sketch of the low-pressure gas separation rig used in the experiments

3.1.1 Uncertainty in Cyclone Efficiency Measurements

The separation efficiency for the cyclone is measured on basis on the captured liquid and the carry over. The formula that has been used is:

$$\eta_{cycl} = \frac{\dot{Q}_{l,drain}}{\dot{Q}_{l,drain} + \dot{Q}_{l,CO}} = \frac{\dot{M}_{l,drain}}{\dot{M}_{l,drain} + \dot{M}_{l,CO}} = \frac{M_{l,drain}}{M_{l,drain} + M_{l,CO}} \qquad (3.1)$$

$M_{l,drain}$ and $M_{l,CO}$ are the liquid that have been accumulated in the drain and liquid carry-over vessel respectively, during one test run. Provided that all the liquid carry-over are collected in the filter coalescer, the uncertainty in the efficiency calculations is dependent on the uncertainties in the weight scales $\delta M_{l,drain}$ and $\delta M_{l,CO}$. Gauss' formula for error propagation can be used:

$$\delta f(x_1, x_{2,}, ...x_n) = \sqrt{\left(\frac{\partial f}{\partial x_1}\delta x_1\right)^2 + \left(\frac{\partial f}{\partial x_2}\delta x_2\right)^2 + ... + \left(\frac{\partial f}{\partial x_n}\delta x_n\right)^2} \quad (3.2)$$

When Equation (3.2) is used to calculate the uncertainty in the expression in Equation (3.1) the uncertainty becomes:

$$\delta\eta = \sqrt{\left(\frac{\partial \eta}{\partial M_{l,drain}}\delta M_{l,drain}\right)^2 + \left(\frac{\partial \eta}{\partial M_{l,CO}}\delta M_{l,CO}\right)^2} \quad (3.3)$$

The uncertainties in both weight scales are the same and are related to the resolution on the panel of the scale (10 grams) i.e.:

$$\delta M_l = \delta M_{l,drain} = \delta M_{l,CO} \quad (3.4)$$

Solving the right side of Equation (3.3) then results in

$$\delta\eta = \sqrt{2} \cdot \delta M \frac{M_{l,CO}}{(M_{l,drain} + M_{l,CO})^2} \quad (3.5)$$

The uncertainty decreases with increasing amount of liquid that is being collected during a test run. Therefore a combination of high liquid loading and long test run is favourable to minimize uncertainty.

3.1.2 Uncertainty in Efficiency Measurements of Other Internals

The efficiency for internals without a shielded drain compartment like the combined efficiency for an inlet vane + mesh pad is calculated on basis of the injected liquid and the collected liquid on the two weight scales:

$$\eta = 1 - \frac{\dot{Q}_{l,drain} + \dot{Q}_{l,CO}}{\dot{Q}_{l,pump}} = 1 - \frac{M_{l,drain}/t_s + M_{l,CO}/t_s}{(\dot{Q}_{l,pump}) * \rho_l} \quad (3.6)$$

The uncertainty in the sample time is small and can be neglected. By combining Equation(3.6), (3.4) and (3.2) the equation for the uncertainty becomes:

$$\delta\eta = \sqrt{\left(\frac{\partial \eta}{\partial M_{drain}}\delta M\right)^2 + \left(\frac{\partial \eta}{\partial M_{CO}}\delta M\right)^2 + \left(\frac{\partial \eta}{\partial Q_l}\delta Q_l\right)^2 + \left(\frac{\partial \eta}{\partial \rho_l}\delta \rho_l\right)^2} \quad (3.7)$$

Solving the right side of the equation results in:

$$\delta\eta = \sqrt{2}\frac{1/t_s}{\dot{Q}_l \rho_l}\delta M + \frac{M_{drain}/t_s + M_{CO}/t_s}{\dot{Q}_l^{\,2} \rho_l}\delta \dot{Q}_l + \frac{M_{drain}/t_s + M_{CO}/t_s}{\dot{Q}_l \rho_l^2}\delta\rho_l \quad (3.8)$$

The uncertainty in the ultrasonic flow meter that measures the injected liquid rate is maximum 0.5% if the set up is otherwise correct. Exxsol D60 has not got a constant liquid composition and the density can therefore vary ± 1 kg/m^3 (temperature variation also taken into consideration).

3.2 High-Pressure Rig

The high-pressure rig is specially designed for scrubber testing with live natural gas fluids, but can be used for all kinds of fluids in theory. The rig is therefore built in such a way that it can cope with all safety issues that occur when high pressure and flammable gas is involved. The rig can test various types of separation equipment over a wide range of gas and liquid loads at pressures up to 100 bara and temperatures ranging from –20 to +50 ^{o}C. It can measure the separation efficiency of both total scrubber solutions and the individual internals. For all tests, a set of differential pressure measurements can also be carried out. In addition, a laser diffraction technique has been adapted and tested in order to obtain information about the droplet size distribution of the gas/liquid mixture at various stages of separation.

The rig is built inside two containers placed on top of each other as seen in Figure 3.2. These process containers are classified as hazardous zone 1, which means that explosive atmosphere is to be expected occasionally. All electronic equipment is therefore classified in accordance with the Ex-standard for hazardous operation. Both the atmosphere in the process containers and the process itself are temperature controlled and the containers can therefore be regarded as a climate chamber. The climate utility system is placed in a utility container next to the process container. This container, which is not classified as hazardous area, also contains other utility systems like pressurized instrument air and all kinds of electric equipment that is not classified in accordance with the Ex-standard. High-pressure gas and liquid samples can be taken from the container seen to the left of the process containers in the figure. This container is also used for storage of the fluids and for filling gas and liquids onto the process loop. The rig is being operated from PC's that are placed in a remote control room.

Figure 3.2 The picture shows the HP-rig. The two process containers on top of each other contain the actual rig. To the right is a technical container that carries several utility systems like the climate, power and air supply system. To the left is the gas-filling container where the fluids can be sampled, stored or filled into the process loop.

3.2.2 Process Description

The rig is built as a closed loop where the liquid is initially charged and gas is used to pressurize the rig. Liquid can also be charged under pressure by use of a piston pump. The rig is designed to operate at pressures up to 100 bara. A gas blower with an adjustable speed motor circulates the gas in the loop. The gas blower is submerged in a temperature controlled glycol bath which provides control of the gas temperature in the loop. Liquid can be injected in the gas stream through either two injection points in the inlet piping or through a nozzle within the test scrubber. A sketch of the main process can be seen in Figure 3.3. The liquid that is captured in the test scrubber can be drained to two separate drain tanks, while the entrained liquid is being captured by a bulk scrubber (vessel quipped with a mesh pad) with a diameter twice as large as the test scrubber. If the gas load is high or the droplets are very small, some liquid might escape the demister as well. In this case the remaining liquid will be separated by a tangential cyclone scrubber and a large filter coalescer further downstream. In the present experiments all the captured liquid has been measured by liquid accumulation tests in the drain tanks, bulk scrubber, tangential cyclone scrubber and filter coalescer. The liquid accumulation has been measured by use of differential pressure cells that detect the increase in

liquid level (see Equation (3.9)). The gas flow and injected liquid rate is continuously being measured by Coriolis meters.

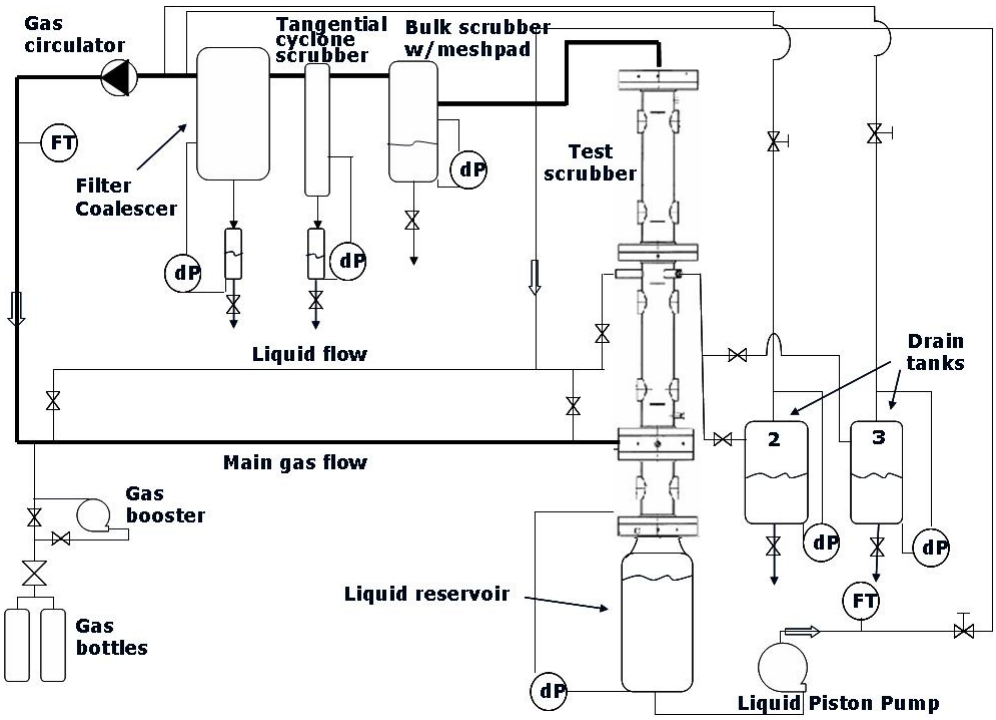

Figure 3.3 A simplified principal sketch of the HP-rig . The main gas flow is marked by the thick line.

Details of the test scrubber can be seen in Figure 3.4. The test scrubber is equipped with five window sections at different heights that provide visual insight into the process stream. The height of the test scrubber is two meters from the inlet to the top. This design offers the possibility to test total scrubber solutions within a large range of internal distances between the internals.

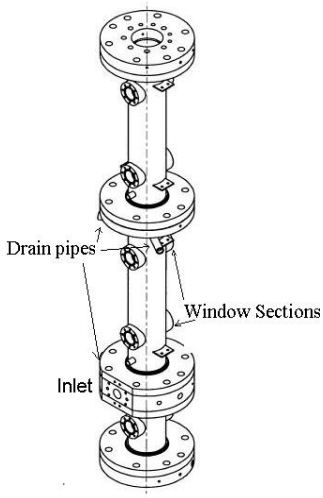

Figure 3.4 Details of the HP-rig test scrubber with 5 window sections

Other technical data of the rig are listed in Table 3.2 and Table 3.3

Table 3.2 Technical data for the HP-rig

	Diameter [mm]	**Cross sectional Area [m^2]**
Scrubber inlet pipe	49.24	0.001904
Test scrubber	150	0.01767
Bulk scrubber with mesh pad	298.6	0.07003
Tangential cyclone scrubber	202.7	0.03227
Filter coalescer	460	0.1662
Drain tank 2	298.6	0.0700
Drain tank 3	295.4	0.0685

Table 3.3 Gas and liquid operating range for the HP-rig

	Pressure [bara]	**Flow [m^3/hr]**
Gas	1 – 100	0 - 60 (at 100 bara)
Liquid	1 – 150	0.05 – 1.0

3.2.3 Equipment for Droplet Size Measurements

In order to gain information about the droplet size distribution in the test scrubber, a laser diffraction system has been adapted to the scrubber. The laser scattering instrument is an Insitec X supplied by Malvern Instruments Ltd.

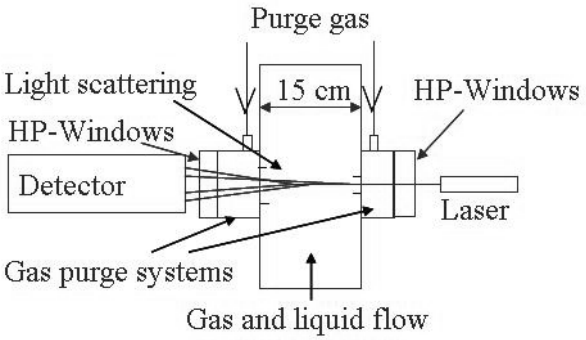

Figure 3.5 The sketch shows how the laser scattering technique has been adapted to the HP rig.

The principles of the laser scattering technique in the HP-rig have been sketched in Figure 3.5. A 10 mm thick laser beam passes through a thick window that withstands the high pressure of the process stream. The light is then being scattered by the droplets in the gas stream and the scattered light proceeds through another HP-window on the opposite side of the test scrubber. The light scattering pattern is measured by a specially designed light detector and by use of Mie scattering theory, the correspondent Droplet Size Distribution (DSD) can be calculated. The measurement of droplets in high-pressure gas is very challenging and to avoid disturbance of the light, the windows must be totally clean and free from any liquid. To achieve this, a special gas purge system has been developed. Dry gas from the process stream is boosted to a higher pressure and injected to two gas purge chambers shown in Figure 3.6 and Figure 3.7.

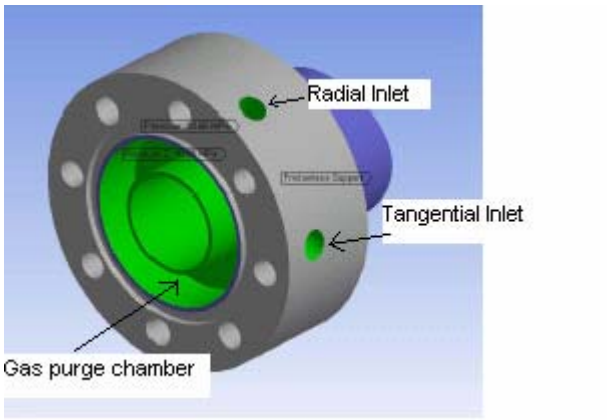

Figure 3.6 The gas purge system for the end where the scattered light leaves the process.

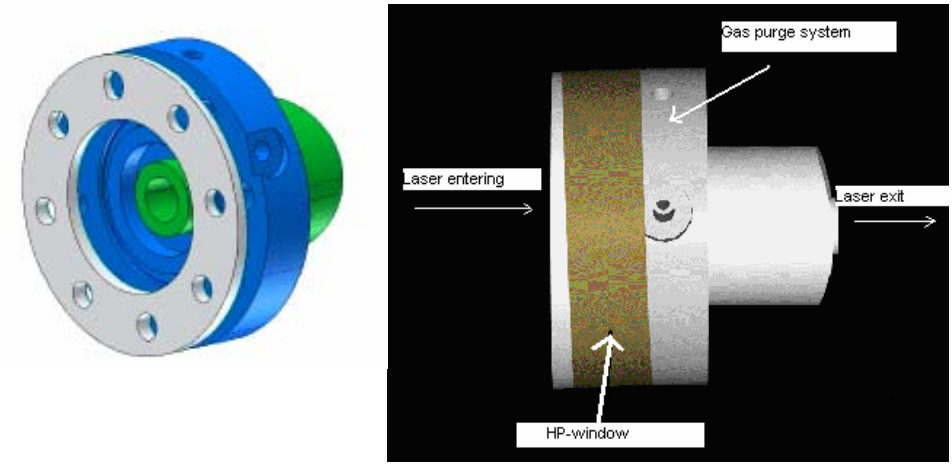

Figure 3.7 The gas purge system on the side where the laser light enters the process.

The HP-window is mounted on the gas purge system. Between the window and the inner cylinder of the purge chamber there is a 1mm gap where gas can flow. The purge gas has both a radial and a tangential oriented inlet. If all the purge gas is introduced through the radial inlet, liquid droplets from the process stream tend to be sucked along the cylinder wall and onto the window. If, on the other hand, the entire gas purge is being introduced through the tangential inlet, a low pressure zone in the centre of the flush cylinder will suck in liquid from the process stream and drop it off on the window. The solution is to combine the radial and tangential gas purge so that both the suction along the wall and in the centre of the cylinder is avoided.

When the instrument is mounted, the detector must be aligned such that all the light passes through a 200 micron diameter hole in the centre of the detector. The alignment takes place when no liquid is present in the gas stream such that the light

can pass un-scattered. When the light is scattered by droplets, the scattered light is caught by a Fourier lens and spread onto various parts of the detector. The detector is made up by 32 rings placed in various distances from the centre. The smallest droplets will spread the light at the largest angles and, hence, be detected by the outer rings of the detector, while the largest droplets will be detected on the inner rings. Three different lenses have been used in order to focus the light onto the detector. The different lenses have a different range of detectable droplet size ranges as seen in Table 3.4. The larger the lens is, the wider the detectable droplet size range is, but larger lenses are also more sensitive to disturbances. The surfaces of the HP-windows are not perfectly parallel and therefore they have a small lens effect on the laser beam that might defocus the light so much that proper alignment of the detector is impossible. The problem with defocusing of the light appears on the inner rings closest to the centre hole. In addition, small bruises on the surface of the window might scatter some of the light such that will hit some of the detector rings. Reflection from one window to the other one and back again might also cause light on some of the detector rings, and therefore the window on one side have been angled by 2^0 (indicated on the right picture in Figure 3.7). Due to the described problems, only the 200 mm lens has been used with satisfactory results. This has led to a narrow range of conditions where the droplet size measurements are available since the largest droplets in the gas stream are larger than 400 mm in most cases.

Table 3.4 the nominal droplet size range of the three different lenses that were available.

Lens focal length [mm]	Min. and max. [microns]	Median size/$D_v(50)$ [microns]
200	1-400	5-250
300	1.5 - 600	8-375
400	2.25 -850	12-500

If there are temperature gradients in the process stream, this might result in inhomogeneous refraction index of the gas. The variation may be so large that it causes defocusing of the laser beam. At low pressures (< 10 bara) this is not a problem but as the pressure increases it becomes increasingly difficult to focus the laser light. In practice the gas temperature has to be controlled so that gradients in the loop are kept below 0.3 ^{0}C. For this reason, also the temperature of the purge gas must have the same temperature as the process gas. When the purge gas is taken from the main gas flow, it is a saturated vapour at its equilibrium temperature and pressure. When the gas is boosted to a greater pressure the temperature is increased as well, so the purge gas has to be cooled before it enters the purge system. Small process variations might lead to condensation of some of the vapour, so in practice the dew point of the gas must be lowered through a gas conditioning process that involves a heat-exchanger and a dew-point control separator.

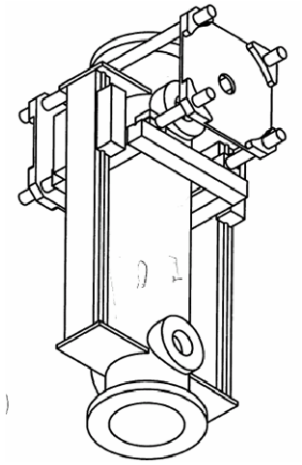

Figure 3.8 A specially designed bench has been made in order to provide maximum control of the alignment of the Insitec X instrument.

3.2.4 Fluids and Fluid Properties in the HP-rig

Two different fluid systems have been used in the tests. The simplest system consisted of Exxsol D60 as liquid and nitrogen as gas. The rig was filled with Exxsol D60 to the required level and then nitrogen was used to pressurize the rig to the required pressure. Independently of pressure (within the range 1-100bara), the Exxsol D60 mainly remains in the liquid phase while the nitrogen mainly remains in the gas phase (only a small amount of liquid is dissolved in the gas phase and vice versa).

The more complex natural gas fluid system consisted of a mixture of methane, ethane and pentane. The rig was initially filled with pentane to a minimum level and then a mixture of premixed methane and ethane gas was used to pressurize the rig to the required pressure. The gas and liquid phase were then circulated until equilibrium was established. The composition of each phase could be calculated on basis of the initial amount of liquid pentane, actual temperature and pressure at equilibrium (the total volume of the rig was known).

Fluid Properties for the Nitrogen-Exxsol D60 Test Fluid

Exxsol D60 is not an exact composition since it is a paraffin distillation cut, but the composition does not vary a lot and the supplier therefore gives typical values of its fluid properties. In Table 3.5 a typical composition of Exxsol D60 is given. The different fractions are groups of components with the specified number of carbon atoms that have been lumped to one fraction with a characteristic molecular weight. This characterized composition has been used as a basis for calculations of the fluid properties of the Exxsol/nitrogen mixture that was used in the HP-rig.

Table 3.5 The fluid composition for the nitrogen/Exxsol D60 fluid. This composition has been used as a basis for the calculation of the key fluid properties.

	Exxsol D60/nitrogen		
Component	Fraction [mol %]	Mol wt [g/mol]	Liq. Dens. [kg/m^3]
N2	33.034	28.014	
C9	0.832	121	781
C10	13.517	134	792
C11	28.066	147	796
C12	19.376	161	810
C13	5.175	175	825

The gas density calculations have been calculated using the Soave-Redlich-Kwong equation of state (EOS) (Soave, 1972). Peneloux et al. (1982) suggested a volume correction for this EOS, and this has been used in the present calculations.

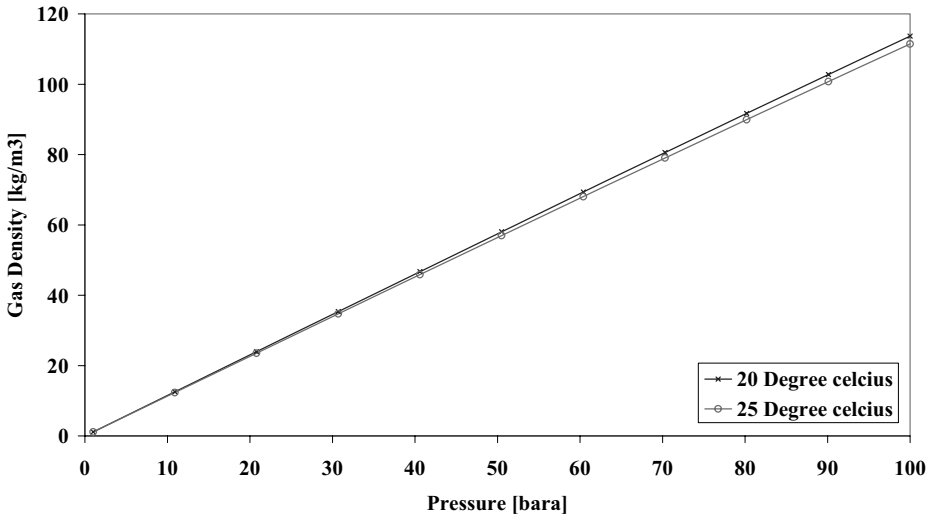

Figure 3.9 The calculated density of the gas phase that consists of nitrogen with a small amount of solved components from the Exxsol.

For the liquid density, a set of measurements have been carried out using a high-pressure density cell supplied by Anton Paar. In the measurements, Exxsol D60 saturated with nitrogen at the actual temperature and pressure has been used. The density variations within the pressure operating range of the HP-rig is less than 1% as can be seen from Figure 3.10. The initially density drops off when pressure is increased since more gas is dissolved in the liquid, but when the pressure exceeds approximately 10 bara, the density is more dominated by the pressure and hence, it increases with increasing pressure.

The uncertainty in the density instrument is given as 0.1 kg/m^3, but the uncertainty is more dependent on the actual composition that can vary from one barrel to another when it comes to Exxsol. The measurements should therefore not be considered to be more accurate than 1 kg/m^3 if they are used as an input in equations of a general Exxsol fluid.

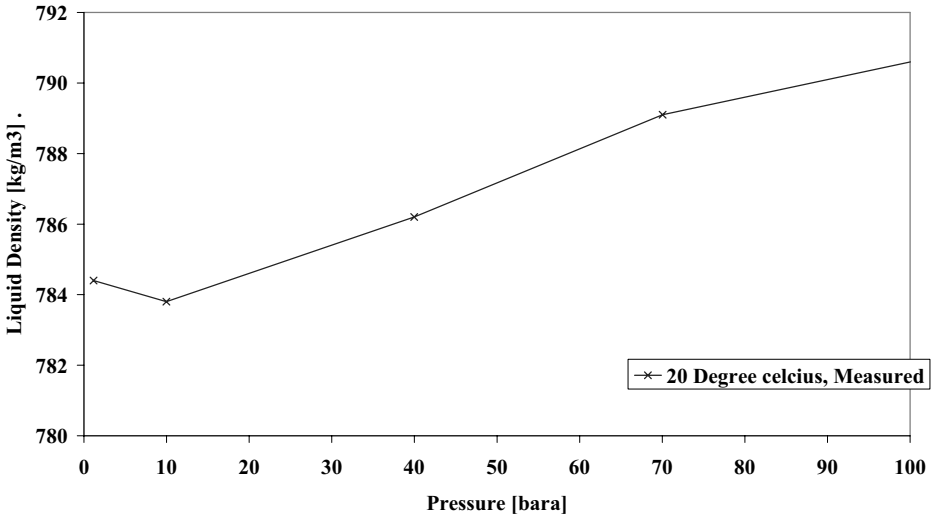

Figure 3.10 The measured liquid density of the Exxsol D60 when it was saturated with small amounts of nitrogen.

The gas and liquid viscosity calculations are based on the corresponding states principle in the form suggested by Pedersen et al. (1987).

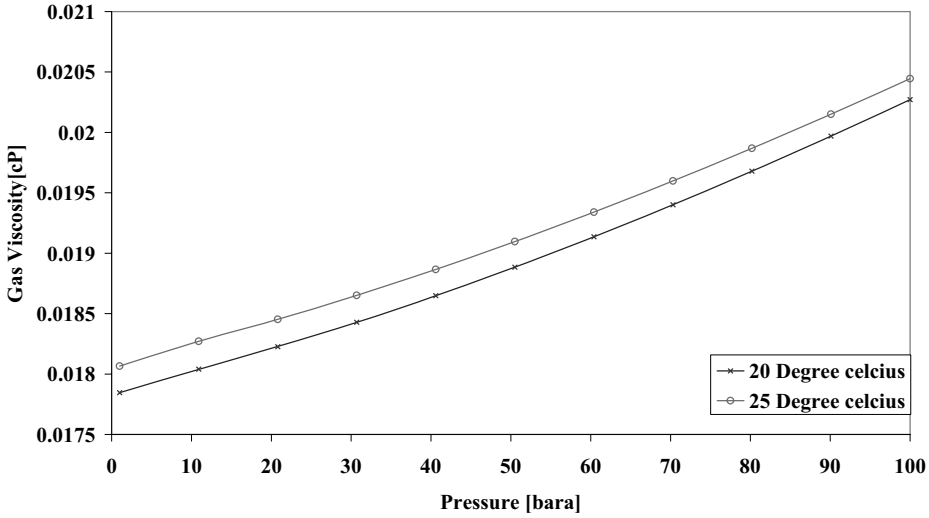

Figure 3.11 The calculated gas viscosity of nitrogen containing small amounts of Exxsol D60 components.

The supplier gives a typical value of 1.58 cP for the liquid viscosity of pure Exxsol D60 at 25 ^{o}C and atmospheric pressure. That value is approximately 20 % higher than the calculated value in Figure 3.12. The uncertainty is due to both uncertainties in the prediction model, the characterization of the heavy C9- C13 components, the molar composition of the actual sample and the fact that nitrogen is dissolved in the Exxsol used in the calculations.

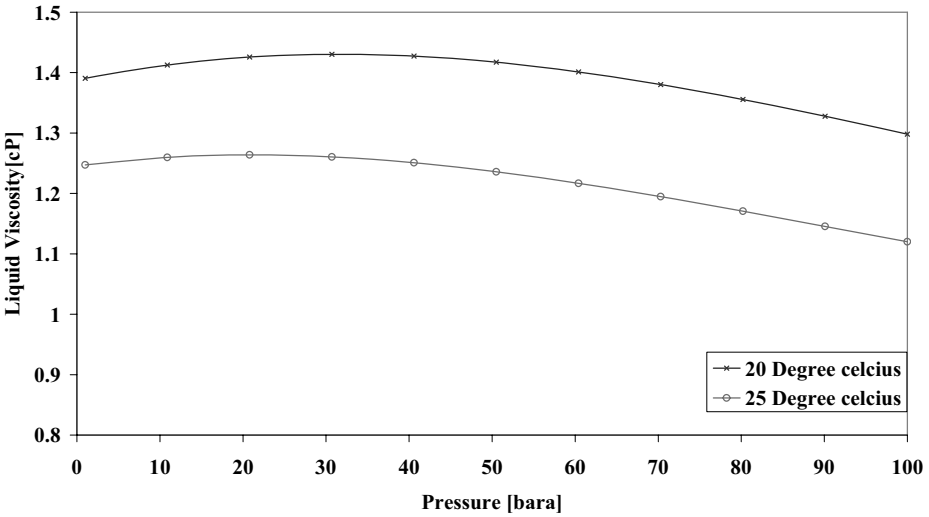

Figure 3.12 The calculated viscosity of Exxsol D60 when it is saturated with small amounts of nitrogen

The calculated interfacial tension is shown in Figure 3.13. The calculations are based on the simple procedure that Weinaug and Katz (1943) used for a Methane-Propane mixture. The accuracy of these calculations depends on the accuracy of the density calculations. Since the uncertainty can be quite large in the latter, the interfacial tension should ideally be measured. High-pressure interfacial tension measurements are very challenging and therefore only a few measurements are done, for pressures ranging from 2 to 6 bara. These measurements show an interfacial tension between 24 and 25 mN/m at 20 ^{o}C, so the calculations seem to under-predict the interfacial tension by up to 10 % in the low-pressure range covered by the measurement range.

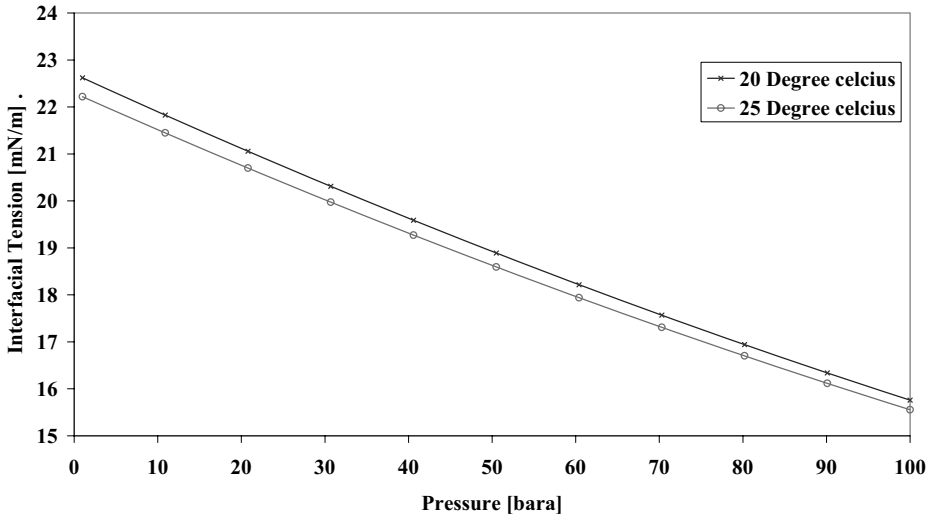

Figure 3.13 The calculated interfacial tension of Exxsol D60 and nitrogen

Fluid Properties for the Synthetic Natural Gas

For the tests with synthetic natural gas, a three component mixture of methane, ethane and pentane was used. The rig was filled with an initial amount of liquid pentane at 20 ^{o}C, then a premixed gas consisting of 85 mol % methane and 15 mol % ethane on batteries of nine 50 litres bottles was used to pressurize the rig. The rig was operated at three different pressures, 20, 50 and 92 bara, when the synthetic natural gas was used. All tests were performed at temperatures within the range 20-23 ^{o}C. The total fluid compositions were calculated with the SRK EOS (Soave, 1972) with Peneloux volume correction (Peneloux et al. 1982) for each operating pressure. Since all the pentane is filled initially and only methane and ethane is added, the fluid composition is changing with pressure as seen in Table 3.6. The fluid is becoming lighter as the pressure is increased. In Figure 3.14 the phase envelopes for the fluid composition corresponding to the three different test pressures are shown

Table 3.6 The calculated fluid compositions for the three different operating pressures at 21 °C

Fluid Composition		20.1 bara	50.2 bara	92 bara
Methane	[mol%]	45.6	64.6	73.6
Ethane	[mol%]	8.0	11.4	13.0
N-Pentane	[mol%]	46.4	24.0	13.4

.

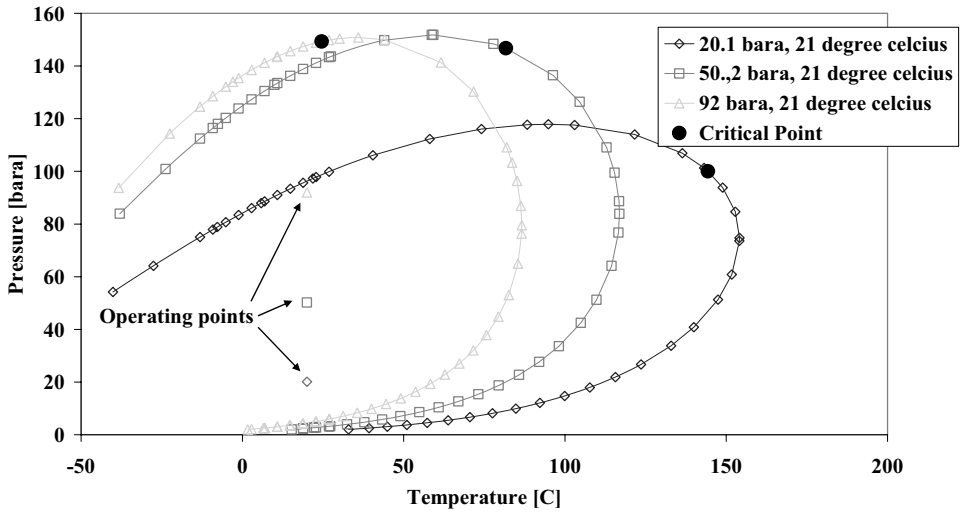

Figure 3.14 The figure shows the calculated phase envelopes for the three fluid compositions given in Table 3.6. The operating points where within the two-phase region of the fluid as indicated in the figure

The calculated composition was used as a basis for fluid properties calculations. In order to verify the fluid composition calculations, a gas sample from the rig was taken at 92 bara and analyzed in a gas chromatograph. The analysis was then compared to the calculated gas composition at the actual pressure and temperature for the sample. The analysis was in good accordance with the calculations as seen in Table 3.7

Table 3.7 A comparison of the calculated and the measured gas composition

	91.7 bara / 20.7C		
Gas Composition	Calculated [mol%]	Analyzed GC [mol%]	Deviation [%]
Methane	85.09	85.61	0.6
Ethane	11.70	11.34	-3.2
N-Pentane	3.21	3.05	-5.4

78 litres of pentane were used when the rig was charged and approximately 900 litres of premixed methane/ethane at 100 bara. Given the larger amounts needed, 100 % pure fluids could not be used. For instance, the pentane was delivered with >99 % purity. This means that traces of other components like for instance propane, iso-pentane, carbon-dioxide and nitrogen could also be found in the fluid. Nitrogen and propane were the trace components with the largest concentrations, 0.87 and 0.23 mol%, respectively. The trace components have been ignored and the analyzed composition in Table 3.7 is normalized with respect to methane, ethane and pentane.

The fluid properties of the synthetic natural gas have been calculated with the same methods as described for the nitrogen/Exxsol D60 fluid. The physical properties are listed in Table 3.8.

Table 3.8 The calculated fluid properties at gas-liquid equilibrium at 20 ^{0}C for the three different fluid compositions given in Table 3.6

Calculated Fluid Properties		20.1 bara	50.2 bara	92 bara
Gas Density	[kg/m^3]	17.2	45.2	97.0
Liquid Density	[kg/m^3]	602.2	551.3	469.5
Gas viscosity	[cP]	0.011	0.012	0.015
Liquid Viscosity	[cP]	0.207	0.150	0.096
Interfacial Tension	[mN/m]	11.4	6.8	2.2

The properties of the simple three component natural gas system can be calculated with greater accuracy than the nitrogen/Exxsol fluid since the actual composition is known and consists of well defined components that are easier to model.

The quality of the gas and liquid density calculations has been checked by adding the same pentane to methane/ethane ratio in sample cylinders. The liquid and gas density of these samples where then measured with the Anton Paar high-pressure density cell. The gas and liquid compositions and densities were then calculated the same way as they were calculated for the HP-rig. The calculated and measured densities were then compared. In addition, the actual gas composition was analyzed in a Gas Chromatograph (GC). The analyzed composition was then used as an input in a second density calculation. While the first calculation approach includes uncertainty in both models and composition, the second approach eliminates most of the uncertainty in the composition. In that way it was possible to evaluate whether the uncertainty in the calculated composition gave a dominant contribution to the uncertainty in gas density calculations or if the accuracy of the calculations were mostly restricted by the accuracy of the model itself. The comparisons have been listed in Table 3.9. The calculations are within 2.4% of the measured density regardless of which composition has been used. As expected the deviation is generally larger when a calculated composition has been used instead of the measured, but the calculations generally agree well with the measurements.

Measurements of the other fluid properties i.e. viscosity and interfacial tension, are not available. However, despite the simplicity of the model of Weinang and Katz (1943), it should be suitable for this mixture. Weinang and Katz developed the model by use of methane and propane –two components that have very much the same chemical properties as the components used in this project. Also, the density calculations have been seen to be fairly good. The density calculations are used as input in the interfacial tension calculations.

Table 3.9 A comparison of the calculated vs. the measured densities for different pressures. The fluid compositions that have been used as input in the calculations are either the measured compositions (GC-comp.) or the calculated compositions. Measured compositions were only available for the gas phase since the GC cannot handle liquid.

	Press.	Temp.	Density			Deviation	
			Measured	Calc. w/GC-comp.	Calc. w/calc. comp.	Meas./GC-comp	Meas./calc.-comp
	[bara]	[°C]	[kg/m^3]	[kg/m^3]	[kg/m^3]	[%]	[%]
Gas Phase	92.5	25	96.1	95.9	96.9	0.2	-0.8
	61.7	25	56.1	56.5	57.1	-0.7	-1.8
	20	20	16.8	17.2	17.2	-2.4	-2.4
Liquid Phase	92.5	23	484.4	N/a	467.8	N/a	3.4
	61.7	23	541.7	N/a	528.8	N/a	2.4
	20	20	602.5	N/a	599.5	N/a	0.5

.

3.2.5 Efficiency Calculations and Uncertainties

The efficiency in the HP-rig is calculated on basis of the accumulated liquid in the drain tanks. In order to calculate the level increase, differential pressure cells are mounted wherever liquid is collected in the rig. The increase in differential pressure ΔP can be related to the increase in liquid level Δh by the following expression

$$\Delta P = (\rho_l - \rho_g) g \Delta h \tag{3.9}$$

The accumulated liquid can then be found if the vessel cross section is known.

$$\dot{Q}_l = A_{vessel} \Delta h_l \tag{3.10}$$

Cyclone Efficiency

The efficiency of internals that have a drain chamber can be found by using the liquid volume rates that is collected in the demister and drain tank. In the experiments of this work, the cyclones are being drained to drain tank 2. Hence, the efficiency is defined as:

$$\eta_{cycl} = \frac{A_{De} \cdot \Delta h_{l,De}}{A_{De} \cdot \Delta h_{l,De} + A_{l,drain} \cdot \Delta h_{l,drain}} = \frac{A_{De} \cdot \Delta P_{l,De}}{A_{De} \cdot \Delta P_{l,De} + A_{l,drain} \cdot \Delta P_{l,drain}} \tag{3.11}$$

The expression is valid as long as the gas and liquid densities are the same in the different vessels. This is true for the HP-rig since it is a closed loop that operates with a fluid at its equilibrium. The uncertainty of the efficiency can be calculated by use of Gauss' formula for error propagation, Equation (3.2). The uncertainty is dominated by the uncertainty in the differential pressure measurements and therefore the uncertainty in cross section areas is ignored in the following expression:

$$\delta\eta_{cycl} = \frac{\sqrt{\left(A_{dem}\cdot A_{Drain}\cdot\Delta P_{l,dem}\right)^2\cdot\delta(\Delta P_{l,dem})^2 + A_{Drain}^2\cdot\delta(\Delta P_{l,Drain})^2}}{\left(A_{dem}\cdot\Delta P_{l,dem} + A_{Drain}\cdot\Delta P_{l,Drain}\right)^2} \quad (3.12)$$

The standard deviation will decrease if the total amount of liquid increases and thereby the differential pressure. Since the sizes of the vessels are fixed, the cross sections in Equation(3.12) can be regarded as constants.

Inlet Vane + Mesh Pad Efficiency

The efficiency of the inlet vane and mesh pad cannot be calculated on basis of accumulated liquid solely, since the scrubber bottom also is the reservoir were the liquid is pumped from during the tests. Instead, the mass rate of injected liquid is being continuously measured and used as a basis for efficiency measurements:

$$\eta = 1 - \frac{\dot{M}_{drain} + \dot{M}_{dem}}{\dot{M}_{inlet}} = 1 - \frac{\frac{\left(A_{drain}\cdot\Delta h_{drain}\right)\cdot\rho_l}{t} + \frac{\left(A_{dem}\cdot\Delta h_{dem}\right)\cdot\rho_l}{t}}{\dot{M}_{inlet}} \quad (3.13)$$

The liquid height can be found by rearranging Equation (3.9) into

$$\Delta h = \frac{\Delta P}{(\rho_l - \rho_g)g} \quad (3.14)$$

The uncertainty of the efficiency calculations for the inlet vane + mesh pad is much more complex than the cyclone efficiency since it depends on uncertainties in pressure differential measurements, injected liquid mass rate measurements and calculated liquid and gas densities (uncertainties in cross section area and sample time are negligible). The complex expression is not given here but in general the uncertainty decreases with increasing liquid concentrations in the rig, similar to the results from the uncertainty of the cyclone efficiency measurements.

3.3 Large Scale High-Pressure Rig (K-lab)

The Kårstø complex in western Norway (see Figure 3.15) holds one of Europe's largest facilities for natural gas processing. The facility receives raw natural gas from several offshore fields on the Norwegian continental shelf. At Kårstø the gas is being processed into lean sales gas which is then transported through a pipe line system to Emden and Dornum in Germany. The condensate (light oil) is being fractioned and shipped out by boat. The Kårstø metering and technology laboratory - K-lab is an integrated laboratory at the site and has unlimited access to gas from the production facility.

Figure 3.15 An overview over the Kårstø gas plant (Photo: Øyvind Hagen, Statoil)

3.3.1 Process Description

K-lab is a large-scale laboratory which is specialised in research and development of normal-sized equipment for gas metering, testing and in the qualification of gas-related processes and equipment being operated under realistic conditions.

The test facility for wet gas equipment can be operated at pressures of up to 150 barg, and recently a test rig for gas scrubbing has also been finalized. The aim is to test near-full-sized scrubber solutions under realistic conditions prior to installation in processing facilities. Realistic conditions in this sense, means a typical natural gas fluid at elevated pressures, large scale and gas and liquid flow rates within typical design ranges for most scrubbers. The diameter of the test scrubber is 840

mm, but the largest high-pressure separators today may be up to 3000 mm in diameter.

The test scrubber where the scrubber solutions are tested is a pressure vessel capable of withstanding pressures up to 156 barg. An interior shell can easily be removed from the test scrubber through a quick-opening cover at the top of the vessel. The demisting internals are mounted within this shell before it is mounted in the test scrubber. This solution provides a simple and quick way of changing test scrubber internals.

The test rig is a closed wet-gas loop were a large vessel –the guard separator- is charged with stabilized condensate from tankers. The loop is then pressurized with lean sales gas from the production facility and gas and liquid is recombined into a live natural gas fluid.

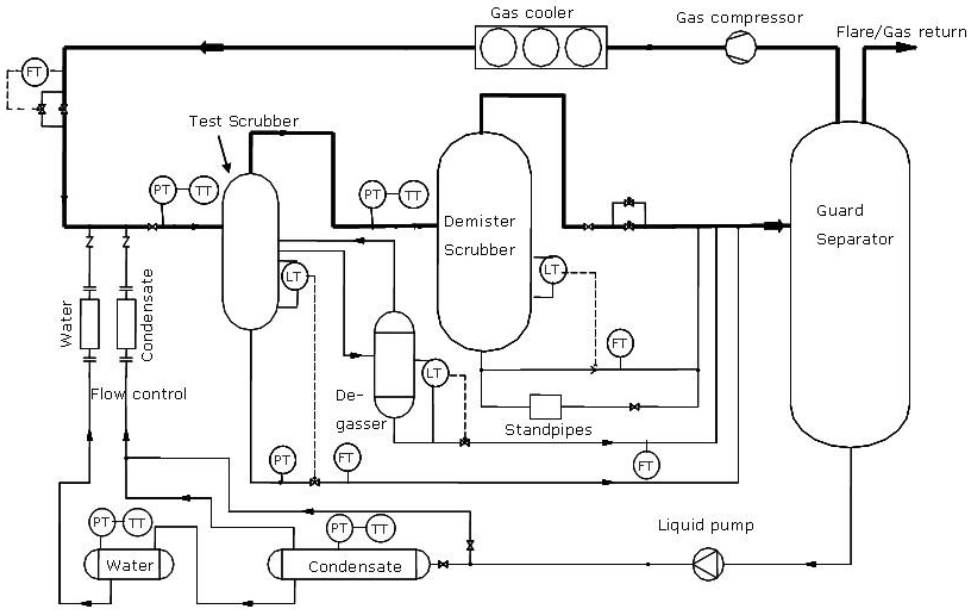

Figure 3.16 A simplified PFD of the wet gas loop at K-lab. The main gas flow is marked by the thick line, while the thin lines represent the liquid flow.

The simplified process flow diagram (PFD) of the K-lab loop is shown in Figure 3.16. The large guard separator acts as a gas and liquid reservoir. The gas is taken from the top of the guard separator and through a gas compressor that drives the gas flow in the gas loop. Liquid from a condensate tank is continuously being measured and injected into the gas loop several meters upstream of the test scrubber. The gas is in equilibrium with the injected liquid when it enters the test scrubber. This statement is supported by Brenne et al. (2005). Brenne et al. carried out temperature measurements in the liquid film at the bottom of the two-phase pipe and observed that mass transfer occurred in the range of milliseconds after liquid injection through a wet gas compressor at K-lab. This is likely to be caused

by the large gas-liquid surface area that exists when a large proportion of the liquid is dispersed as a fine mist. Separate samples of the gas and liquid phase taken upstream of the test scrubber have also confirmed that the fluid is in equilibrium.

If only small amounts of liquid are captured in the inlet arrangement of the test scrubber, this liquid is measured by liquid accumulation tests in the bottom. The liquid level is measured by both level radars and pressure differential cells. It is also possible to monitor the level visually through level gauges mounted on the tank. If the liquid flow rate is large, it is continuously being measured by one of two coriolis meters mounted at the liquid pipe in the bottom of the scrubber.

The liquid that is captured by demisting internals with a separate drain chamber is drained to the degasser. The liquid in the degasser is either measured by liquid accumulation tests or by a coriolis meter as described for the bottom of the test scrubber.

The liquid carry-over from the test scrubber is collected in the demister scrubber downstream of the test scrubber. The demister scrubber and the test separator can be seen in Figure 3.17. The internal diameter of the demister scrubber is 1800 mm i.e. more than twice as large as the test scrubber (840 mm). The internals of the demister scrubber is an inlet vane, a mesh pad and a deck of filter coalescers that can remove droplets down to sub-micron size.

Figure 3.17 The K-lab test facility. The large scale test separator can be seen to the right. The demister scrubber is the column to the left in the picture.

If only very small amounts of liquid are separated in the demister scrubber, it can be drained to one of two stand pipes of 2" or 6" in diameter. If the liquid load is so large that the 6" standpipe is overloaded during a test, a liquid accumulation test in the bottom of the demister scrubber is possible. Larger liquid rates in the demister scrubber can be measured by continuously draining the liquid through one of two coriolis meters that have different ranges of flow rates.

The K-lab test rig can operate at a large range of operating conditions as can be seen from Table 3.10. Liquid concentrations ranging from 0.01 – 3 vol% and K-values up to 0.35 m/s should cover the vast majority of vertical scrubbers currently in operation. Due to limitations in the compressor, the rig cannot be operated below 20 barg. The upper limit of 148 barg is not the upper limit of scrubbers in operation today as several examples of scrubbers operating at pressures above 200 barg can be found.

Table 3.10 The operating range of the K-lab test rig

Design pressure	[barg]	156
Operating pressure	[barg]	20 - 148
Design temperature	[^{0}C]	-46 - 100
Operating temperature	[^{0}C]	20 - 60
Gas rate	[Am^3/hr]	40 - 1900
Liquid rate	[Am^3/hr]	0.01 - 60
Liquid concentrations	[vol%]	0.01 - 3
K-value	[m/s]	0.03 – 0.35

The design of the rig is such that the total efficiency should be possible to calculate with an accuracy of 99.95% within the operating conditions specified in Table 3.10. The efficiency is calculated as the average over a test period that normally runs for 15 – 30 minutes. The process conditions are held as stable as possible during a test.

3.3.2 Fluid Properties at the K-lab Test Rig

Three different test pressures were used during the K-lab tests -28, 55 and 113 barg. For each pressure a new fluid composition was calculated since the rig was only charged with gas and not liquid.

As opposed to the conditions of the HP-rig which is placed in a temperature controlled climate chamber, the temperature at K-lab are changing and some mass transfer will therefore occur. The gas pressure is also varying in the gas loop since the loop is equipped with a compressor instead of a circulator. For instance, when

liquid is injected in the gas upstream of the test scrubber, some mass transfer must occur before a new gas-liquid equilibrium is established. For this reason, an integrated fluid calculation system constantly recalculated the physical fluid properties when temperature, pressure and flow rates changed. Increased liquid rates due to condensation were accounted for in the efficiency calculations. Due to the size of the rig, it was impossible to keep it absolutely gastight. Therefore, the fluid composition was also recalculated each time a considerable drop in the system pressure was observed e.g. before start-up in the morning.

In order to evaluate the accuracy of the fluid composition calculations, samples of the initially stable condensate and samples of the gas and liquid under two different pressures (at equilibrium) were taken. The samples were then analyzed at West Lab Services AS that uses a GC in accordance with the ASTM D-1945 standard for gas composition analyses, and a frequency densitometer in accordance with the ASTM D-4052 standard for liquid density measurements. The liquid composition was analysed by use of a HP 5890 Plus/Perkin Elmer Autosystem XL chromatograph in accordance with an internal West Lab standard.

The gas and liquid used at K-lab were real natural gas (i.e. not synthetic). A real fluid has got numerous of different components as opposed to the simple three-component system used in the HP-rig. The gas samples were analysed up to a C8 fraction while the liquid samples were analysed up to a C9 fraction. For the gas composition calculations the C9+ fraction and for the liquid composition calculations the C10+ fractions were lumped into one fraction with a corresponding characteristic density and mol weight.

The thermodynamic equations that were used were exactly the same ones as described for the HP-rig fluid calculations i.e. the SRK EOS modified with the Peneloux volume correction (Soave, 1972; Peneloux et al., 1982). The analysed composition was compared to the fluid composition calculations in the first test run after the sample was taken. The analyses of the two pressurized liquid samples can be seen in Table 3.11 while the gas comparison can be seen in Table 3.12.

Table 3.11 A comparison between the analysed and calculated liquid composition. The temperature and pressure refer to the equilibrium conditions in the Guard separator (reservoir)

		Calculated	Sample	Calculated	Sample
T	**[°C]**	29.3	30.4	31.4	31.1
P	**[barg]**	49.2	50.1	111.7	111.6
Component					
N_2	**[mol%]**	0.13	0.03	0.32	0.06
CO_2	**[mol%]**	0.71	0.62	1.18	1.04
C1	**[mol%]**	19.07	18.66	36.92	31.94
C2	**[mol%]**	5.60	5.37	8.12	7.79
C3	**[mol%]**	1.11	1.11	1.47	1.6
IC4	**[mol%]**	0.37	0.46	0.25	0.35
NC4	**[mol%]**	3.28	4.25	1.99	2.84
IC5	**[mol%]**	6.71	7.06	4.16	4.92
NC5	**[mol%]**	6.85	7.5	4.36	5.34
C6	**[mol%]**	9.39	9.24	6.42	6.99
C7	**[mol%]**	12.92	12.48	9.37	10.17
C8	**[mol%]**	13.89	13.32	10.29	10.73
C9	**[mol%]**	6.98	6.57	5.24	4.89
C10+	**[mol%]**	12.99	13.33	9.93	11.34

Table 3.12 A comparison between the analysed and calculated gas composition. The temperature and pressure refer to the equilibrium conditions in the Guard separator (reservoir)

		Calculated	Sample	Calculated	Sample
T	**[°C]**	29.3	30.0	31.4	31.1
P	**[barg]**	49.2	49.3	111.7	111.6
Component					
N_2	**[mol%]**	1.85	1.31	1.83	1.25
CO_2	**[mol%]**	1.37	1.38	1.39	1.46
C1	**[mol%]**	89.09	89.93	88.29	88.82
C2	**[mol%]**	5.79	5.52	6.25	5.87
C3	**[mol%]**	0.40	0.38	0.52	0.52
IC4	**[mol%]**	0.06	0.08	0.05	0.07
NC4	**[mol%]**	0.41	0.5	0.33	0.42
IC5	**[mol%]**	0.39	0.39	0.40	0.47
NC5	**[mol%]**	0.31	0.31	0.35	0.42
C6	**[mol%]**	0.17	0.12	0.26	0.32
C7	**[mol%]**	0.09	0.05	0.17	0.21
C8	**[mol%]**	0.04	0.02	0.11	0.15
C9+	**[mol%]**	0.01	0.01	0.04	0.02

The absolute uncertainty in the composition analysis varies for the different components as shown in Table 3.13. More details of the compositions can be found in Appendix A

Table 3.13 The absolute uncertainties of the composition analyses

N2	±0.05 mol%	**Ethane**	±0.07 mol%	**Pentanes**	±0.03 mol%
CO2	±0.03 mol%	**Propane**	±0.04 mol%	**Hexane's +**	±0.10 mol%
Methane	±0.7 mol%	**Butanes**	±0.03 mol%		

As can be seen from the tables, the liquid calculation is more inaccurate at 112 barg than at 49 barg and the gas compositions are more accurate than the liquid compositions. The deviation is generally larger than the uncertainties in the composition analyses, though indicating that there is an inaccuracy related to the calculation routines. The inaccuracy reflects the difficulties related to

- Measure the total volume of the large test rig
- Calculate the composition and amount of the gas leak
- Calculate and characterize the large amount of components in the fluid
- Small variations in lean gas composition (constant composition is assumed)

- Impurities from previous tests
- The quality of the thermodynamic equations

The fluid composition in the test scrubber is changing slightly with small changes in process conditions (pressure, temperature and flow rates). However, the small variations do not change the calculated values of the physical fluid properties more than ± 0.5 % for each test pressure. Typical values of the physical properties are listed in Table 3.14.

Table 3.14 Typical physical fluid properties in the test scrubber at the three different test pressures

Typical Calculated Properties		28 barg	55 barg	113 barg
Gas Density	**[kg/m^3]**	22.0	46.0	104.0
Liquid Density	**[kg/m^3]**	704.0	682.0	640.0
Gas viscosity	**[cP]**	0.012	0.013	0.016
Liquid Viscosity	**[cP]**	0.450	0.385	0.260
Interfacial Tension	**[mN/m]**	14.5	10.9	5.0

The quality of the calculated values is difficult to evaluate, but the liquid density is continuously being measured by coriolis meters. The coriolis meters measure a liquid density that is within 1.4 % of the calculated value for all tests. The densities of the liquid samples in Table 3.11 were measured at the actual temperature and pressure of the guard separator at the time of the sampling. The measured density was 0.7% less than the calculated density for the lowest pressure and 2.2 % larger for the highest sample pressure.

There are not any viscosity or interfacial tension measurements available that can verify the calculated values. The values have been calculated the same way as described for the HP-rig in Section 3.2.4. However, the presence of heavier components in the fluid will increase the uncertainty of the calculations compared to the synthetic three component system used in the HP-rig.

3.4 Tested Demisting Internals

A standard scrubber configuration was used during the experiments in the three different rigs. The distances between the internals were kept approximately the same in the different rigs. The exception is the distance between the inlet vane and the mesh pad at K-lab, which had to be larger due to the position of the nozzle of which a drain pipe from the cyclone deck had to go through. A principal sketch of the three different setups is shown in Figure 3.8. The diameters of the different vessels in the sketch are scaled so that the ratio of the diameter is the same as built.

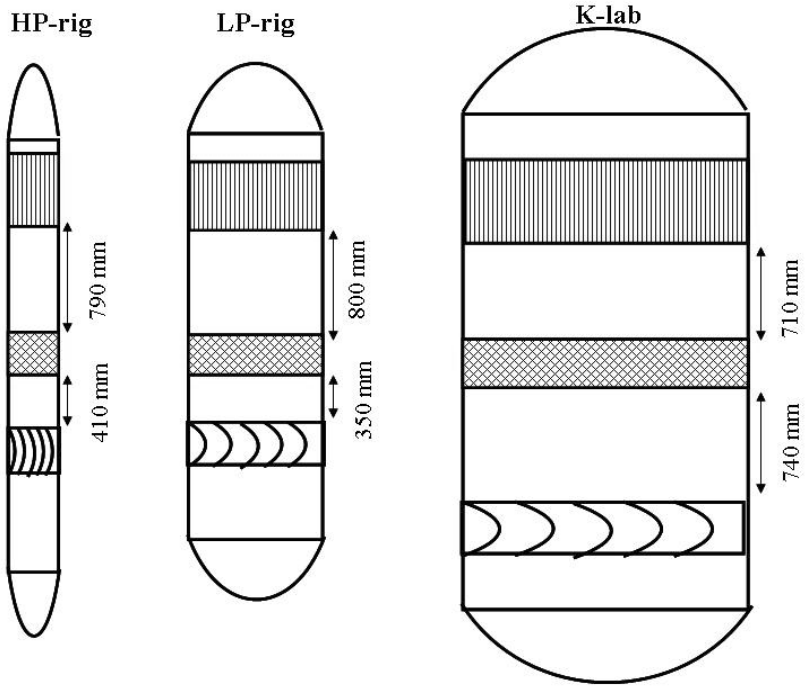

Figure 3.18 A scaled principal sketch of the setup in the three different experimental rigs

The standard configuration consists of an inlet vane, a 15 mm mesh pad and a deck of axial flow cyclones (AFC).

3.4.1 Inlet Vanes

The three different inlet vanes in Figure 3.19 have been used in the three different test rigs.

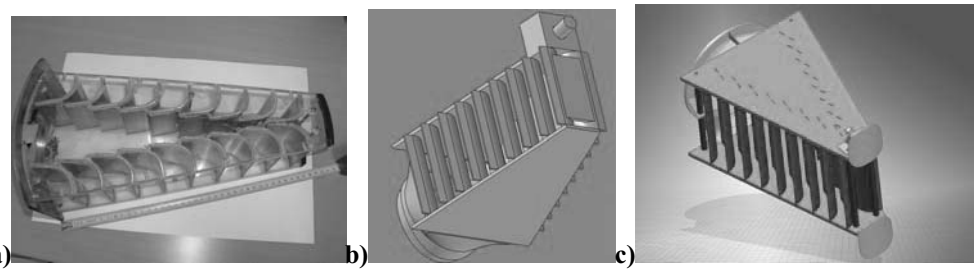

Figure 3.19 The figures shows the three different inlet vanes used for the experiments in a) the LP-rig, b) the HP-rig and c) the K-lab rig

Table 3.15 Some key geometrical data for the three different inlet vanes used in the experiments.

	LP-rig Vane	HP-rig Vane	K-lab Vane
Length [m]	0.39	0.15	0.84
Vane Area [m^2]	0.0474	0.0070	0.2010
Vessel Cross Sectional Area [m^2]	0.1195	0.0177	0.5542
Blocked Area [%]	39.7	39.5	36.3
Inlet pipe diameter [m]	0.08	0.049	0.257

3.4.2 Wire-Mesh Mist Eliminator

The mesh pads used in the three different rigs have been produced by Costacurta S.p.A Vico, and are identically to mesh pad 'Style A' investigated experimentally and theoretically by Brunazzi and Paglianti (1998). The mesh pads are constructed in stainless steel, AISI 304 and the general properties of a mesh pad are shown in Table 3.16

Table 3.16 The properties of the mesh pad used in all three rigs

Style	A
Wire diameter d_w [mm]	0.27
Packing density [kg/m^3]	144
Specific Area A_s [m^2/m^3]	274
Void fraction ε	0.98
Pad thickness [mm]	150
No. of layers [-]	65
Equiv. mesh diameter [mm]	2.35

A picture of the 150 mm diameter mesh pad used in the HP-rig can be seen in Figure 3.20. The mesh pad is constructed by rolling mats of 150 mm plain (65 layers high) until the diameter of the mat meets the requirements -150 mm diameter in this case.

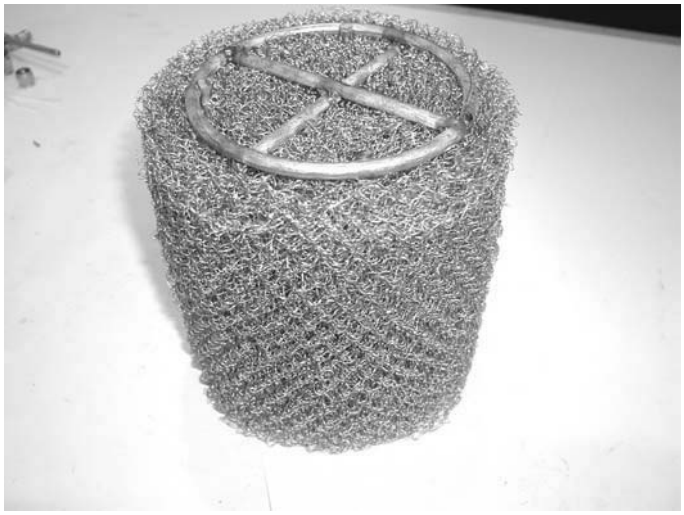

Figure 3.20 The 150 mm diameter mesh pad from Costacurta S. p. A. Vico that were used in the HP-rig.

3.4.3 Axial Flow Cyclone

Several principal sketches of different AFC geometries are given in open literature (Swanborn 1988; Bürkholz 1989; Verlaan 1991; Nieuwstadt and Dirkzwager 1995; Hoffmann and Stein 2002). Later, Yuan (2005) has published the geometry for an AFC that by the writer has been named the Sheffield design. The work by Verlaan and Yuan are the only publications that contain sufficient geometrical details in order to reproduce the cyclones and since the work by Yuan was not published at the start of this project, the Verlaan cyclone was chosen as the AFC in the standard setup for the scrubber in this project. A sketch of the Verlaan cyclone is shown in Figure 3.21. The left sketch shows a modified version that includes a vortex finder in the top of the cyclone. The modification will be discussed more thoroughly in Section 4.1.2.

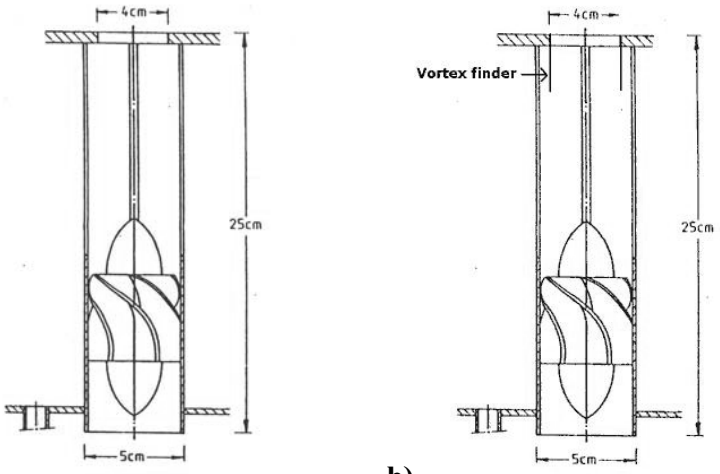

a) **b)**

Figure 3.21 A sketch of the generic geometry used for this report. (Picture taken from Verlaan (1991)). a) The sketch to the left shows the original cyclone, b) the right sketch shows a modified version with a vortex finder in the top.

Even though Verlaan gives a quite detailed description of the recommended cyclone geometry, some assumptions have been made when constructing the cyclone tested in this work. The tested cyclone have been built in accordance with Figure 3.21 and Figure 3.22, but the exact shape of the swirl vanes and the size of the drainage slits are examples of geometric details that where not given by Verlaan. The produced cyclones (Figure 3.23) are mounted in parallel in a multi cyclone packages adapted to each of the three test rigs.

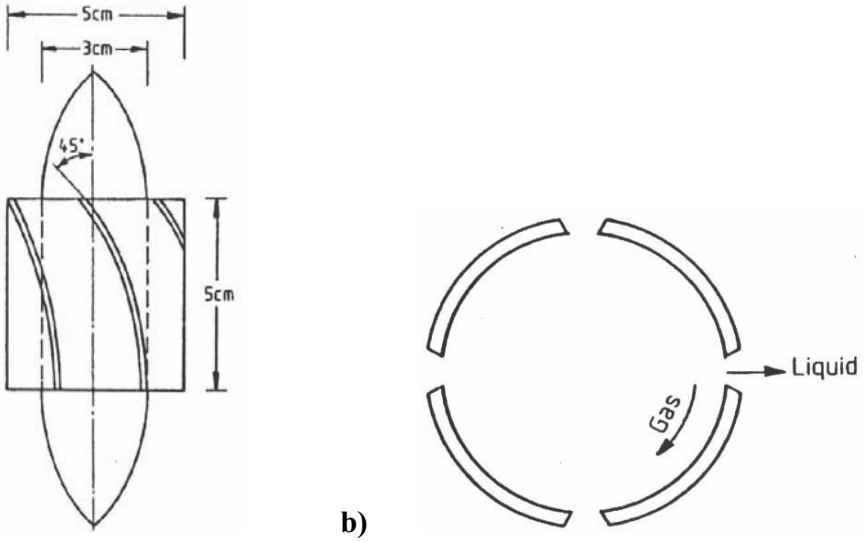

a) **b)**

Figure 3.22 The geometry of the cyclone recommended in Verlaan (1991) a) Details for the swirl vanes b) Details for the drainage slits (pictures taken from Verlaan (1991)

The chosen geometry for the cyclone has an exit angle for the blades on the swirl element of 45^{o} as indicated in Figure 3.22 a), and the vertically oriented slits are designed with a sharp edge as indicated in Figure 3.22 b)

a) 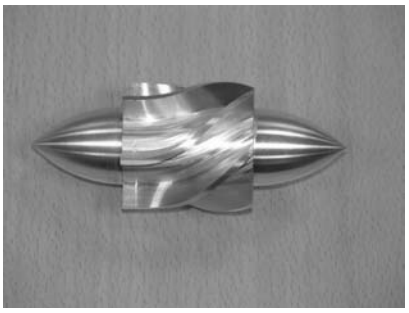 **b)** 

Figure 3.23 The generic cyclone design built from drawings given by Verlaan (1991) a) the swirl vanes with 45 degree exit angle b) the cyclone body with the vertical drainage slits

One common principle of commercial AFC's is not included in the Verlaan cyclone and that is the use of a secondary gas flow to help the liquid through the drainage slits. There are two ways of adding the secondary flow; either by recycling some gas back to the low-pressure zone downstream the swirl vanes in the centre of the cyclone body (see Figure 3.24) or by adding secondary outlets at the top of the drain chamber.

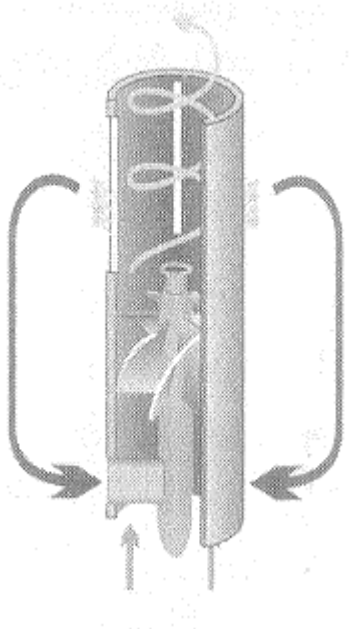

Figure 3.24 The picture shows a cyclone with recycling secondary gas (picture taken from Hoffmann and Stein, 2002)

The cyclone in this study does not have a recycling flow, but since the swirl is at its highest magnitude just downstream of the swirl vanes and decrease upwards in the cyclone, the pressure is higher at the lower end of the drainage slits than further up in the cyclone. This pressure difference drives a kind of secondary gas flow that flow through the lower end of the slits and re-enters at the upper part of the slits. This behaviour can be seen from the CFD calculation in

Figure 3.25 and is disadvantageous in terms of liquid drainage efficiency.

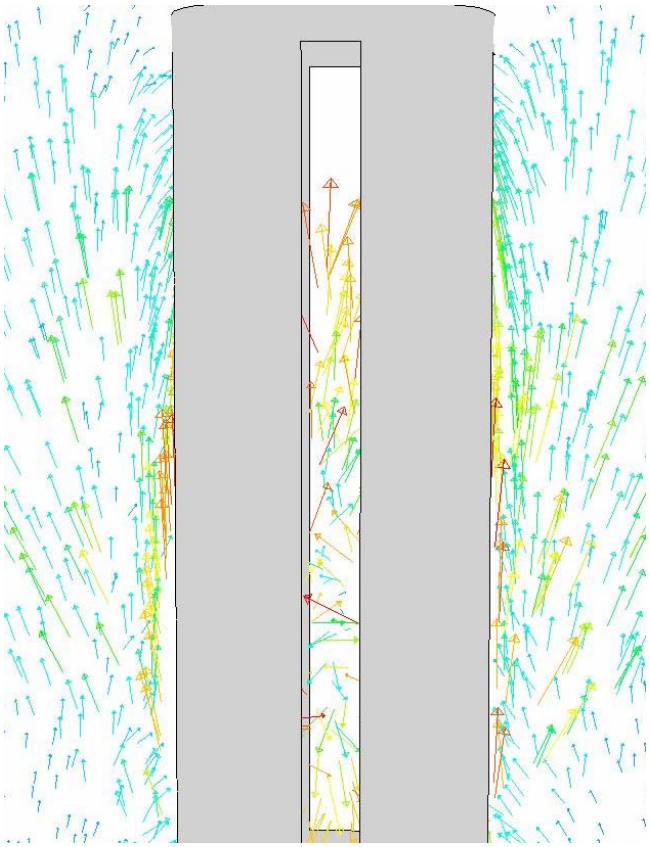

Figure 3.25 The gas flow pattern in the drain-chamber when no re-circulation or secondary outlet is used

The cyclones have been arranged in parallel in a cyclone deck for each rig as shown in Figure 3.26. The packing density of the setups can be defined as the ratio of the added sum of the cyclone cross sections to the total scrubber cross section i.e.

$$packing\_density = \frac{A_{cycl}}{A_{scrub}} \cdot 100\% \qquad (3.15)$$

a)  b) 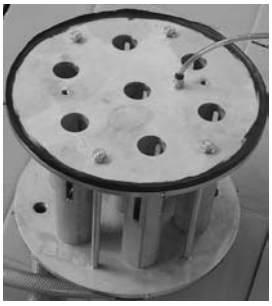 c) 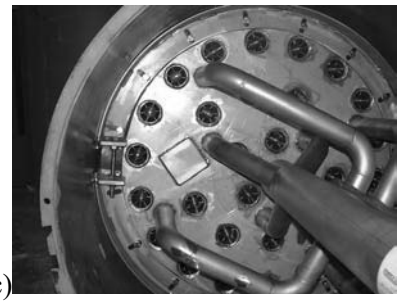

Figure 3.26 The axial flow cyclone mounted in parallel in a multi-cyclone deck. The cyclone decks are the ones installed in the a) HP-rig, b)LP-rig and c) K-lab rig

The packing densities in the different rigs are listed in Table 3.17. As seen, the packing densities for the LP-rig and the K-lab rig are approximately the same while the packing density in the HP-rig is twice as large compared to the two others.

Table 3.17 The packing densities for the cyclone decks in the three different experimental rigs.

		HP-rig	**LP-rig**	**K-lab**
Scrubber diameter	[m]	0.150	0.390	0.840
# cyclones	[-]	2	7	31
Packing density	[%]	22.2	11.5	11.0

Due to the differences in packing densities, the total scrubber efficiency in the HP-rig at a given gas and liquid load cannot be compared to the total efficiency of the two other rigs since the superficial cyclone velocity in the two latter rigs will be approximately twice the velocity of the HP-rig.

CHAPTER 4

Results and Discussion

The three different rigs described in Chapter 3 have been used to produce the results in this chapter. Each rig has got different set of possibilities and advantages over the other two rigs. The LP-rig is easy to operate in terms of safety and operational costs. This rig is also big enough to put in cyclone banks of different sizes. The small scale HP-rig can also operate with the same fluids as in the LP-rig. This makes it possible to compare experiments with the same fluids but at two different scales. In addition, this rig can operate with live hydrocarbon fluids, hence, offering the opportunity to compare experiments carried out with a model system (e.g. N_2-Exxsol D60) to experiments carried out with a live fluid -under otherwise equal conditions.

Even if experiments are carried out with realistic fluid properties, the results from a small scale unit cannot be used to accurately predict the performance of a large real scrubber. There can be variations in the gas- and liquid-distribution throughout the scrubber that is not being reflected in a small scale unit. For this reason tests have also been carried out in large scale at K-lab, since this scrubber will give answers that are close to what one could expect in a real scrubber.

4.1 Low-Pressure Rig Results

The low-pressure rig has been used in order to check the performance of

1. The Verlaan cyclones (Verlaan, 1991)
2. A modified set of Verlaan cyclones
3. The standard scrubber setup (see Section 1.5)

4. Demonstration of separation performance for water vs. hydrocarbon experiments.

Two different configurations have been used. A principle sketch of these configurations can be seen in Figure 4.1. The configuration to the left was used in order to check the performance of the Verlaan cyclones in combination with an inlet vane arrangement upstream. Liquid was introduced either through a liquid nozzle above the inlet vanes or through a nozzle in the upstream piping. In the configuration to the right the standard scrubber setup is shown.

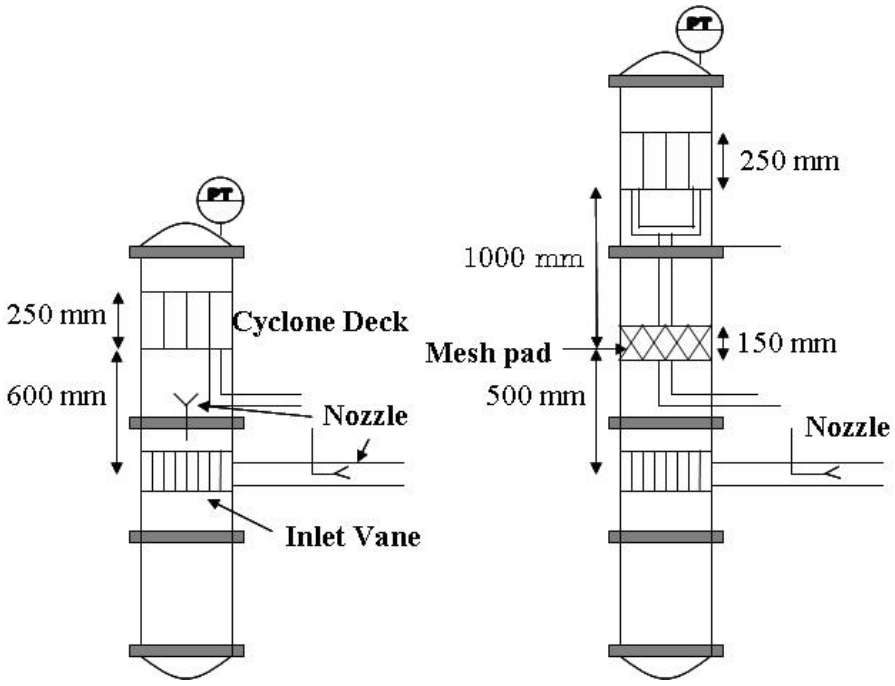

Figure 4.1 The two different test setups in the low-pressure rig

Since varying amounts of liquid were required in the scrubber, different nozzles were used in different tests. The nozzles that were used were produced by Delavan Spray Technologies and are of type BLM-5, BF-12 and BNM-39. The two former nozzles produced a spray angle of 90^{o} (BLM-5 and BF-12) while the latter produces a spray angle of $90 – 120^{o}$ dependent on pressure (larger pressure gives smaller angle for this design). The liquid flow rate through the nozzle depends on the differential pressure. The pump could deliver pressure up to approximately 12 bara so the maximum differential pressure varied from 6 – 11 bara during the testing. The characteristics of each nozzle can be seen in Figure 4.2.

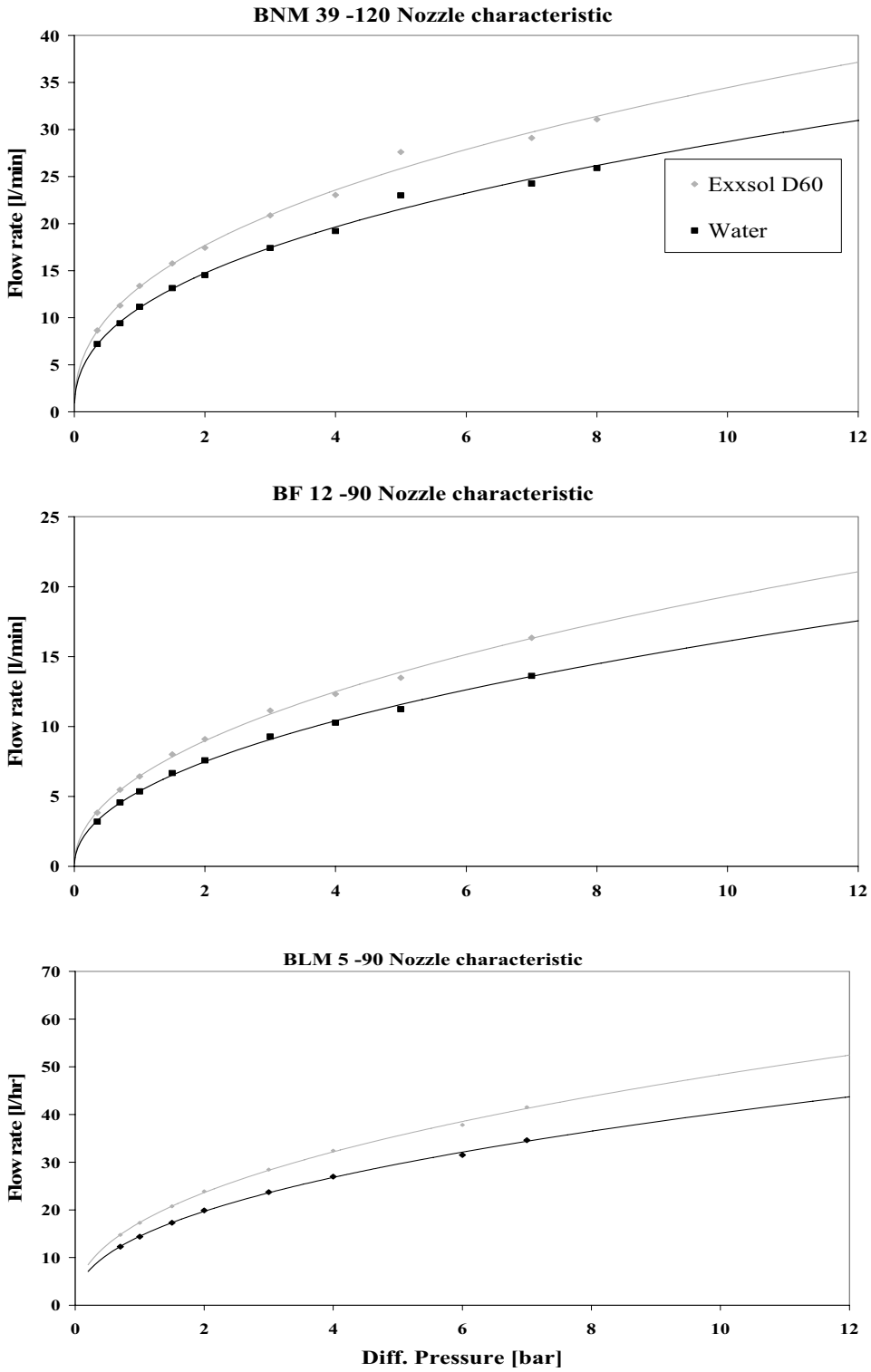

Figure 4.2 The characteristics of the three nozzles used in the LP-rig

4.1.1 The Verlaan Cyclone with Air/Exxsol and Air/Water

The work performed by Verlaan (1991) was carried out with an air/water system under ambient conditions. Verlaan has presented results for efficiency as functions of the volumetric gas flow through the cyclone.

Collocation of present results and Verlaan's result

It can be seen in Figure 4.3 that in both Verlaan's results and in the present ones (except for one case) the separation efficiency drops off as the gas flow increases.

As discussed in Chapter 2, if the droplets are so small that the cyclone separation efficiency is determined by the droplet size, one would expect an increase in efficiency with increasing volumetric gas flow and probably with increasing liquid loading. However, if re-entrainment is the determining factor, the efficiency would be expected to drop off with higher volumetric gas flow and liquid loadings.

In the LP-rig experiments, at the largest liquid flow rates the bulk liquid is in the form of larger droplets, and the droplet size should not play an important role –if any at all- in determining the separation efficiency. The shape of the curves in Figure 4.3 supports this statement. The atypical behaviour of the curve corresponding to the lowest loading, where efficiency increases with increasing gas flow rate, may indicate that in this case a sufficient amount of liquid was dispersed into small droplets comparable to the cut-size of the cyclone.

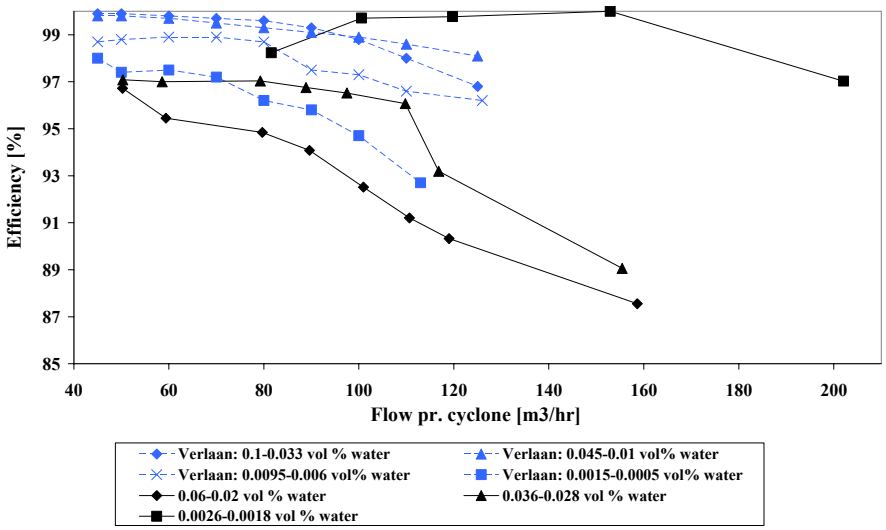

Figure 4.3 A collocation of the results obtained by Verlaan and results obtained in the LP-rig. Seven cyclones and gas densities ranging from 2.1 - 7.5 kg/m^3 were tested in the LP-rig, while one cyclone and gas density fixed to 7.5 kg/m^3 was tested in the work by Verlaan (1991).

In Figure 4.3 the actual liquid load to the cyclone has been reported. Since some of the liquid will be separated and drain to the bottom of the test scrubber, the injected liquid concentration will always be higher than the concentration in the cyclone inlet. During the first experiment 0.1 vol% liquid was injected, but only 0.06 – 0.02 vol% reached the cyclone inlet. In the two following experiments, the amount of liquid was therefore controlled such that approximately 0.03 and 0.002 vol% reached the cyclone deck.

Water is a fluid with physical properties that makes it easier to separate than hydrocarbons due differences in interfacial tension, density and viscosity. Since the main focus for this work is to investigate scrubbers for hydrocarbon services, the test fluid mainly used in the LP-rig is Exxsol D60. The same tests as shown in Figure 4.3 have also been carried out with Exxsol as liquid. The results are shown in Figure 4.4 for identical test geometries. As opposed to the collocation in Figure 4.3, the results are compared in terms of the superficial velocity in the cyclones $u_{g,s}$ since superficial velocity also makes it easier to compare cyclones of different diameter.

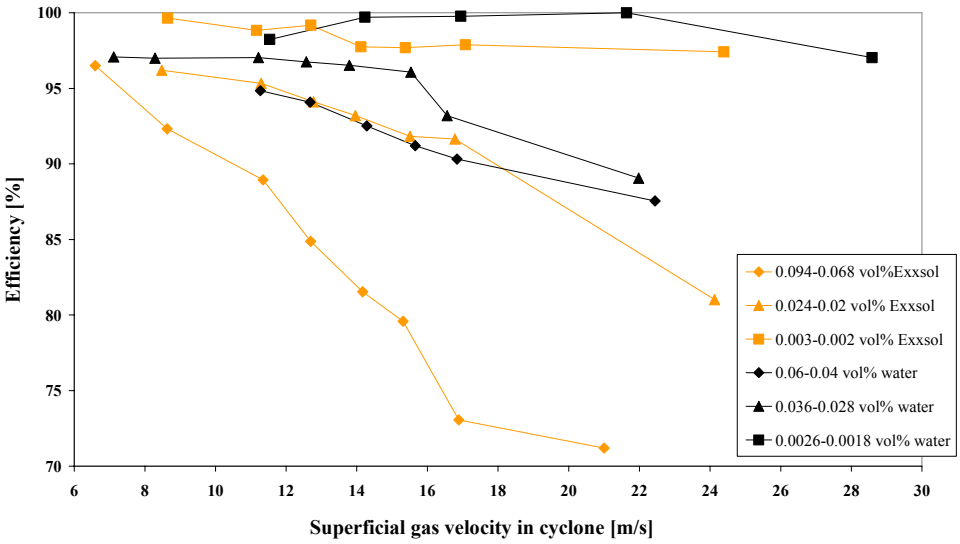

Figure 4.4 A comparison between the cyclone efficiency when Exxsol D60 and water was used as liquid respectively. Water is easier to separate than Exxsol D60 for all tested cases

The cyclones are performing a lot worse when Exxsol is used as liquid instead of water. If these results are analyzed in terms of absolute amount of liquid that escapes instead of efficiency, one can see that the liquid carry-over is up to three times as large when Exxsol is used. This clearly reveals the importance of taking into account the fluid properties when lab-results are used as basis for the design of real scrubbers. All experiments in the LP-rig has therefore been carried out with air

and Exxsol D60 except for the three curves shown in both Figure 4.3 and Figure 4.4

The results from Figure 4.3 and Figure 4.4 have been plotted against liquid load to the cyclone in Figure 4.5. This plot reveals a difference in the dependency on liquid load. The work by Verlaan shows that separation efficiency generally increases with increasing liquid load (within the narrow range of liquid load tested!). The efficiency of the cyclones in the present tests show that the efficiency decreases with increasing liquid load. This is true for both the water tests and the Exxsol tests.

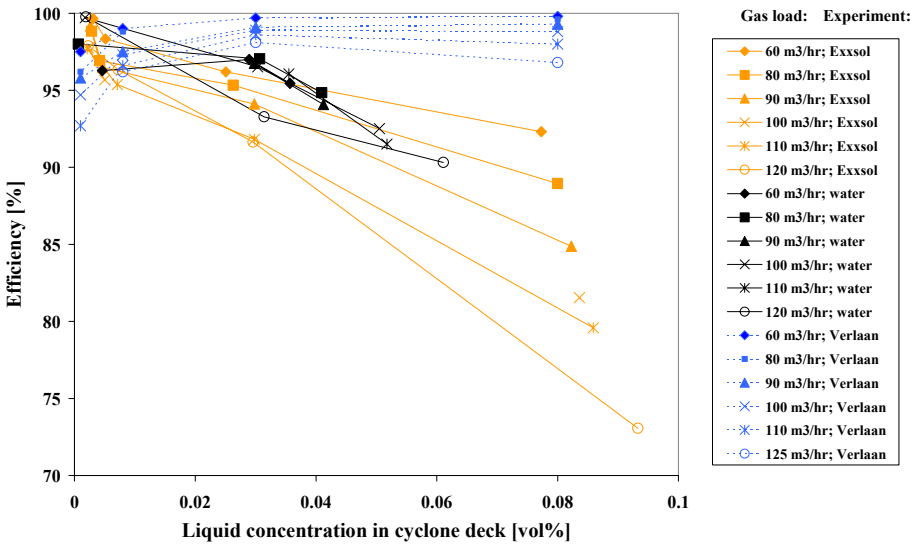

Figure 4.5 The efficiency of the investigated cyclones shows different liquid load dependence than the cyclone tested by Verlaan.

Discussion of Differences Between Present Results and Verlaan

The LP rig has been operated at pressures ranging from approximately 2 – 6.5 bara during the present work. The volumetric gas flow was controlled by throttling the gas flow as described in section 3.1. Decreasing pressure results in decreasing gas density in the test scrubber. The gas density will influence the results in a comparison between the results from the LP-rig and Verlaan's results since Verlaan operated with constant density 7.2 kg/m^3. In addition to the deviation in gas density also the following points were or might have been different:

- Differences in the drainage slit geometry etc.
- Differences in the swirl vane geometry

- Different droplet sizes in the various experiments
- Uneven liquid and/or gas distribution in the present multi cyclone setup

When it comes to the first point on the list, one possible difference that might be important is the configuration of the drainage slits. For reasons related to the manufacturing of the cyclones, the drainage slits do not go all the way up to the end of the cyclone body, but stop about 1 cm below the edge (se Figure 3.23 b). This edge is supposed to stop rivulets that are flowing upwards along the slits or bands of liquid that escape the drainage slits. Before the liquid enter the end of the cyclone body and gets re-entrained by the gas leaving the cyclone, the edge is supposed to stop this. Since the drainage slits do not proceed to the very end of the cyclone body, a small area is left behind where liquid can build up and finally get re-entrained since it has not got a chance to drain to the drainage chamber from this area. In addition to this, the v-shape angle of the slits is small and the wall is relatively thick. This might decrease the efficiency of the slits slightly.

If the swirl vanes are well designed there is a reduced chance of gas recirculation zones between -and downstream of- the vanes. Such recirculation zones can decrease the grade efficiency of the cyclone. Good swirl vane design might be the reason why the cyclones in the current study perform better than in the Verlaan study when the liquid load is low i.e. below 0.01 vol% as seen in Figure 4.5

The difference in the experimental setup between Verlaan and this study is primarily related to the use of a multi cyclone arrangement instead of a single cyclone, and the use of inlet vanes for distribution of the gas over the cross-section of the scrubber. As mentioned, there is a possibility of liquid mal-distribution caused by a combination of the nozzle characteristics and an inhomogeneous gas flow pattern upstream of the cyclone inlet. Uneven liquid distribution is likely to reduce the efficiency since the efficiency of cyclones in the current study generally drops off with increasing liquid load. The influence of liquid mal-distribution is discussed more thoroughly in section 4.1.3.

Since the LP-rig cannot operate the volumetric gas flow and gas density independently, the gas density will vary from one experiment to another. However, since Verlaan operates at a constant gas density, that is greater than (or in some cases equal to) the gas density for all the experiments in the LP-rig, the results by Verlaan should be negatively influenced compared to the operating conditions in the LP-rig. Since the results of Verlaan generally shows a better performance at higher liquid loadings, some of the other issues discussed must be the main reason why the performance of the cyclones in the current study is worse than reported by Verlaan for liquid loadings above 0.01 vol%.

4.1.2 Modified Verlaan Cyclones

To improve the cyclone performance two simple modifications to the cyclone were tested (see Figure 4.6). The modifications included a vortex finder at the exit and a hole in top of the drain chamber, where some of the gas that enters through the slits and into the drain chamber could escape. This extra gas flow is called the secondary gas flow.

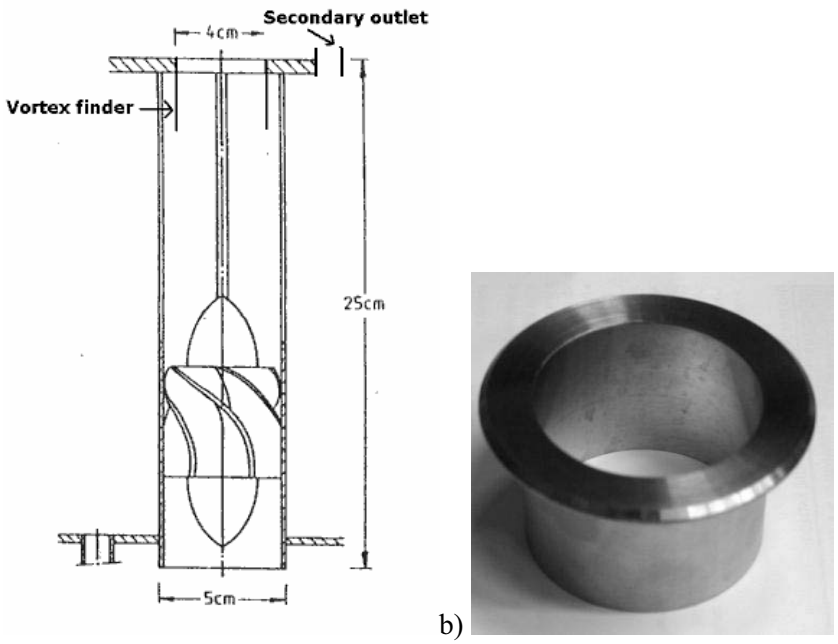

Figure 4.6 The pictures show the modifications to the original cyclone. In picture a) both the new vortex finder and the secondary outlet for the gas is shown. Picture b) shows the vortex-finder that was mounted in the cyclone as seen in figure a)

The idea behind the vortex finder was to protect the liquid that accumulates in the top against the swirling gas flow. By shielding the liquid in this section, the liquid was given a better chance to drain instead of being re-entrained by the gas.

Effect of Vortex Finder

The installation of a vortex finder has had a very positive influence on the cyclone in terms of efficiency as can be seen in Figure 4.7. For the tests with the least amount of liquid, the efficiency was close to or actually 100 %, meaning that it was not possible to detect any liquid in the gas outlet. For the tests with the greatest amount of liquid and highest gas load, the efficiency was improved from 71 to 90 %, which is a large improvement for such equipment.

There is no obvious reason that the vortex finder should contribute to increased grade efficiency. If it should have any effect at all on the grade efficiency, it should be negative since the effective length for the droplets to settle is decreased when the vortex finder is introduced. This large improvement in efficiency therefore indicates that cyclone efficiency in the LP-rig is related to some kind of re-entrainment from the cyclone.

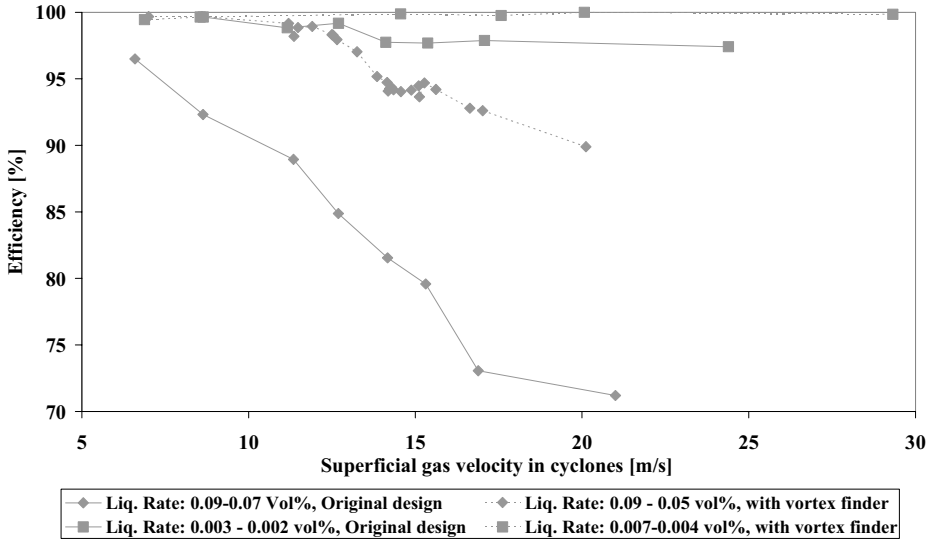

Figure 4.7 The air/Exxsol separation efficiencies of the Verlaan cyclone with and without vortex finder. The vortex finder in the top of the cyclone has got a positive effect on the efficiency

Effect of Secondary Outlets

In order to induce a secondary gas flow through the drain slits, four 3/8" pipes where mounted through the top plate in the multi cyclone arrangement in Figure 3.23 c). No efforts were made to quantify the amount of secondary gas flow since the objective was to see if such a simple change in geometry could have a potential for efficiency improvement that was worthwhile working on.

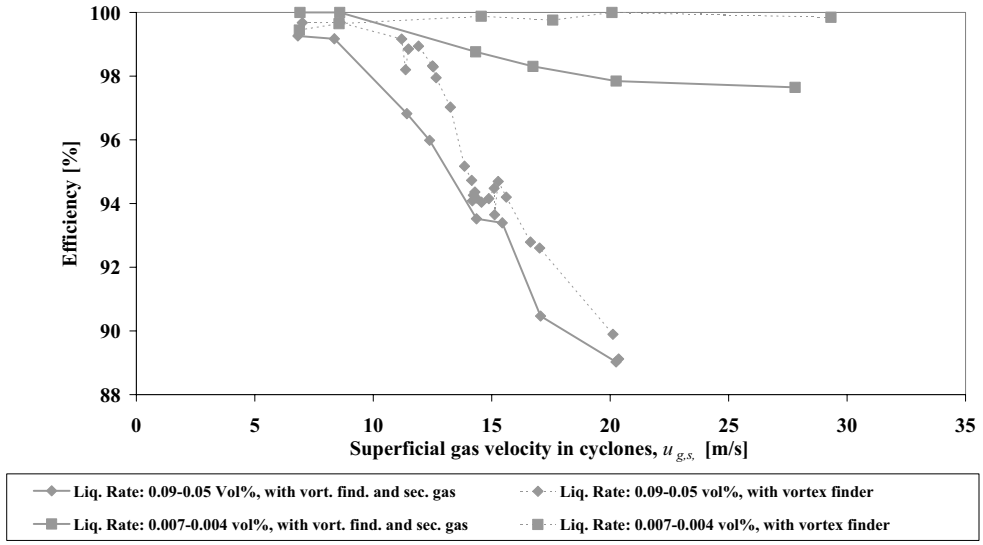

Figure 4.8 The air/Exxsol separation efficiencies for the Verlaan cyclone with and without secondary gas flow (all tests with vortex finder in the top of the cyclone).

Contrary to other design solutions for secondary gas flow (see Swanborn, 1988; Verlaan, 1991; and NG, 2005), the secondary gas flow in the current design has the potential of bypassing the cyclone. Bypassing in this sense means that small droplets in the drain chamber can follow the secondary gas flow through the roof and, thereby, increase the total liquid carry-over. On the other hand, the secondary flow can help the separated liquid through the drain slits and thereby decrease the chance of re-entrainment. For almost all tested cases the secondary outlet had a negative effect on the efficiency as can be seen from Figure 4.8. The negative effect is most evident for the test with the least liquid load, since a relatively larger fraction of the liquid in the drain chamber is distributed as small droplets in these tests. This has also been observed visually during the tests.

Since the tests with secondary outlets did not improve the efficiency, this modification was not used for further experiments with gas/liquid separation.

4.1.3 Uncertainties and Reproducibility

The uncertainty in the efficiency results in section 4.1.1 and 4.1.2 are calculated with Gauss' formula for uncertainty (Equation (3.2)) and in all the present experiments it is found to be below 0.01%. The largest contribution to the uncertainty in these 2D-plots is probably not the uncertainty in the measurements but variations in the process conditions under which the measurements have been carried out. To investigate the variations in the experiments, the curve tagged '0.09-0.05 vol % w/vortex finder' in Figure 4.7 and Figure 4.8 were determined with a lot

more experimental points than the rest of the curves. The experiments behind this curve were carried out in random order, with varying test durations and at different days. In addition, many of the experimental points were also repeated, but considering the size and the complexity of the rig, it was difficult recreate the exact process conditions for each repetition. Five repetitions were made for superficial gas velocity 14 m/s, and the liquid load was 70 l/hr pr. cyclone. Based on these repetitions a standard deviation could be estimated by the expression:

$$s_\eta^2 = \frac{1}{N-1}\sum_{i=1}^{N}(\eta_i - \langle \eta \rangle) \tag{4.1}$$

Using the results from the five repetitions in Equation (4.1) resulted in a standard deviation $s_n = 0.25\%$

During the experiments where the liquid was introduced through a nozzle above the inlet vane, it was observed that gas and liquid flow was strongly unevenly distributed. If the gas had been evenly distributed above the inlet section, the liquid would have been distributed as a cone from the nozzle tip and upward. This was not the observed flow pattern during the experiments but a strongly inhomogeneous swirling flow pattern was observed above the inlet vane. A principal sketch of the effect that the swirling gas flow had on the liquid from the nozzle is shown in Figure 4.9. The liquid was forced to the left on the picture. This had a bad effect on the liquid distribution, especially when only a small amount of the liquid capacity in the nozzles was used. In addition, it was seen that the nozzle BF-12 (see Figure 4.2) was much more affected by the swirling gas flow compared to the effect it had on nozzle BN-39. It seemed like the latter one was designed in a way that forced more of the liquid out in the cone pattern that both nozzles were supposed to create. This flow pattern may cause a much higher liquid loading on some of the cyclones in the multi cyclone setup.

The inhomogeneous flow pattern above an inlet vane was investigated in a master thesis at the University of Bergen (Kvinnesland, 2004). An experimental study of the flow pattern was compared to Computational Fluid Mechanics (CFD) simulations of the same geometry. An example of the swirling nature of the gas flow above an inlet vane identically to the one used in the HP-rig (see Figure 3.19b) is shown in Figure 4.10. The swirl pattern is seen from above and the inlet is placed on the opposite side of the vessel compared to the sketch in Figure 4.9. (inlet gas is streaming from left to right).

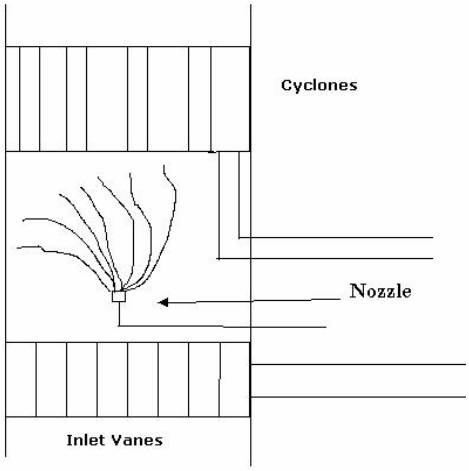

Figure 4.9 Liquid mal-distribution from nozzle due to uneven gas flow pattern downstream the inlet vane

Even though the simulated geometry is different to the inlet geometry used in the LP-rig (see Section 3.4.1), the main structures in the flow pattern can be expected to be the same. This was also supported by visual observations done during the tests.

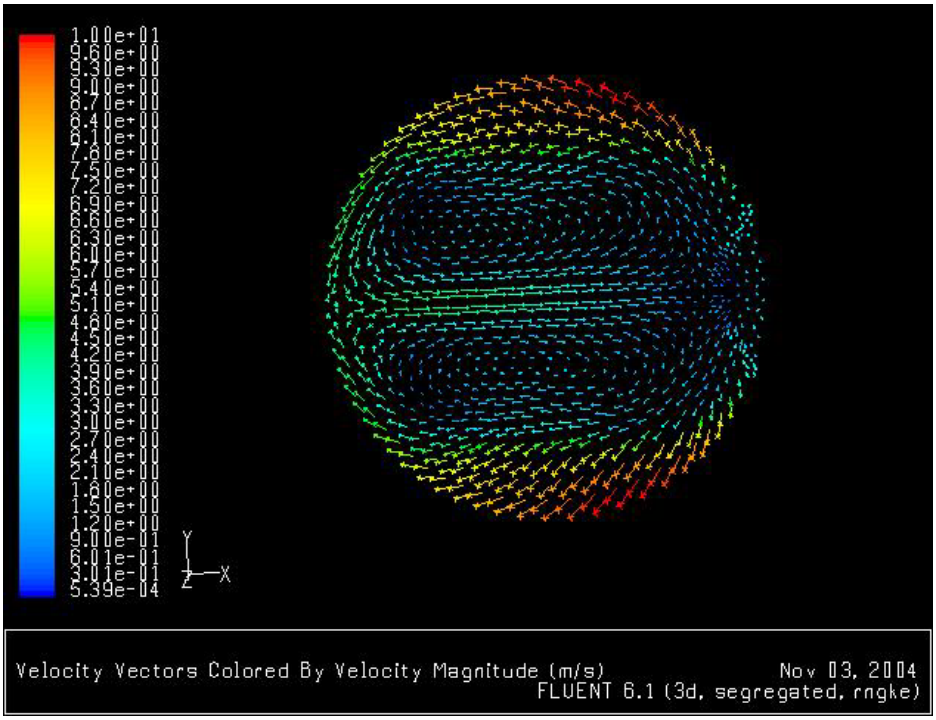

Figure 4.10 A CFD simulation of the 2D flow pattern above an inlet vane identically to the one used in the HP-rig. The picture shows the inhomogeneous nature of the gas flow pattern. (Picture taken from Kvinnesland, 2005)

Uneven liquid distribution of the liquid to the cyclone deck influences the total performance since the efficiency of the individual cyclone is dependent on liquid load. The curves in Figure 4.11 show how the cyclone efficiency drops off with increasing liquid load.

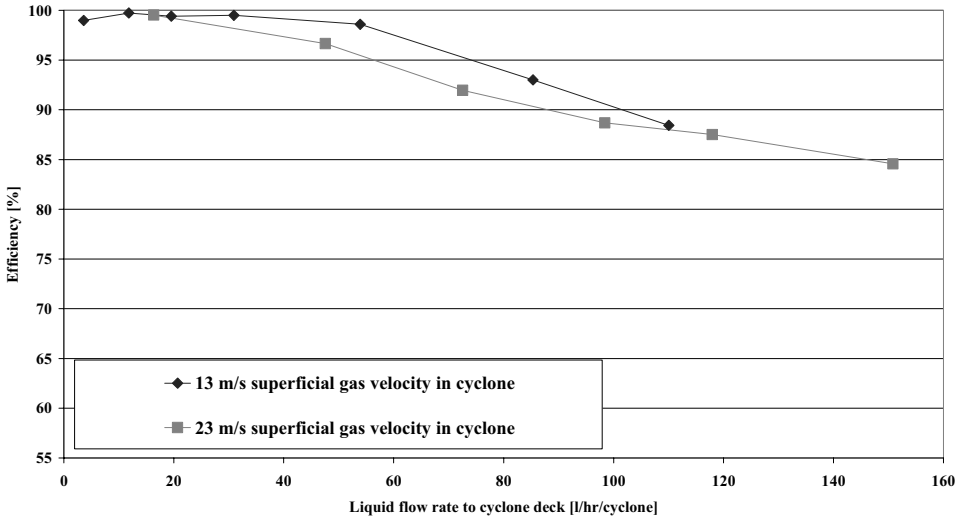

Figure 4.11 The cyclone efficiency for varying liquid flow rate at two different gas flow rates. Exxsol was introduced through nozzle BN39.

To demonstrate how sensitive the performance of the cyclone deck is to the liquid distribution, the same tests where carried out with three different ways of injecting the liquid. In two of the experiments, the liquid was injected through two different nozzles, while it was injected in the upstream piping during the third experiment. The nozzles used were BN-39 and BF-12. The results of the different methods of liquid injection are shown in Figure 4.12. Since uneven liquid distribution is expected to result in lower efficiency, the best distribution of the liquid with the three different methods will result in the highest efficiency.

The results in Figure 4.12 show that the liquid distribution to the cyclone deck is most even when the liquid is introduced through the inlet vanes and most uneven when the liquid is introduced through nozzle BF12. This is true for a superficial gas velocity in the cyclones up to 15 m/s which corresponds to a scrubber K-value of approximately 0.13 m/s. When the superficial gas velocity exceeds 20 m/s (Scrubber $K \approx 0.15$ m/s), the trend is the opposite, i.e. BF12 results in the most even liquid distribution.

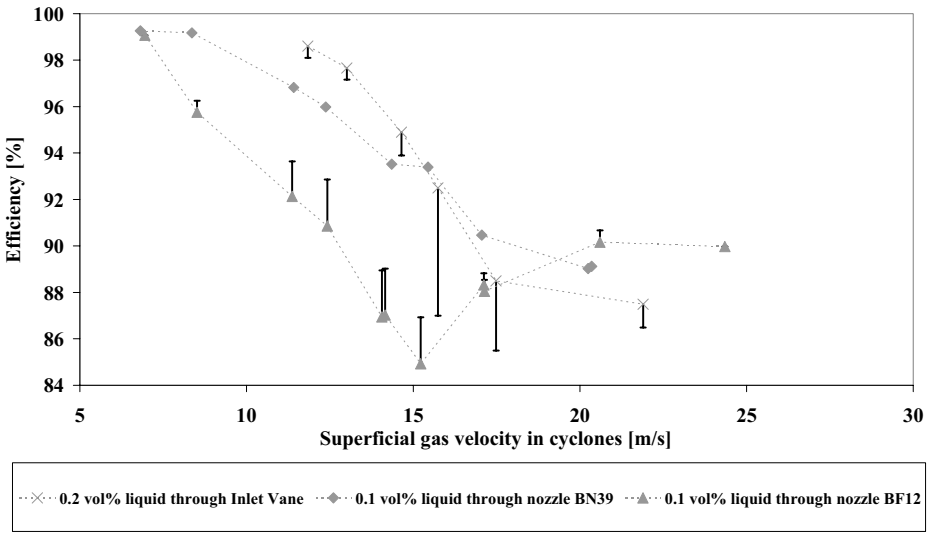

Figure 4.12 The efficiency is dependent on the way the liquid is introduced in the scrubber. The figure shows the efficiency for three different ways of introducing the liquid. Since different liquid flow rates reached the cyclone deck during the different experiments, the error bars reflect the relative deviation to the curve produced with nozzle BN39 is shown. The best efficiency indicates the best liquid distribution.

The separation efficiency is dependent on the liquid load to the cyclones as shown in Figure 4.11. In order to compare experiments with different liquid injection methods, the same amount of liquid must therefore reach the cyclone deck. However, this is not the case for the experiments shown in Figure 4.12. Varying amounts of liquid reached the cyclone deck for the different liquid injection methods even when the gas flow rate was identical. Therefore, with basis in the curves in Figure 4.11, an estimate were made for each experiment showing how much the efficiency could deviate from the measured efficiency if the same amount of liquid reached the cyclone deck as the corresponding experiments carried out with nozzle BN39. Corresponding in this sense means identical gas flow rate. The maximum estimated deviation in efficiency due to difference in liquid load between the BN39 experiments and the two other experiments is indicated with error bars for each experimental point in Figure 4.12. For instance, when the superficial velocity in the cyclones was 13 m/s, the average liquid load was 60 l/hr per cyclone when 0.1 vol% liquid was introduced through BN39, but only 40 l/hr when 0.2 vol% liquid was introduced through the inlet vane. If more liquid was introduced through the inlet vane such that the average liquid load was 60 l/hr per cyclone, the efficiency would have been lower. Based on the curves in Figure 4.11 this expected difference in efficiency was estimated to be -0.5%, and hence an error bar of -0.5% was added to the experimental point.

The error bars in Figure 4.12 indicate that differences in liquid load alone cannot be the explanation for the differences in efficiency with the different methods of

introducing the liquid. Therefore it is concluded that there is an uneven distribution of the liquid below the cyclone deck and that this is likely to cause a decrease in the efficiency.

4.1.4 Inlet Vane and Mesh Pad

The standard scrubber solution has been tested in the LP-rig in order to serve as a reference for experiments in the HP-rig and at K-lab. The setup to the right in Figure 4.1 has been used for the experiments in this section and K-values from 0.1-0.16m/s have been tested. The liquid concentrations have been kept constant in terms of volume percentage, and five different concentrations have been tested for seven variations in K-value. In addition to this, the rig has been tuned in order to find the flooding point of the mesh pad for each liquid concentration curve. The flooding point has been identified by visual observations. The K-value was increased in small steps and at the same time, the liquid rate was increased to keep the liquid concentration constant. The flooding point was then defined as the point where the liquid accumulation in the mesh pad reached the top surface. The transition from a demisting pad to a flooded mat is a gradual process and the exact flooding point is therefore difficult to identify exact.

The individual separation efficiencies of the inlet vane and the mesh pad cannot be calculated, but the combined separation efficiency of both scrubber internals can be calculated on basis of the injected liquid and the collected liquid in the cyclones and the filter coalescer (see Equation (3.6)). For the uncertainty calculations Equation (3.8) have been used and in all experiments the efficiency uncertainty was < 0.3 %.

The combined efficiency of the inlet vane and the mesh pad is shown in Figure 4.13. The flooding point for each curve is also indicated and as can be seen, the flooding point is not just dependent on the K-value but also on the liquid concentration. The connection between liquid rate and flooding point has also been identified by Bürkholz (1989). The reason for this is that liquid hold-up in or below the mesh pad reduces the free area where gas can flow and therefore the local gas velocity vectors increase, an effect not accounted for in the K-factor, which is based on the superficial velocity.

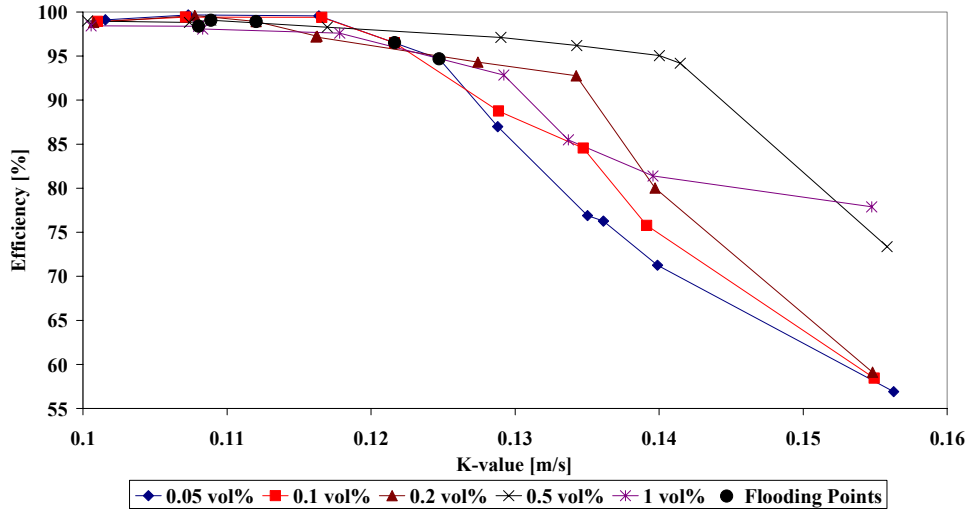

Figure 4.13 The primary separation efficiency (inlet vane and mesh pad) as function of the gas load (K-value). All tests are carried out with air/Exxsol

The efficiency never exceeds 99 % for the lowest K-values where the mesh pad is operated below flooding conditions. This indicates that approximately 1% of the liquid from the inlet vane distribute as fine droplets that are too small to be caught in the mesh. The mesh typically has a cut size (d_{50}) around 5 microns at atmospheric conditions (Brunazzi and Paglianti, 1998).

The fractional efficiency increases with increasing liquid concentration up to 0.5 vol %. The efficiency for the 1 vol% trend line is better than the some of the trend lines with lower concentrations, but he total liquid carry over does not decrease. However, the absolute liquid carry-over increases with increasing liquid concentration. The results in Figure 4.13 are plotted in terms of liquid carry-over from mesh pad against liquid concentration in Figure 4.14. From the figure it can bee seen clearly that more liquid in the inlet vane results in larger liquid carry-over from the mesh pad. It can also be seen that higher gas load results in larger carry-over.

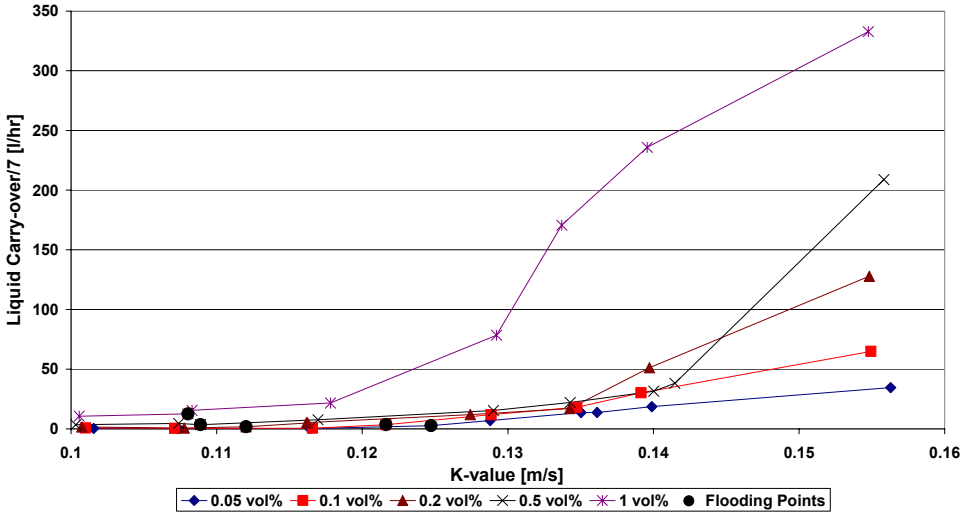

Figure 4.14 The liquid carry-over from the mesh pad as a function of the liquid concentration in the inlet pipe.

4.1.5 Total Scrubber Efficiency

In Figure 4.15 a comparison of the cyclone efficiency is made when liquid is introduced through nozzle BN39 and when the liquid is entrained from mesh pad can be seen.

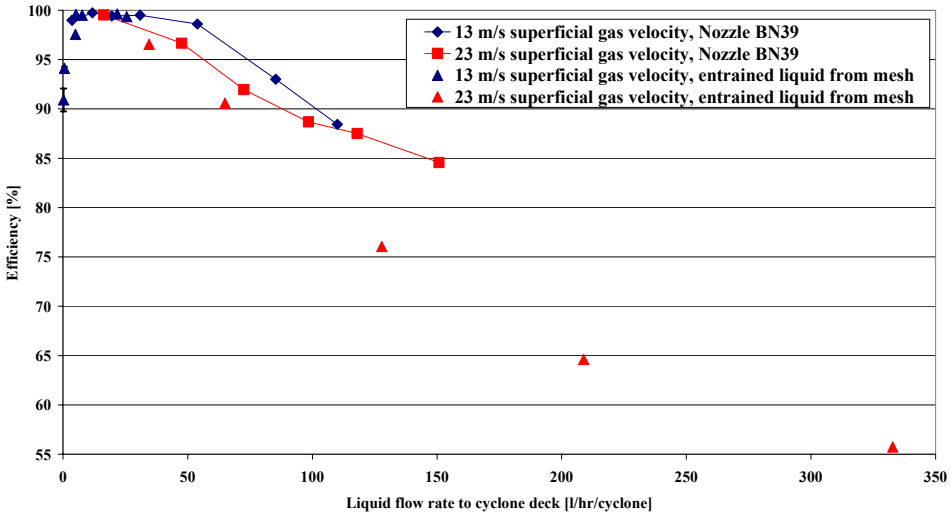

Figure 4.15 The cyclone efficiency as function of liquid load when Exxsol is either introduced through nozzle BN39 or as entrainment from the mesh pad.

A superficial gas velocity of 13 m/s corresponds to a K-value in the vessel equal to 0.117 m/s. That means that the mesh pad is slightly below or slightly above the flooding point, -dependent upon the liquid concentration. When the mesh pad is below the flooding point, it acts as a filter and only small droplets pass and enter the cyclone. This explains the reduced efficiency for these points. When the mesh pad is operated above the flooding point, larger droplets are entrained and the liquid is evenly distributed to the cyclones. For these experimental points, the liquid carry-over from the mesh pad is evenly distributed to the cyclones and maximum efficiency is therefore expected (no liquid mal distribution). The efficiency for the points marked as '13 m/s, cyclone above mesh pad' agrees well with the results obtained by use of nozzle BN39 injections. However, when the gas and liquid loads are increased further the liquid above the mesh pad starts to pulsate. This transient behaviour is related to liquid hold-up in the mesh pad. When a large amount of liquid is present inside and on top of the mesh pad, the pressure builds up below the mat. Finally, when the pressure exceeds a certain limit, a gas jet discharges through the mat causing liquid entrainment in the form of a liquid jet to the cyclones. At regular intervals, the cyclone therefore experiences a sudden increase in liquid and that behaviour has a bad influence on the performance. When the superficial velocity in the cyclones is 23 m/s, the vessel K-value is 0,156 m/s. Now, the efficiency is reduced compared to the corresponding results obtained by use of the nozzle despite the fact that the mesh pad is placed approximately 0.8 m below the cyclone deck –which is a relative large distance in a scrubber.

The total scrubber efficiency is influenced by the liquid jet to the cyclones as well as uneven gas and liquid distribution. The total scrubber efficiency of the experiments shown in Figure 4.13 and Figure 4.14 has been plotted in Figure 4.16. As seen, the efficiency is above 90 % for all experiments. The efficiency decreases with increasing gas and liquid load.

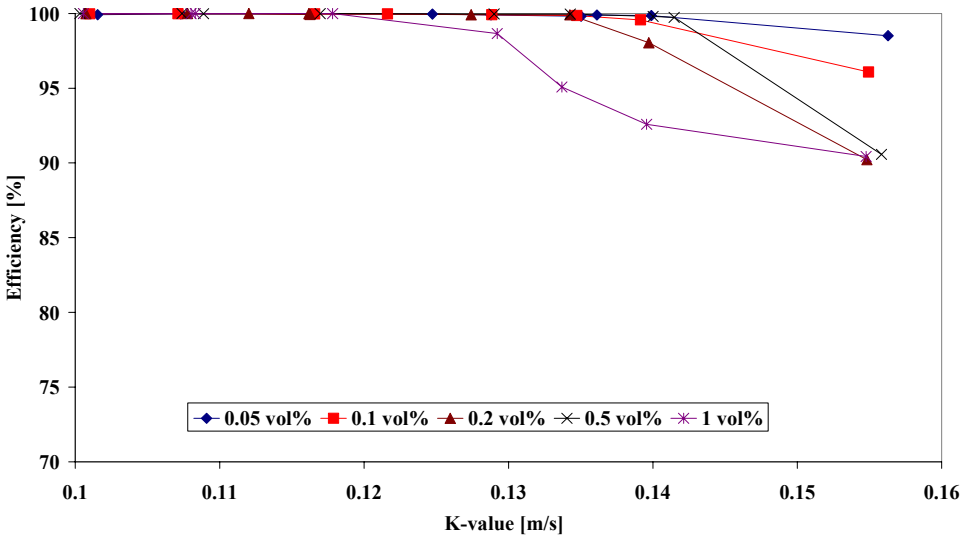

Figure 4.16 The total scrubber efficiency of the experiments where liquid is injected in the upstream piping.

4.1.6 Pressure Drop

The pressure drop over the cyclones and mesh pad was measured in all experiments, but in the air/water experiments the measurement was corrupted due to water in one of the legs in the pressure difference meter.

Cyclone Pressure Drop

The measurements for all air/Exxsol D60 experiments are shown in Figure 4.17. The pressure drop is presented in terms of the Euler number, Eu, (pressure drop coefficient):

$$Eu = \frac{\Delta P}{\frac{1}{2}\rho_g v_g^2} \tag{4.2}$$

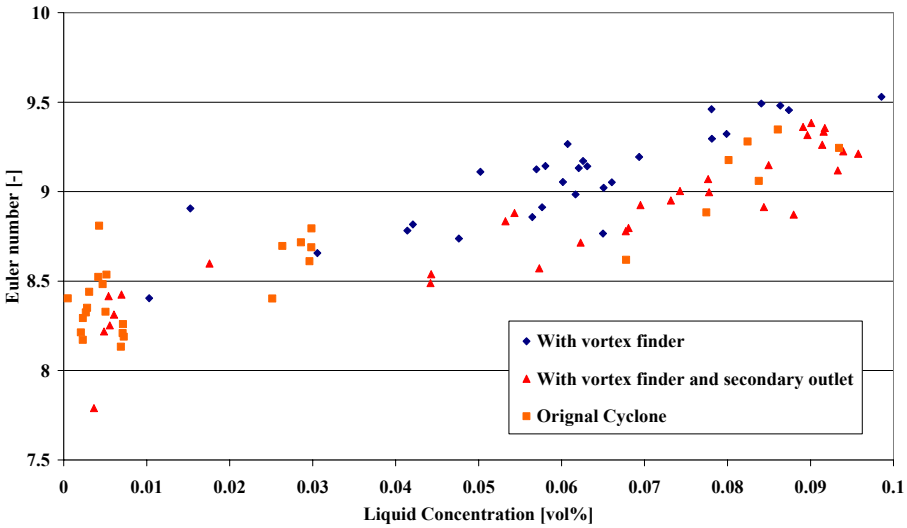

Figure 4.17 The pressure drop coefficient for the cyclone in the air/Exxsol D60 experiments. The different colours refer to the different versions of the cyclone.

The Euler Number is a characteristic for the pressure drop over a dry cyclone. However, when liquid is present the Euler Number is not constant but becomes dependent on the liquid load. The pressure drop in a reverse flow cyclone with tangential inlet is expected to decrease when liquid (or solid) is introduced3. A decrease in the pressure drop cannot be seen in the present experiments and that is similar to results achieved with swirl tubes (Hoffmann and Stein, 2002). The different modifications to the cyclone have got little effect on the pressure drop, but generally the presences of the vortex finder increases the pressure drop, while opening the secondary outlet decreases the pressure drop. The latter result is also consistent with the results of NG (2005).

Pressure Drop over Mesh Pad

The pressure drop over the mesh pad is shown in Figure 4.18. The pressure drop is very low when the mat is operated below the flooding point. During flooding, the liquid is held up in the in the mesh pad thus forming a layer of liquid and bubbles, which at increased gas velocities, mounts from the bottom to the top of the mesh where it finally breaks through. This process is accompanied by a large increase in pressure drop. Dependent on the liquid load, the pressure drop increases with a factor 5 – 10 when the K-value is increased from 0.10 – 0.14 m/s. When the gas load is further increased, the increase in pressure drop is not as steep as it is during flooding. This behaviour is more distinct for low liquid concentrations.

[3] This statement is valid for concentrations up to 50 g/m3 solid loading (Hoffmann and Stein, 2002)

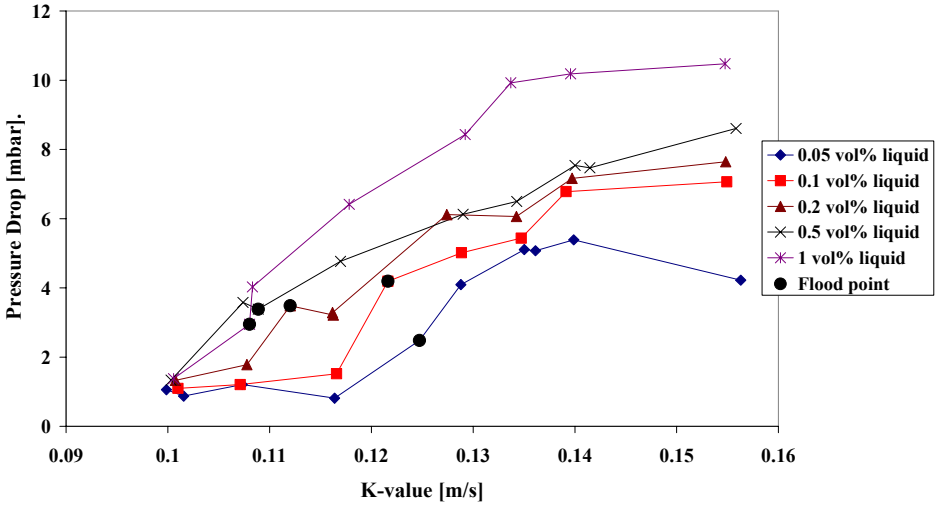

Figure 4.18 The pressure drop over the mesh pad for different liquid concentrations in the inlet pipe.

4.2 High-Pressure Rig Results

The HP-rig has been used in order to produce results that do not need to be extrapolated to conditions that are relevant for real scrubbers. The term "real scrubbers" refer to scrubbers that are in operation in the fields today, as distinct from most results from low-pressure laboratory rigs that most often operate with non-relevant fluids and very limited pressure and temperature ranges. The previous described LP-rig is a laboratory rig in this category.

The HP-rig has been used to investigate the difference between a model fluid (N_2/Exxsol) and a natural gas system. The N_2/Exxsol D60 model system can be considered as two separate phases where only small amounts of liquid are dissolved in the gas phase and vice versa. The natural gas system on the other hand, is a three-component system in two-phase equilibrium. The physical properties of the natural gas system are much more dependent on pressure than the N_2/Exxsol system where only the gas density varies significantly with pressure. Three different operating pressures have been used as a basis for the experiments in the high pressure rig: 20, 50 and 92 bara. All experiments are carried out in the temperature range 20 – 25^{o}C.

Two cyclones are placed in parallel in the top of the test scrubber for the HP-rig tests. The cyclone deck is placed 865 mm above the mesh, which in turn is placed

485 mm above the inlet vane. These ratios of internal distance to vessel diameter are large compared to real scrubber solutions.

As opposed to a real scrubber, the drain pipe from the cyclone deck does not proceed down to the liquid sump in the bottom of the test scrubber, but penetrates the scrubber wall and the liquid is thereby collected in a separate drain tank.

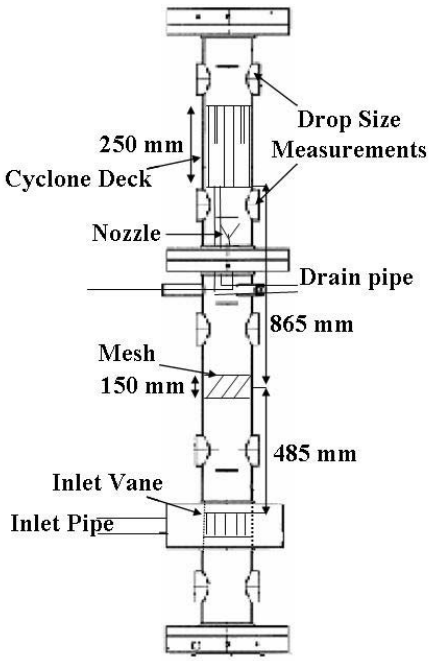

Figure 4.19 The setup in the I.D. 150 mm test scrubber in the HP-rig

4.2.1 The Modified Verlaan Cyclone

The modified cyclone as shown in Figure 4.6 has been used as the demisting cyclone in the setup for the HP-rig. This cyclone geometry has been tested by introducing the liquid through the nozzle below the two cyclones (Figure 4.19). Taking into account the relatively small diameter of the test scrubber (0.15 m), the gas and liquid flow is assumed to be evenly distributed to the cyclone deck. The separation efficiency at different pressures is plotted against the superficial gas velocity in the cyclone in Figure 4.20. In these experiments the rate of injected liquid was controlled such that in total 90 l/hr reached the cyclone deck (45 l/hr per cyclone). For all cases, the efficiency decreased with increasing gas load. For the 20 and 50 bara cases, the experiments agreed well when N_2/Exxsol D60 and the natural gas fluid were used, respectively. When the pressure was increased to 92 bara, the efficiency was radically lower for the natural gas fluid case indicating that the different physical properties of the two cases are crucial for the performance. The differences are mainly in the interfacial tension, liquid density and liquid

viscosity. In those cases where the natural gas case has slightly better efficiency than the corresponding N_2/Exxsol case, the gas density of the natural gas is lower and is likely to cause the difference.

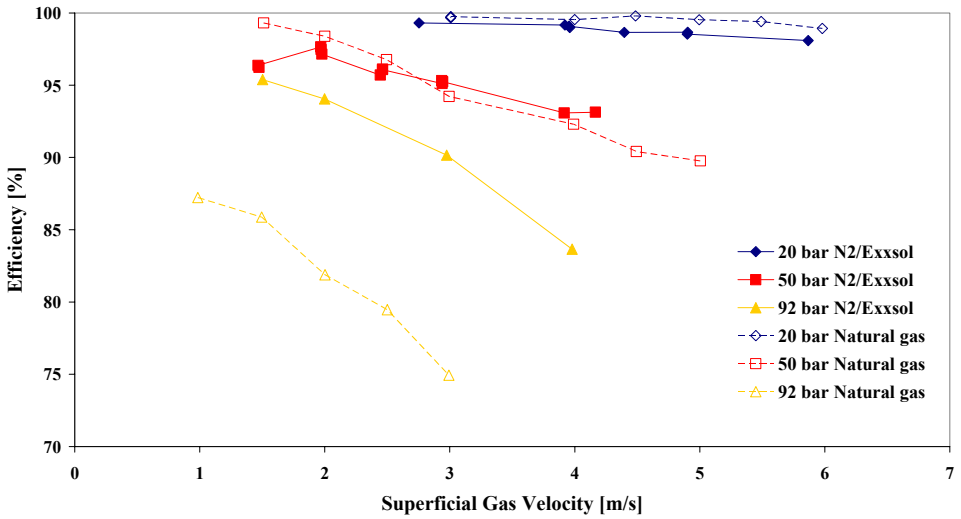

Figure 4.20 The cyclone efficiency when the liquid load to the cyclones was kept constant at 45 l/hr per cyclone

The gas dynamic pressure ($\rho_g v_g^2$) increases if the superficial gas velocity is kept constant while the pressure is increased (and hence increasing gas density). The gas flow capacity of the rig is related to the gas dynamic pressure and therefore the cyclones were generally tested at lower velocities at high pressure than at low pressure. 3 m/s superficial gas velocity was the only velocity that was tested at three pressures. At this velocity, the K-values in the vessel were 0.11 m/s at 20 bara and 0.26 m/s at 92 bara pressure.

The amount of liquid influences the performance and therefore the liquid load was varied while the superficial gas velocity was kept constant at 3 m/s. The result is plotted in Figure 4.21.

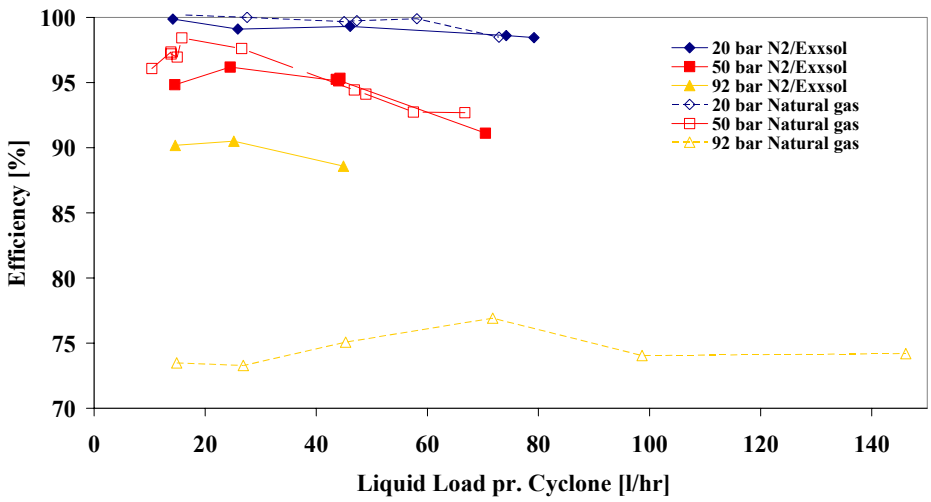

Figure 4.21 The cyclone performance at varying liquid loading. The superficial gas velocity was constant, 3 m/s, for all experiments in the plot.

In most cases, the efficiency dropped off when the liquid load was increased. The only exception was when liquid load was below 20 l/hr. At these low liquid rates, a larger fraction of the liquid was distributed as a fine mist and the separation efficiency of small droplets may determine the efficiency rather than re-entrainment.

Once again the efficiency was very much lower when natural gas was used compared to N_2/Exxsol at 92 bara.

Due to capacity limitations in the drainpipe from the cyclone deck, only results from experiments with liquid load less than 80 l/hr per cyclone are plotted. However, in the 92 bara natural gas case, the liquid was drained more efficiently and some additional tests at higher loads are plotted for this case. During these latter experiments, a valve above drain tank 2 was slightly open (see Figure 3.3). This valve was connected to piping further downstream in the process loop were the pressure was slightly lower. The pressure difference helped the liquid from the cyclone drain chamber down in the drain tank.

4.2.2 Inlet Vane and Mesh Pad

The inlet vane and the mesh pad are expected to do the bulk separation before the remaining liquid enters the demisting section (cyclone deck). The combined efficiency of these units is therefore referred to as the primary efficiency. The primary separation efficiency of the scrubber was tested by injecting liquid in the

inlet pipe two meters upstream of the inlet vane. The K-value in Equation (4.3) was varied identically for all three test pressures and both fluid systems. In Figure 4.22 the liquid concentration has been kept constant at 0.2 vol% in all experiments and the resulting efficiency for the inlet vane + Mesh (primary separation) has been plotted as function of the K-value.

$$K = u_{g,s}\sqrt{\frac{\rho_g}{\rho_l - \rho_g}} \tag{4.3}$$

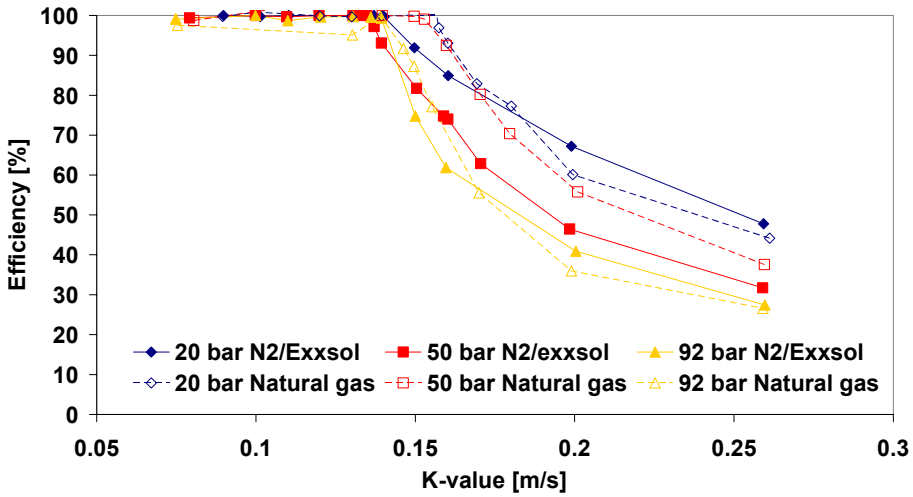

Figure 4.22 The primary separation efficiency as function of the K-value for two different fluid systems with 0.2 vol% liquid at three pressures

The primary efficiency is above 95 % for all experiments below K = 0.14 m/s. Most experiments in this region have efficiency close to 100 % but some of the experiments, especially the 92 bara Natural gas case show lower efficiency. During these experiments the mesh pad was operated below flooding conditions so the measured carry-over is most probably related to small droplets that penetrate the mesh pad.

The sudden break in the curves is associated with flooding conditions in the mesh pad. The break in the curve generally occurs at lower K-values for the N_2/Exxsol system compared to the natural gas system even though the physical properties of the last system are more severe in terms of separation efficiency. There are two possible reasons for this:

- The K-value over-compensates for the liquid density so that the resulting superficial gas velocity is reduced too much when experiments with two different liquid densities are compared
- Since the superficial gas velocity is less in the natural gas cases compared to the corresponding N_2/Exxsol cases at the same K-value, the absolute amount of liquid is also less since the experiments are compared in terms of equal liquid concentration (vol%) and not absolute liquid rate (l/hr). The flooding velocity is dependent on liquid rate (Sherwood et al., 1938) as discussed in Chapter 0. This is not accounted for in the expression

The deviation in break point in the curves in Figure 4.22 is probably a combination of the two mentioned effects. The deviation is better illustrated by the pressure drop as will be commented in Section 4.2.4.

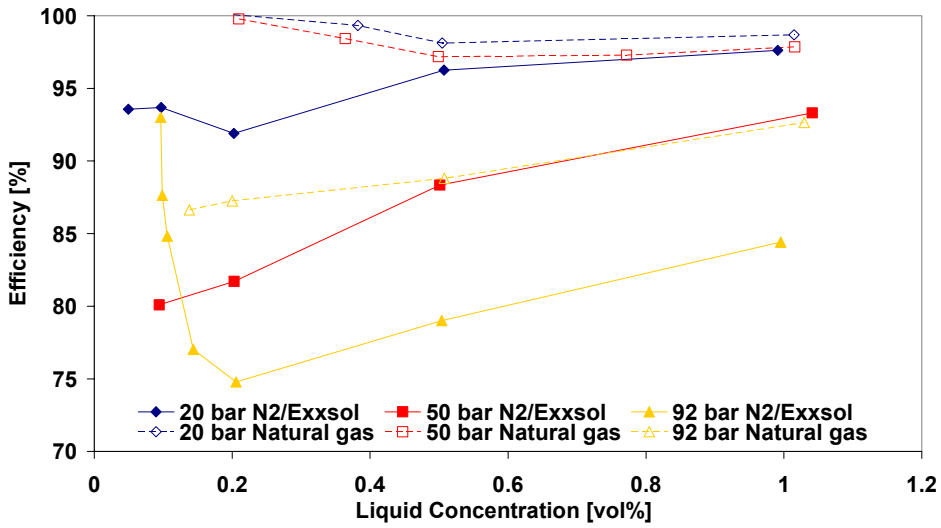

Figure 4.23 The primary separation efficiency of the test scrubber at K = 0.15 m/s for varying pressures and fluids.

In Figure 4.23, the primary separation efficiency is shown as function of liquid concentration. In the majority of these experiments, the mesh pad is operated under flooded conditions. The fractional efficiency is generally increasing with increasing liquid concentration, (but the absolute liquid carry-over from the mist mat is not decreasing). An exception from this behaviour is found at small liquid concentrations, but the reason for this is that the experimental points are very near to the flood point when the K-value is 0.15 m/s. When the mesh pad is at its flooding point or slightly above, the efficiency drops off with increasing liquid load. When the liquid load is further increased i.e. operating conditions are tuned further above flood point, the efficiency increases. This behaviour is best demonstrated by the curve for N_2/Exxsol at 92 bara where a steep decrease in

efficiency was found between 0.1-0.2 vol% liquid. For this curve the flooding point can be found when liquid concentration is just below 0.1 vol% and K = 0.15 m/s.

For the same reasons as mentioned in comments on Figure 4.22, the natural gas experiments in Figure 4.23 have a generally higher efficiency than the N_2/Exxsol experiments. The flood point for the 20 and 50 bara natural gas cases actually occur at liquid concentrations between 0.3 and 0.5 vol% for this K-value.

At K-values above 0.2 m/s the opposite trend is expected i.e. the natural gas efficiency will be lower than corresponding N_2/Exxsol experiments. In this study the maximum gas load that has been tested is K = 0.26 m/s. In Figure 4.24 the primary separation efficiency for the most severe conditions in this study is plotted. The experiments show that the efficiency is little dependent on liquid concentration within the tested range. Approximately 1/3 of the liquid is captured, so the cyclone deck will receive 2/3 of the liquid from the inlet pipe.

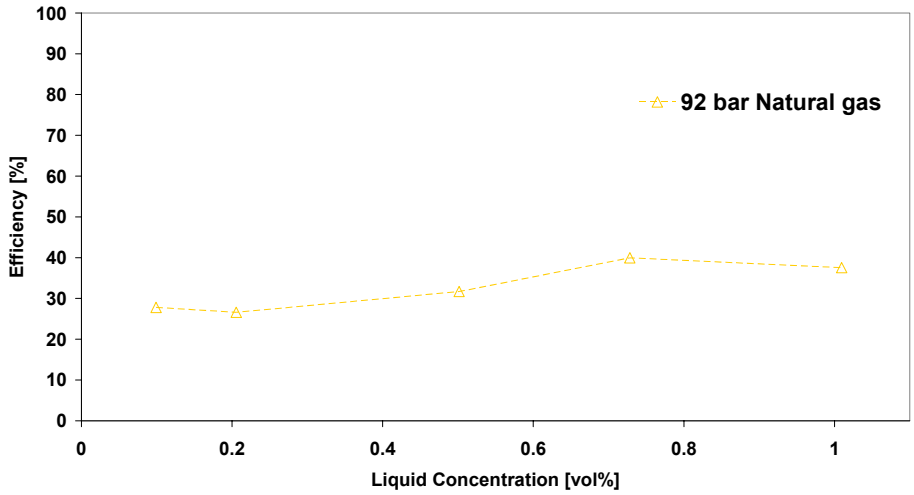

Figure 4.24 The primary separation efficiency at max. gas load and varying liquid concentration

4.2.3 Total Scrubber Efficiency

The total scrubber efficiency for varying gas loads with 0.2 vol% liquid is shown in Figure 4.25. All experiments show efficiency larger than 85%. The trend is that increasing operating pressure is accompanied by decreasing efficiency. For instance, with natural gas at 92 bara, the liquid carry-over is an order of magnitude larger than the carry-over at 20 bara, when the K-value is 0.26 m/s in both cases.

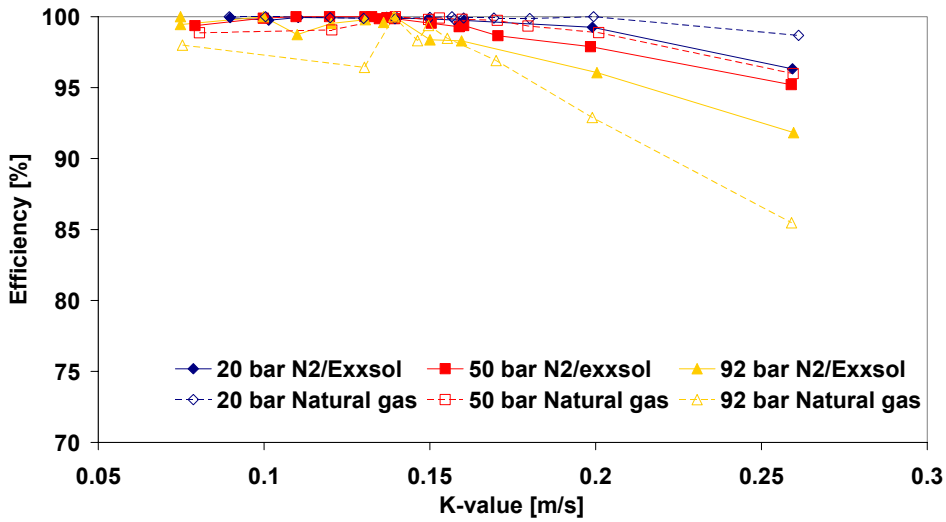

Figure 4.25 The total scrubber efficiency with 0.2 vol liquid concentration in inlet pipe at varying gas loads

At low K-values (below flooding velocities) the total scrubber efficiency and the primary efficiency in Figure 4.22 is much the same. This shows that the majority of the small droplets that penetrates the mesh pad also penetrate the cyclones

The total efficiency of the standard scrubber with K = 0.15 m/s is shown in Figure 4.26. This K-value is the maximum value that is recommended by the NORSOK-standard (2001) for a scrubber of the present configuration (inlet vane, mesh and cyclones). At this K-value the efficiency is not so much dependent on liquid concentration. However, this behaviour should not be extrapolated to liquid concentration levels higher than the tested range, as other effects related to maximum liquid rate in cyclone deck can play an important role.

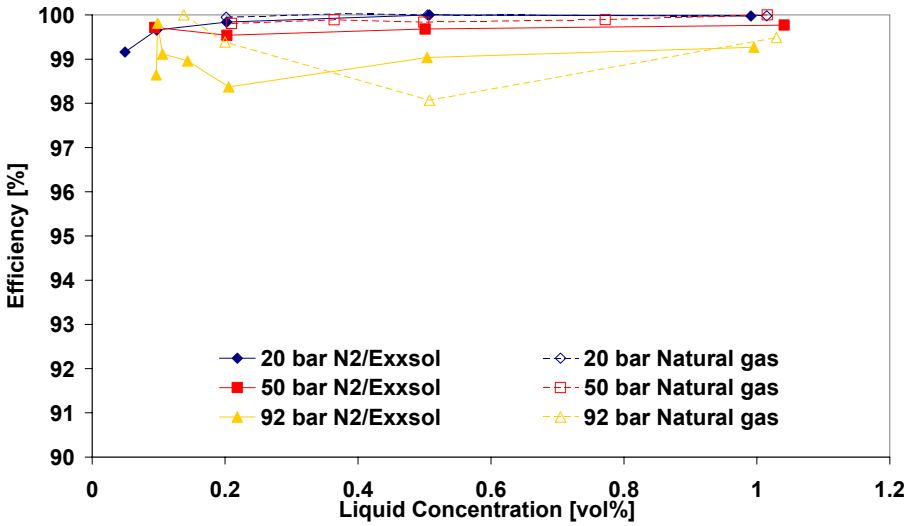

Figure 4.26 The total scrubber efficiency at the maximum K-value recommended by the NORSOK-standard (K=0.15 m/s)

The total efficiency in the region near K = 0.15 m/s, is very influenced by the fact that the operating conditions is very near flooding conditions. Especially the low liquid concentrations in Figure 4.26 are very sensitive for small changes in the process and that is probably the explanation on the spread in the results for 92 bara N_2/Exxsol. At higher K-values the process conditions are more stable and the total efficiency is not much dependent on liquid concentrations as can be seen from K = 0.26 m/s in Figure 4.27. The exception is the point for 1 vol% liquid where the efficiency drops. In this case the liquid loading to the cyclone deck is 100 l/hr pr. cyclone which is around or slightly above the limitation for the drain pipes as described in Section 4.2.1.

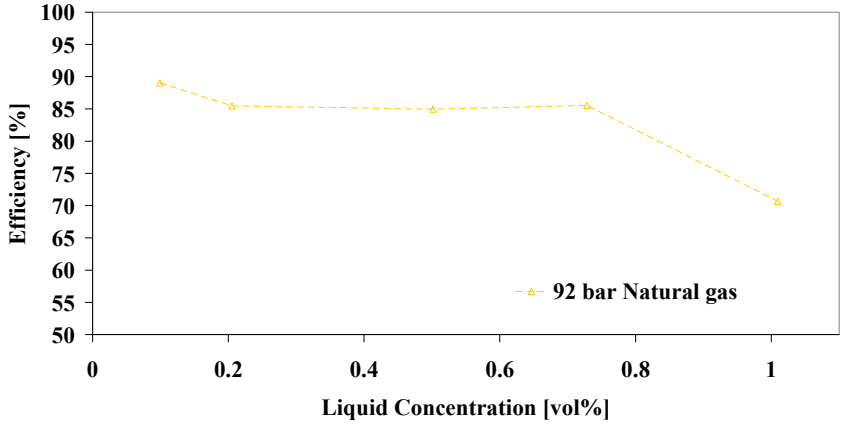

Figure 4.27 The total scrubber efficiency at the maximum gas load tested (K=0.26 m/s)

By comparing this figure with Figure 4.24 one can see that the primary separation units (inlet vane and mesh pad) removes approximately 2/8'th fraction of the liquid, 5/8'th is removed by the cyclone deck while the last 1/8'th of the liquid is carried over top of the scrubber and further downstream. Hence, it is the cyclone deck that has to do the major job at this high K-value and good cyclone design will therefore contribute most to the total efficiency.

4.2.4 Pressure Drop

The setup for the pressure drop measurements in the HP-rig is shown in Figure 4.28. The pressure differential cells are in contact with the system pressure through 1/4" legs that penetrate the scrubber wall. The legs proceed one centimetre into the process and thereby through any possible liquid film on the wall. The exception is the measurement for the drain chamber of the cyclone where the 1/4" pipe is connected through the top plate of the cyclone deck. Measurements have been carried out over the mesh pad and cyclones. In addition pressure drop measurements over the cyclones have been divided in two parts,

1. Pressure drop from below to drain chamber and
2. Pressure drop from drain chamber to outlet.

The sum of these two pressure drop measurements should be equal to the total pressure drop. In order to minimize the influence of any dynamical contribution to the measured pressure above the cyclone deck, a vortex breaker has been installed in order to attenuate a strong swirl that has been observed during the experiments in the LP-rig.

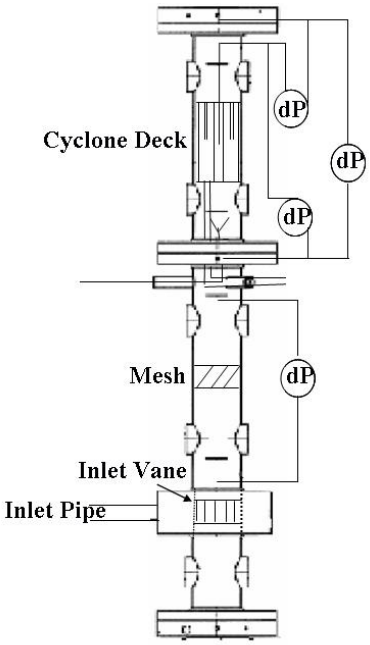

Figure 4.28 The pressure drop measurement in the HP-rig

Cyclone Pressure Drop

The pressure drop measurements have been used to calculate the Euler number $\left(\Delta P \middle/ \left(1/2\,\rho_g v_s^2\right)\right)$ for the different experiments. The Euler numbers are plotted in Figure 4.29.

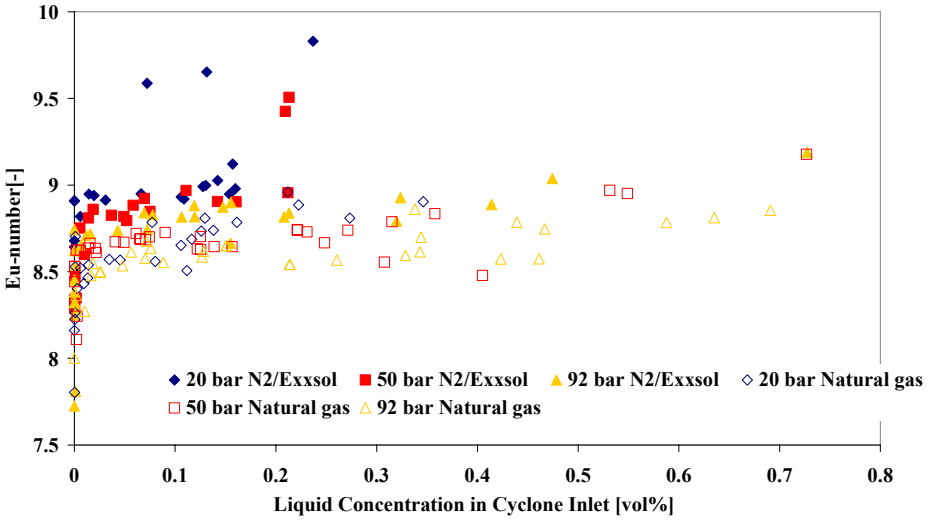

Figure 4.29 The cyclone pressure drop as function of liquid concentration in the cyclone inlet

The experiments show a large spread in Euler Number even at dry conditions (no liquid carry-over from the mesh pad). The reason for this might be uncertainties related to the measurements or it could also be due to differences in gas viscosity (i.e. the Reynolds number), which is a property that is not included in the expression for the Euler Number. The general tendency is that the pressure drop is larger in the N_2/Exxsol experiments than in the natural gas experiments. This is probably due to the higher liquid density for the Exxsol liquid which makes it more energy consuming to carry through the cyclone. There is a weak tendency for the pressure drop to increase as the liquid load increases.

Pressure Drop over Mesh Pad

The pressure drop over the mesh pad is shown in Figure 4.30. This is very much related to the amount of liquid that builds up in the mesh pad which again depends on the gas lift. Therefore the results are plotted against the K-value. At the lowest K-values the pressure drop is dependent on the gas velocity and density. As the K-value increases, a sudden increase in pressure drop can be seen. This increase happens when liquid starts to build up in the mesh pad so the sharp break in the curve is actually a good way of identifying the flood point. When the pressure drop is plotted against the K-value, the flood point for the N_2/Exxsol experiments occur at approximately the same value -independent on operating pressure. This shows that the K-value can be a reasonable way of pressure scaling for simple model fluid systems where physical fluid properties other than gas density, do not change much. However, the results show that K-value is not a good way of scaling natural gas fluids, especially if the scaling is based on experiments with simple fluid systems like the N_2/Exxsol-fluid. Reasons for the mismatch between the flood points between the two different systems are discussed in Section 4.2.2 and include

over-compensation of the liquid density in the K-value, dependency on actual liquid rate and lack of connection between flood point and other physical fluid properties than the densities.

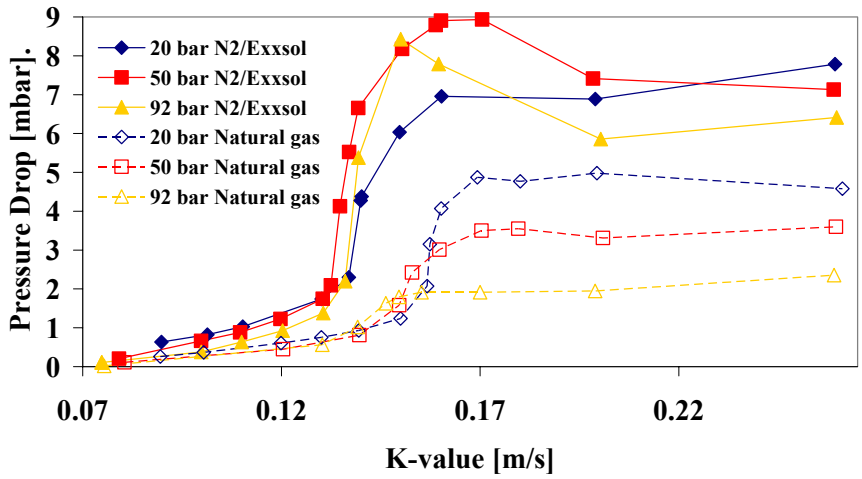

Figure 4.30 The pressure drop over the mesh pad as functions of the K-value for two different systems at constant liquid concentration = 0.2 vol%

When the K-value is further increased above flood point, more and more liquid builds up inside and above the mesh. This liquid build-up is accompanied by an increase in pressure drop until the point where the gas lift becomes so strong that the amount of liquid build-up decreases due to entrainment. When this happens, the contribution to the total pressure drop that is associated with gas-liquid interactions also decreases. For the N_2/Exxsol experiments this contribution decreases more than the increase that is associated with the increased gas flow and, hence, the total pressure drop decreases. For the natural gas experiments, the contribution from the gas-liquid interactions is less and therefore it is matched by the increasing gas flow as the K-value is increased above 0.17 m/s.

4.2.5 Droplet Size Measurements

Measurements of the droplet size distribution (DSD) have been very challenging. The biggest problem has been to keep the windows free from liquid contamination. When liquid contaminated the window, the specially designed purge system (see Section 3.2.3) could remove the liquid film, but still some kind of deposition on occasion remained on the surface of the glass. When this happened, the rig had to be depressurized, the windows demounted and then cleaned. This could only be done when the rig was charged with the relatively cheap nitrogen, but when the rig was charged with natural gas fluid, this was not an option and contamination was therefore very difficult to deal with. In many cases the liquid came from condensed

vapour in the purge gas. Pre-conditioning of the purge gas was therefore needed to ensure that it was absolutely free of liquid.

The 200 mm Fourier lens that was used, had an upper detectable limit for the droplets size of 400 microns. In almost all cases, the largest droplets were considerably larger than the limit. This includes the droplet sizes in the liquid injected through the nozzle upstream of the cyclones, the liquid injected through the nozzle in the inlet pipe and the liquid above a flooded mesh.

Droplets Above a Non-flooded Mesh

When the mesh pad was operated below the flooding point, some droplet measurements were made. At this condition the mesh acted as a filter and removed the largest droplets and only droplets below 400 microns remained in the gas flow downstream. The mean size of the droplets measured above the mesh at constant K-value, increased with increasing pressure as can be seen in Figure 4.31

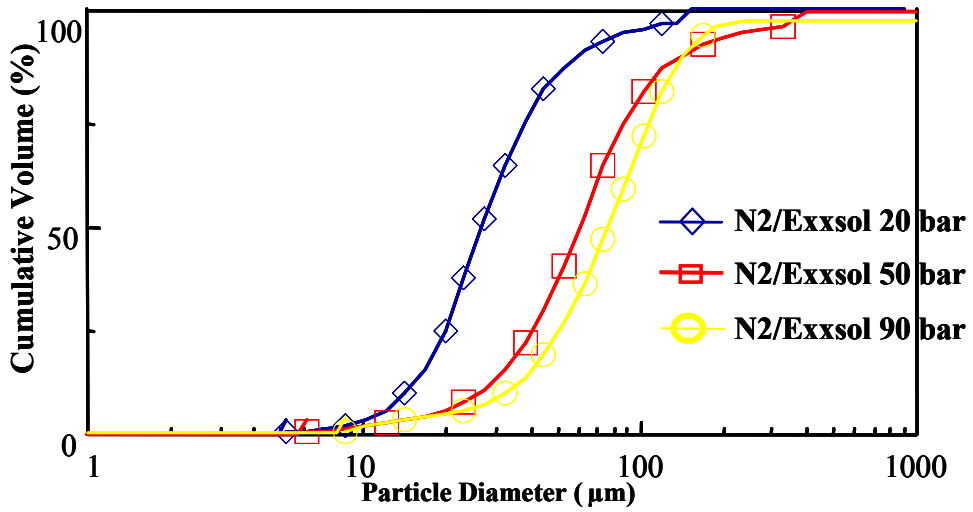

Figure 4.31 The cumulative droplet size distribution above the non-flooded mesh when the scrubber K-value was 0.1 m/s and 1 vol% liquid was injected in the inlet pipe.

However, the liquid concentration also increases with increasing pressure so the shift of the DSD-curve does not mean that fewer small droplets are being offered to the cyclones. The volumetric liquid concentration is increasing from 160 ppm (20bara) to 3000 ppm (50 bara) and 5000 ppm (90 bara). 5000 ppm corresponds to 0.5 vol%. This relatively high liquid concentration is much higher than the concentration calculations based on the gas and liquid flow rates and shows that the liquid hold-up is considerably high. When compared to the measured liquid load to

the cyclones, it shows that the measured concentration is approximately 500 times higher than the calculated based on the flow rates.

Droplet Size Distributions from Natural Gas Condensation

When natural gas has been used as fluid, some few measurements were made when the liquid in the gas was produced by condensation rather than as injected liquid. The liquid condensation occurred when a temperature gradient was induced in the heat-exchanger downstream the gas circulator. The liquid was carried by the gas to the inlet vane –where some of it was separated- and then through the mesh pad. Above the mesh pad the DSD of this fine fog was measured at three different K-values. The measurements were taken at 92 bara pressure and are plotted in Figure 4.32

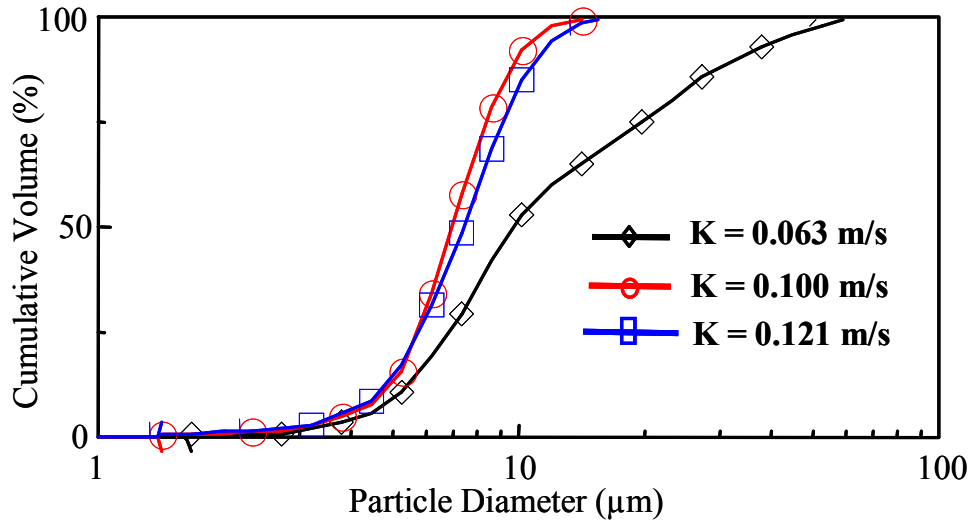

Figure 4.32 The droplet size distribution above the non-flooded mesh when the droplets were formed by natural gas condensation under 92 bara pressure.

These measurements show droplets so small that they might be comparable to the cut size of the cyclone. Typical results from the low-pressure set-up of Brunazzi and Paglianti (1998) showed that droplets below 10 microns generally were difficult to separate in the current mesh pad.

The concentrations of the three measurements were all approximately 640 ppm, so that difference in liquid hold-up is less likely to explain the difference in DSD for the lowest K-value (K = 0.063 m/s). The droplets are so small that they will easily be carried with the gas instead of bouncing up and down above the mesh pad before they eventually reach the cyclone deck.

4.3 K-lab Results

Testing at the K-lab rig is very expensive compared to testing in the LP- and HP-rig, but the produced data are also very unique as scrubber data from this geometry and/or pressure scale has never been published in the public domain. Due to the expenses and time limitations, the total amount of data produced at K-lab is much less compared to the amount produced in the HP- and LP-rig. The focus has been to vary the gas load when 0.2 vol% liquid is injected in the upstream pipe, and to vary the liquid load when K-value was 0.15 and 0.26 m/s. The tests have been carried out around three different operating pressures in the test scrubber: 28, 55 and 113 barg. Note that the pressure in the K-lab loop is not constant throughout the loop due to the gas lift in the compressor. Neither is the loop placed in a temperature controlled climate chamber as opposed to the HP-rig. The actual pressure in the test scrubber may therefore vary ± 1 bar from test to test around the three given test pressures.

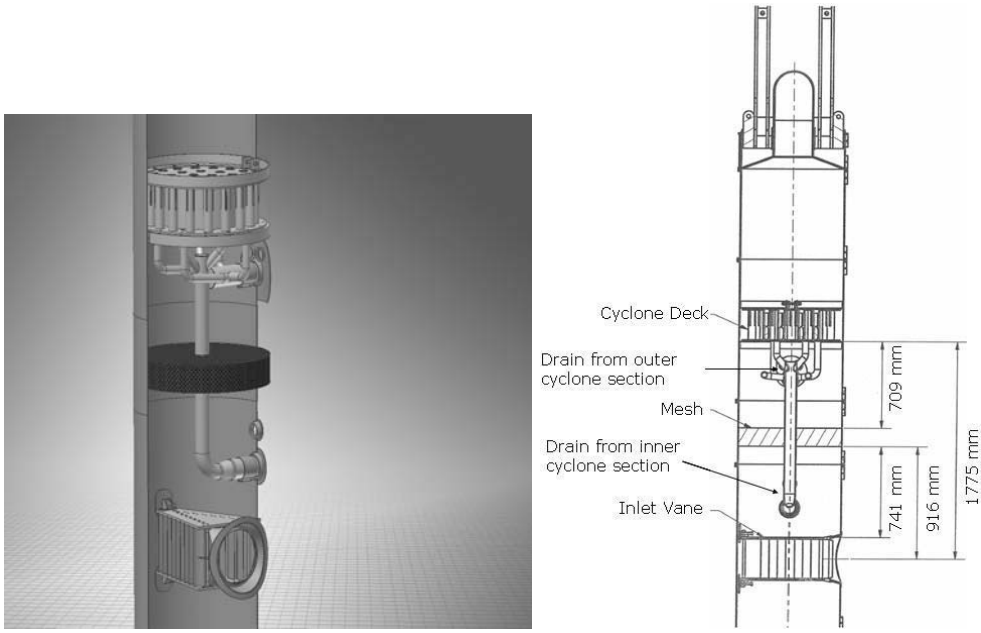

Figure 4.33 The total scrubber configuration in the K-lab tests

The test setup in the K-lab rig is the standard setup that has also been used in the two other rigs. Drawings of the setup are shown in Figure 4.33. The distances between the mesh and the cyclone is the same as in the two other test rigs while the distance between the inlet vane and mesh is somewhat larger as explained in Section 3.4. The cyclone deck holds 31 cyclones, and the drain compartment is divided in two different parts with separate drain pipes as will be discussed in more detail in Section 4.3.5.

The liquid was injected in the straight inlet pipe through nozzles placed more than 10 meters upstream of the inlet vane. As opposed to the HP-rig, no nozzles were placed inside the test scrubber.

4.3.1 The Modified Verlaan Cyclone

In this section the results from the cyclone deck with the modified version of the 31 Verlaan cyclones are presented. The cyclone performance has not been tested independently of the inlet (i.e. no nozzles have been used to inject liquid below the cyclone deck). It was therefore not possible to steer by a fixed liquid load to the cyclones. Hence, it was not possible to investigate the efficiency as function of the gas load at a specific liquid load. For this reason, the cyclone efficiency can only be plotted as function of varying liquid load at a fixed gas rate. The cyclone efficiency when the vessel K-value is 0.26 m/s is shown in Figure 4.34.

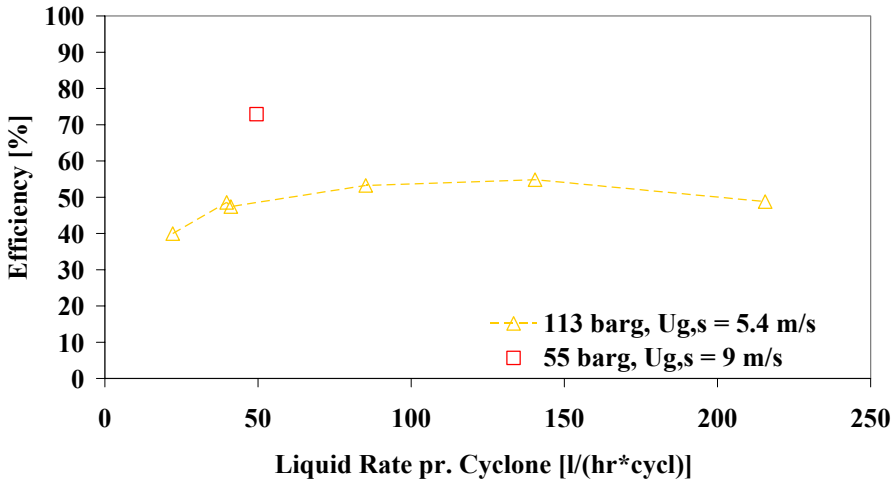

Figure 4.34 The cyclone efficiency as function of the average liquid load per cyclone for vessel K = 0.26 m/s at two different pressures. The velocity in the legend refers to the superficial velocity in the cyclone.

The efficiency seems to increase with increasing liquid load up to 100-150 l/hr per cyclone while at higher liquid loads, the trend is the opposite. The efficiency with the 55 barg operating pressure is better than at 113 barg, for K = 0.26 m/s. At this K-value, the velocity is much higher when the pressure is 55 barg compared to the 113 barg case. The result may indicate that small droplets may contribute significantly at average liquid loadings below 100 l/hr per cyclone, while at higher liquid loadings the liquid carry-over is governed by some kind of re-entrainment mechanisms.

The liquid flow rate was also varied at K = 0.15 m/s, but the liquid load to the cyclone was very low at this K-value -typically less than 1 l/hr.

4.3.2 Inlet Vane and Mesh Pad

The liquid concentration in the inlet pipe was held constant =0.2 vol% for K ranging from 0.1 – 0.26 m/s. The efficiency of the inlet vane and mesh pad – hereafter referred to as the primary efficiency- is plotted in Figure 4.35. The tests with 0.2 vol% liquid concentration have been carried out at two pressures, 55 and 113 barg. As seen, the efficiency declines rapidly when K exceeds 0.17-0.18 m/s. Once again, the efficiency is lowest at the higher of the two tested operating pressures, and at K =0.26 more liquid is entrained than separated by primary separation devices.

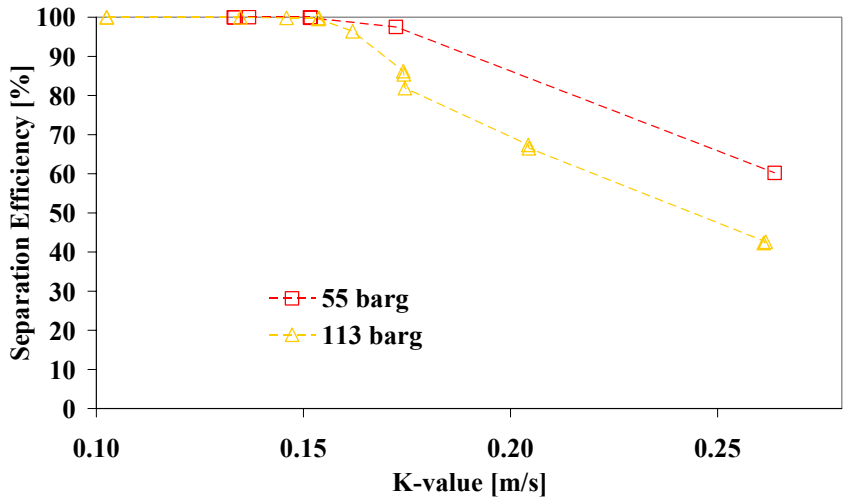

Figure 4.35 The primary efficiency for a liquid concentration in inlet pipe =0.2 vol%

For K = 0.17 at 113 barg pressure, three repetitions have been carried out. In the repetition that gave the lowest efficiency, the liquid flow rate in the test scrubber and degasser was continuously measured by coriolis meters, while liquid accumulation tests were carried out for the two other repetitions. The liquid flow rate in the test scrubber and degasser were in the lower operating range for these experiments. Still the liquid flow rate was so large that the liquid capacity in bottom of the test scrubber only allowed an experiment to last for 10-15 minutes. Such a short test period makes the average test results vulnerable for process variations that would have been more or less neutralized in a 30 minute test period. The described reasons can explain the scatter in the three repetitions for this test conditions.

The primary efficiency has been tested as function of liquid concentration in the inlet pipe at two different *K*-values, 0.15 and 0.26 m/s. The result from these tests can be seen in Figure 4.36 and in Figure 4.37. The NORSOK-standard (2001) recommends that a scrubber with inlet vane + mesh + cyclones, should be designed with maximum *K*=0.15 m/s. The results from Figure 4.36 show that the inlet vane and the mesh are capable of doing the separation without the need of any cyclones in the top of the scrubber. Only for the 113 barg pressure case a significant amount of liquid carry-over has been detected, but the efficiency is still better than 99.5 %. The results indicate that the mesh pad is in a non-flooded condition at $K = 0.15$ m/s within the tested range of liquid concentrations, so the liquid carry over in the 113 barg case may be small droplets that have penetrated the mesh pad.

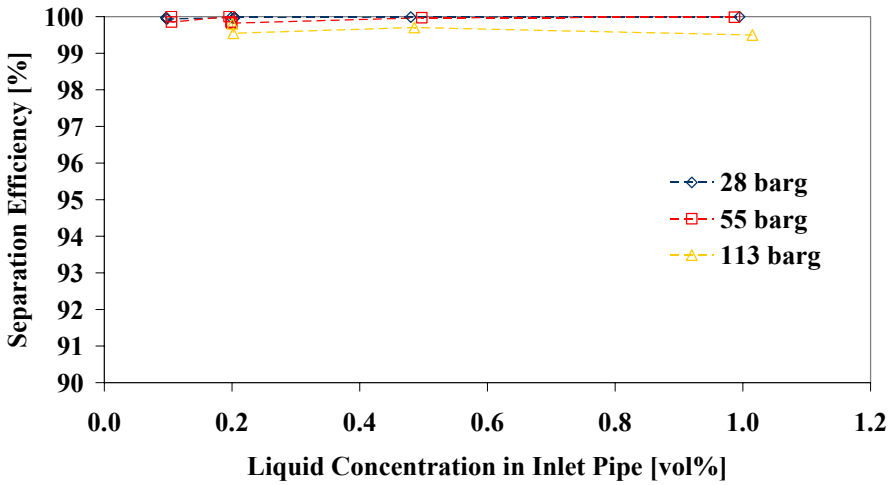

Figure 4.36 The primary efficiency as function of the liquid concentration in the inlet pipe for vessel K = 0.15 m/s

At $K = 0.26$ m/s the mesh pad is in a flooded condition, and the separation efficiency is well below the efficiency that was found at $K = 0.15$ m/s. For the lowest liquid concentrations at the highest test pressure, the primary efficiency drops below 40 %. However, at this *K*-value the efficiency is very dependent on the liquid concentration. For both test pressures the efficiency is increasing with increasing liquid concentration, and for the highest test pressure the efficiency varies from 35 % to nearly 80 % within the tested range of liquid concentrations.

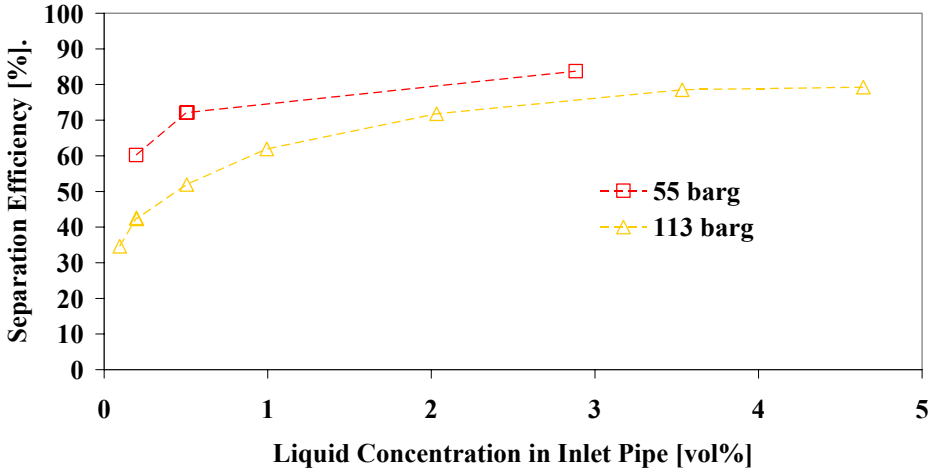

Figure 4.37 The primary efficiency as function of the liquid concentration in the inlet pipe for vessel K = 0.26 m/s

4.3.3 Total Scrubber Efficiency

The total scrubber efficiency for varying *K*-values is plotted in Figure 4.38. The experiments show only the results when the liquid concentration is kept constant = 0.2 vol% in all experiments. The efficiency is close to 100% until the *K*-value exceeds 0.16 – 0.17 m/s. At higher K-values the efficiency drops off rapidly. The trend is more severe at the highest of the two test pressures. Based on the trends from the primary efficiency and the cyclone efficiency in the two previous sections, the total efficiency is expected to be better at liquid concentrations higher than 0.2 vol%.

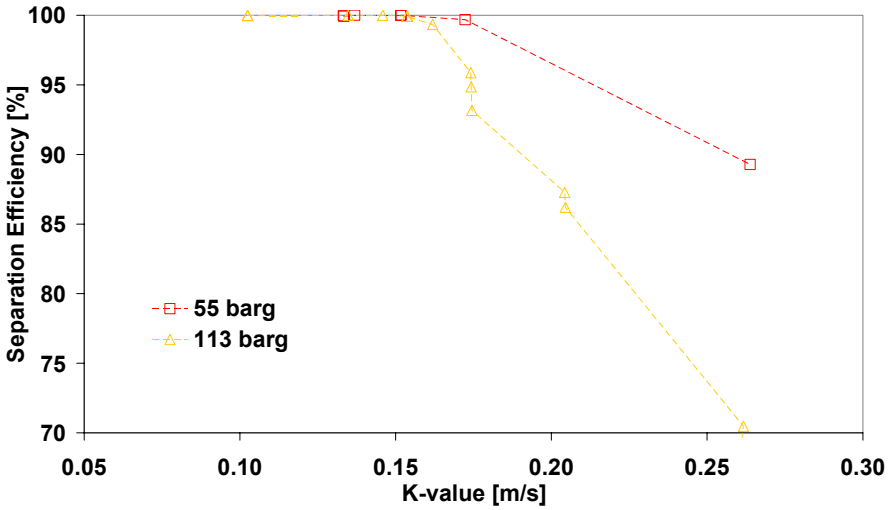

Figure 4.38 The total scrubber efficiency for 0.2 vol% liquid in the inlet pipe at varying K-values

At recommended max. K-value, according to the NORSOK standard (2001), the efficiency is better than 99.9 % in all tested cases as seen in Figure 4.39. The inlet vane and mesh pad is responsible for almost all the separation in this case. If these results are compared with the primary efficiency in Figure 4.36 it can be seen that the cyclones are offered a significant amount of liquid only in the 113 barg case.

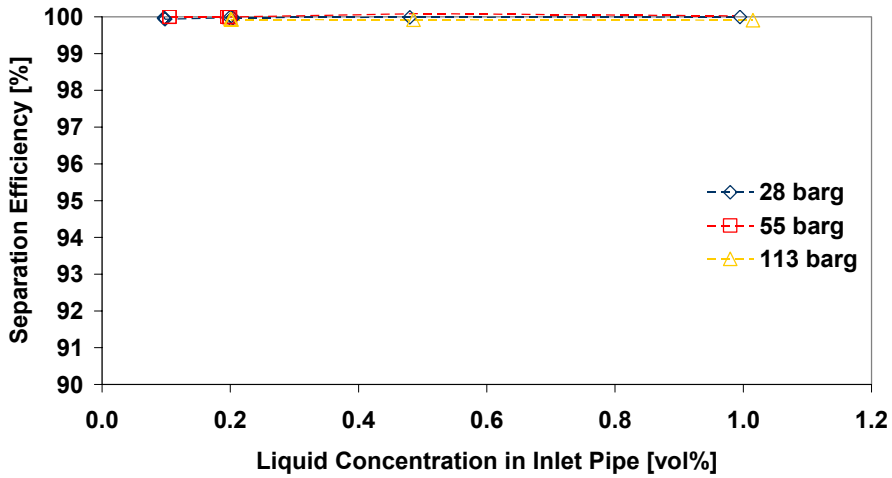

Figure 4.39 The total scrubber efficiency at K = 0.15 m/s for varying liquid concentrations

When the K-value exceeds 0.16-0.17 m/s the primary efficiency declines rapidly and becomes very dependent on liquid load as pointed out in the previous section. The total scrubber efficiency is also very dependent on liquid load for these *K*-values as can be seen from Figure 4.40. The trend of the total efficiency with increasing liquid concentration is comparable with the trend of the corresponding primary efficiency. The total efficiency is hence governed by the primary separation devices. For the lowest liquid concentration at 113 barg, the inlet vane and the mesh pad removes 35% of the liquid while the cyclones remove roughly 25% of the liquid while 40 % is carried over top of the scrubber. At higher concentrations the primary separation becomes increasingly important and the inlet vane and mesh pad removes a larger fraction of the total liquid rate. For 3.5 vol% the inlet vane and the mesh pad removes 79%, the cyclones 13% while 8% is carried over the top of the scrubber.

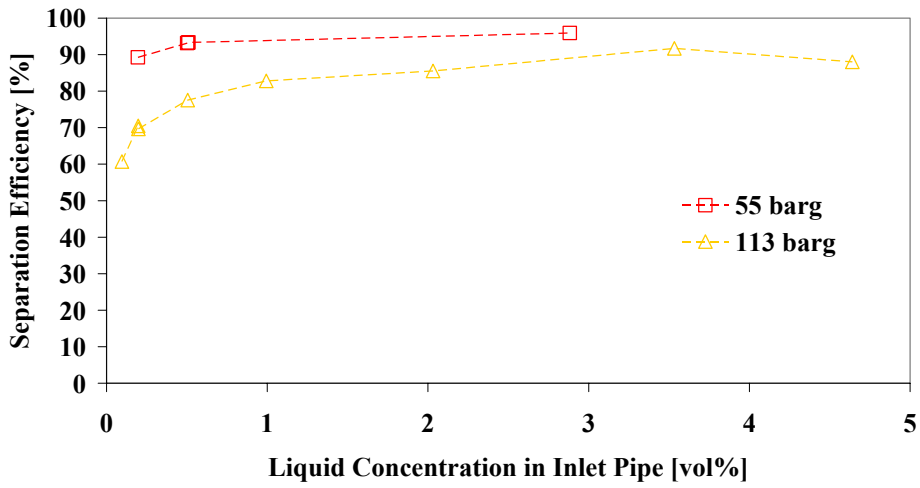

Figure 4.40 The total scrubber efficiency at *K* = 0.26 m/s for varying liquid concentrations

4.3.4 Pressure Drop

Pressure drop measurements have been carried out for all the tests in the K-lab rig. An overview over the different measurements is sketched in Figure 4.41. The pressure drop over the cyclone deck is not measured directly but will appear as the sum of the pressure drop from upstream to the drain compartment and from the drain compartment to downstream the cyclone deck.

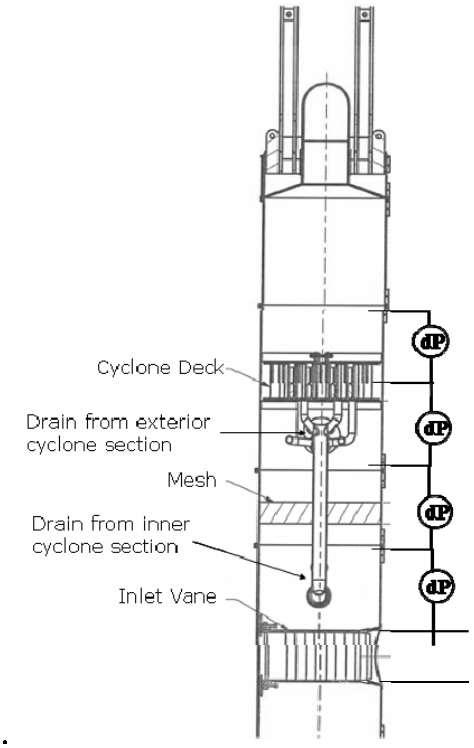

Figure 4.41 An overview of the pressure drop measurements carried out during the K-lab experiments

Pressure Drop over Mesh Pad

Pressure drop measurements over the mesh pad when 0.2 vol% liquid is injected in the inlet pipe are shown as function of K-value in Figure 4.42. The pressure drop information is limited for the 28 and 55 barg cases, but for the 113 barg case a detailed trend of the pressure drop at varying liquid concentration is produced. At a K-value of 0.15 m/s, the pressure drop increases with increasing operating pressure. However, no sudden increase in pressure drop was found as expected around flooding although such an increase had been expected. The pressure is increasing slightly steeper around 0.15 – 0.17 m/s. This may indicate that a transition to fully flooded conditions takes place.

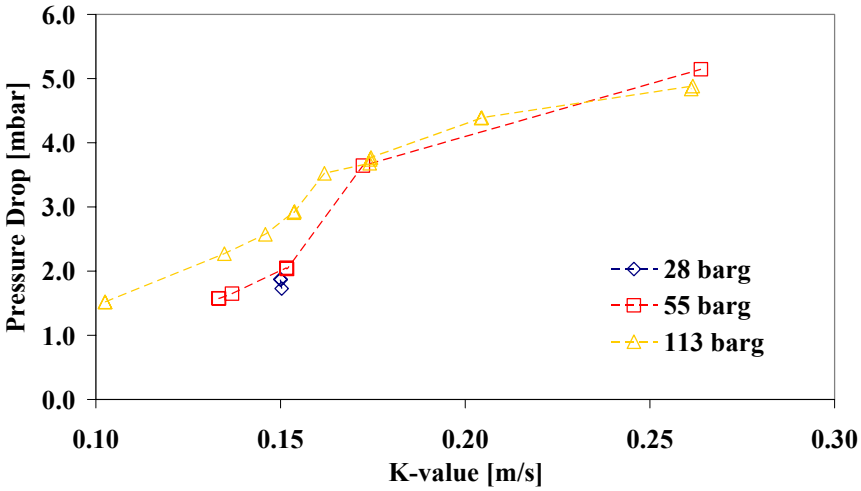

Figure 4.42 Mesh pad pressure drop when 0.2 vol% liquid was injected in the inlet pipe

Note that the pressure drop is larger at the highest pressures when compared on basis of the K-value at the same liquid concentration. This is despite the fact that the liquid density becomes lower with increasing pressure while pressure drop in general is expected to increase with increasing liquid density. This trend may change when the K-value is well beyond the flooding point and for the experiment at K = 0.26, the pressure drop is larger in the 55 barg case than in the 113 barg case.

The differences in the 113 barg case versus the 55 barg case are that both the fluid properties and process conditions are different. The liquid density, liquid viscosity and interfacial tension are lower for the 113 barg case. Since the comparison is made on basis of the K-value, the gas dynamic pressure ($\rho_g v_{g,s}^2$) and the liquid loading in the inlet pipe (not concentration) are also lower in the 113 barg case, while the gas viscosity is approximately 22% higher. The latter is the only differences that could give a contribution to the increased pressure drop in the 113 barg case, since the gas friction coefficient might increase with decreasing Re_g.

A likely explanation for the increased pressure drop at higher pressures might be that the separation in the inlet vane is less efficient in the 113 barg case than in e.g. the 55 barg case. If the inlet vane efficiency is sufficiently lower at the highest pressure, the total liquid loading to the mesh might be higher in this case than at lower pressures despite the fact that less liquid is injected in the inlet pipe in the 113 barg case. Higher liquid loading to the mesh might increase the pressure drop due to a higher transfer of momentum from the gas phase to the liquid phase.

Cyclone Pressure Drop

The pressure drop in the cyclones is measured as the sum of the pressure drop from:

1. Upstream of the cyclone deck to the drain chamber
2. The drain camber to downstream of the cyclone deck

The pressure drop in the cyclones is increasing with increasing liquid concentration in the cyclone inlet as shown in Figure 4.43.

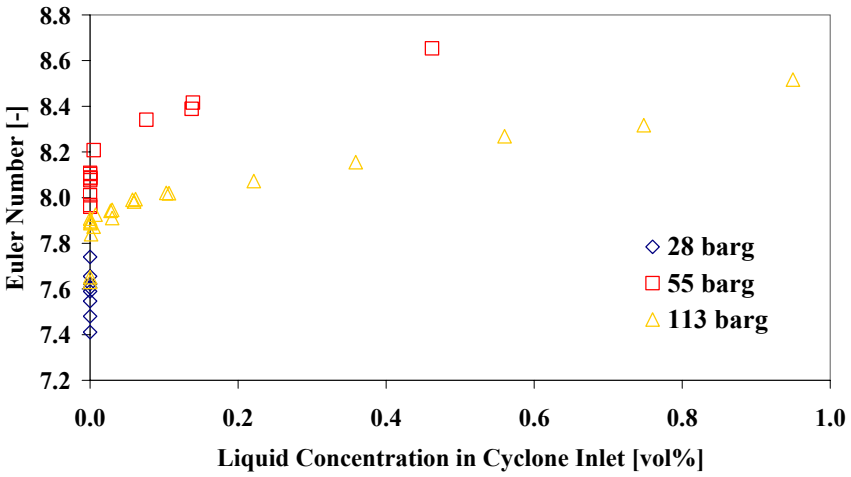

Figure 4.43 The figure shows the Euler number over the cyclone deck at varying liquid concentrations in the cyclone inlet. The liquid concentration is calculated based on the total gas and liquid flow rates to the cyclone deck.

The Euler number is larger in the 55 barg case than in the 113 barg case. This is the opposite trend than the trend found for the pressure drop over the mesh pad. The pressure drop increases with approximately 8% when the liquid load is changed from very small amounts of liquid up to 1 vol%.

4.3.5 Liquid Distribution to the Cyclone Deck

A special layout for the drain chamber made it possible to divide between the liquid separated by the outer and the inner cyclones. Hence, it was possible to give a quantitative measure for any uneven liquid distribution to the cyclone deck.

A drawing of the cyclone deck with the drain system is shown in Figure 4.44. As can be seen, 18 cyclones are located in the outer drain section and 13 cyclones are located in the inner drain section. The liquid from the outer cyclones are routed to

the upper drain manifold, while the liquid from the inner cyclones are routed to the lower drain manifold.

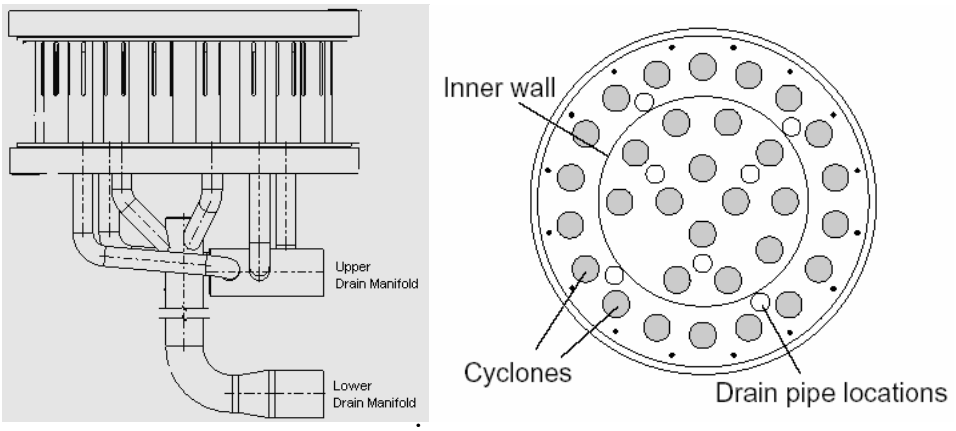

Figure 4.44 The figure shows the special drain arrangement for the cyclone deck. An inner wall was placed in the drain chamber so that the liquid from the outer and inner cyclones were drained separately

The drain pipes from the lower deck were attached to a manifold that were routed out of the test scrubber above the mesh pad, while the drain pipes from the inner section were connected to a manifold that were routed through the mesh pad and the test scrubber wall below the mesh. Once outside the wall, the liquid in the manifolds could either be routed to the degasser or back to the bottom of the test scrubber.

Some few experiments were repeated once. During the first test all the liquid was routed to the degasser, while during the repetition, the liquid from the inner section of the drain chamber where routed back to the bottom of the test scrubber. If the liquid was evenly distributed to the cyclone deck, the amount of liquid during the second test should be 18/31 of the amount that was measured during the first test. However, this was not the case and a large deviation from this was found. The rate between the average liquid loadings captured per cyclone in the outer to the inner section was calculated as:

$$L_{frac} = \frac{\dot{Q}_{drain,outer} \Big/ 18}{\dot{Q}_{drain,inner} \Big/ 13} = \frac{\dot{Q}_{drain,outer} \Big/ 18}{\left(\dot{Q}_{drain,total} - \dot{Q}_{drain,outer} \right) \Big/ 13} \tag{4.4}$$

If the liquid flow is evenly distributed to the cyclones L_{frac} will be equal to unity. However, the relationship in Equation (4.4) showed that the average amount of liquid drained from the outer cyclones were 2 – 2.5 times larger than the average amount of liquid drained from the inner cyclones. Note that the expression for L_{frac}

only accounts for the captured liquid that has been drained from the cyclone deck. Results from the HP-rig showed that the efficiency of the individual cyclones generally drops off with increasing liquid load. For that reason the actual liquid loading per cyclone in the outer section might have been even larger than 2.5 times the cyclones in the inner section but due to lower efficiency for the cyclones with the highest liquid loading. The average liquid loading per cyclone in the inlet cannot therefore be calculated.

There are two obvious reasons for the uneven distribution of liquid below the cyclone deck. First off all, the gas flow pattern above an inlet vane might not provide a homogeneous mixture of liquid and gas. An uneven liquid distribution below the mesh pad might also result in an uneven liquid distribution above. Secondly, the pipes and drain manifold below the cyclone deck (see Figure 4.45) might disturb the gas and liquid flow sufficiently so that the inner cyclones are shielded and more of the liquid enters the outer cyclones.

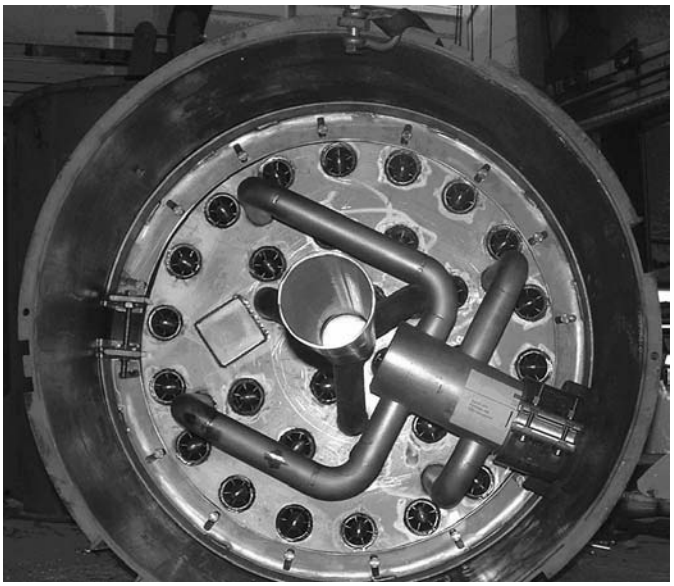

Figure 4.45 The picture shows how the upper and lower drain manifolds are blocking parts of the cross section area below the cyclone deck.

The results show that large scale scrubber performance cannot be predicted on basis of results from small scale rigs solely, since the total performance is influenced by uneven gas/liquid distributions occurring in large scrubbers.

CHAPTER 5

Further Analyses and Discussion

Three experimental rigs have been used to investigate the performance of a standard scrubber design. In this chapter, results from the different rigs are compared in order to point out differences related to the size of the scrubber. Also, the performance of each internal have bee discussed in light of the different results from the different rigs in order to reveal the most important mechanisms behind liquid carry-over. Wherever possible, the impact of the changing fluid properties has been quantified, but also qualitatively analyses have been made.

5.1 Primary separation

The term 'primary separation' refers to the combined performance of the inlet vane and mesh pad. The efficiency was close to 100% whenever the mesh pad was in a non-flooded condition, but as the gas or liquid rates increased above the flooding conditions, the efficiency decreased rapidly. In this section the performance of the inlet vane and the mesh pad in the three different rigs is compared and commented.

5.1.1 Inlet Dynamic Gas Pressure

The inlet dynamic gas pressure is defined as the kinetic energy of the gas phase in the inlet pipe, $\rho_g u_{g,s}$ where the superficial gas velocity is taken as the ratio of the volumetric gas flow to the cross sectional area of the inlet pipe. The NORSOK standard (2001) recommends that the inlet dynamic pressure should be kept below 6000 Pa when an inlet vane is used to distribute the gas and liquid in a scrubber. For further details on this subject it is referred to Section 0.

Since the gas rates in the present study has been varied systematically with the K-value, the actual inlet dynamic gas pressure varied with pressure due to changing $\Delta\rho$ that has an effect on the gas velocity. At increasing pressure the gas velocity is decreasing, and it is increasing more rapidly when natural gas is used instead of N2/Exxsol. Also the ratio of the inlet pipe diameter to the scrubber diameter determines the inlet dynamic gas pressure at a given K-value. This ratio is quite small in the LP-rig where it is 0.205, while it is 0.326 and 0.306 in the HP-rig and K-lab rig, respectively. Smaller ratio means higher inlet dynamic gas pressure at a given K-value.

In Figure 5.1 the inlet dynamic gas pressure in the different rigs used in the present study are shown for various pressures and fluids. As seen, it is much higher in the LP-rig than in the two other rigs. This is both due to the low pressure and the relatively small inlet pipe as discussed above. The inlet dynamic gas pressure is also generally higher in the K-lab rig than in the HP-rig, but it was always kept below the NORSOK limit in these rigs as opposed to the LP-rig.

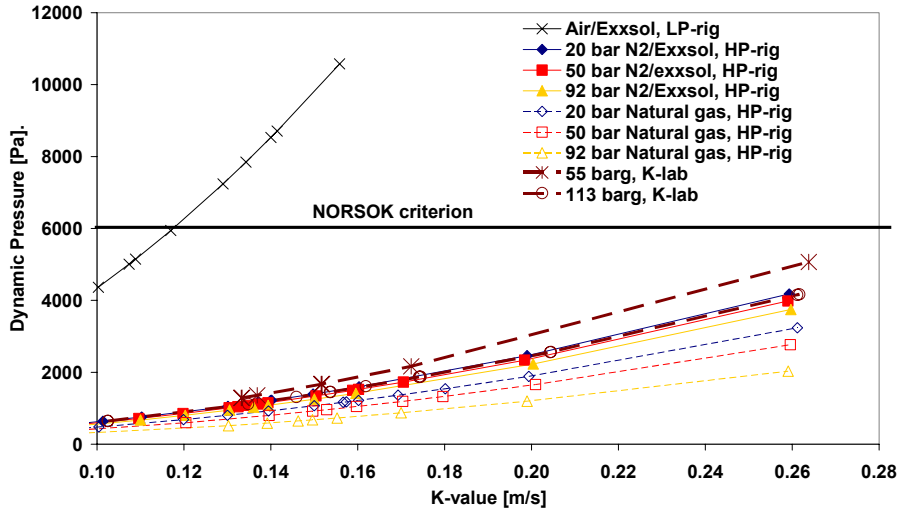

Figure 5.1 The inlet dynamic gas pressure in the three different rigs at different pressures and fluids

The motivation for recommending an upper limit as it is done in the NORSOK standard, is to keep the shear forces between the gas and liquid low. High shear forces may produce a fine mist that is more difficult to separate. However, the criterion is very rough as it does not account for the interfacial tension which obviously must play an important role in determining the size distribution and the amount of mist.

5.1.2 Mesh Pad Flooding

It was not possible to measure the amount of liquid that was separated by the inlet vane in any of the experimental rigs in the present tests. Therefore the exact liquid load to the mesh pad is not known. However, in many cases, an upper value for the K-value is set to ensure that the mesh pad is operated in a non-flooded condition. This criterion does not include the liquid load at all.

The flood point in the present experiments occurs at different K-values in the different rigs. In Figure 5.2 the pressure drop in the LP-rig and HP-rig are compared when 0.2 vol% Exxsol was injected in the inlet pipe. While flooding in the HP-rig was well defined as seen with the sudden increase in pressure drop, the flooding in the LP-rig occurred more gradual. The indicated flooding point in the figure is the point where the first visible liquid started to break through at the top of the mesh pad. However, at K = 0.12 – 0.13 m/s the entire mesh pad was in a flooded condition. Flooding in the LP-rig, hence, occurred at a lower K-value than in the HP-rig

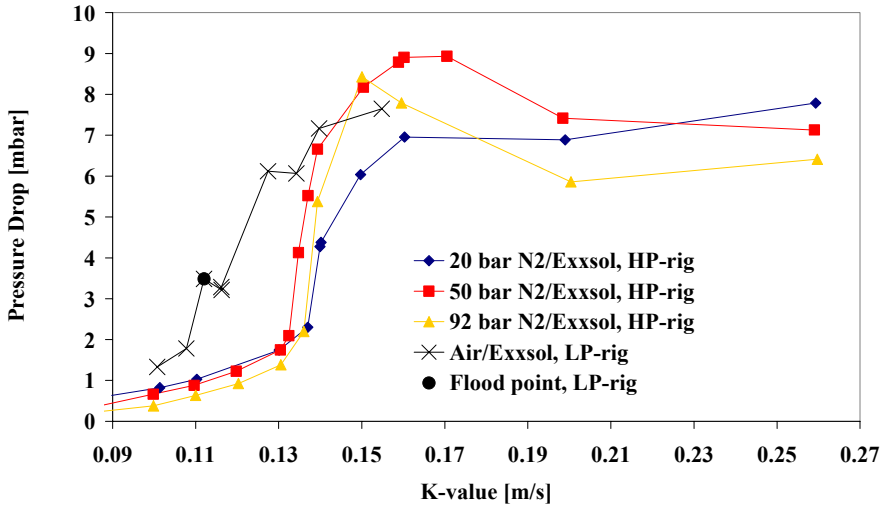

Figure 5.2 The pressure drop over the mesh pad in the LP-rig and HP-rig when Exxsol was used as liquid. The tests are carried out with 0.2 vol% liquid injected in the inlet pipe.

The pressure drop over the mesh pad is shown in Figure 5.3 when natural gas was used as fluid. The results from the HP-rig and the K-lab rig, when comparable fluids were used, are compared. The K-lab rig was not transparent and it could therefore not be seen directly how the flooding process occurred. However, the pressure drop curves from the K-lab tests show no sudden increase as seen in the HP-rig. Instead the pressure drop increases gradually although slightly steeper

around K = 0.15 m/s. The gradual flooding process in the LP-rig was seen through visual sections. This process was accompanied by a pressure drop curve that is comparable to the curve obtained at K-lab, but the curve in the LP-rig is steeper. This indicates that the flooding process at K-lab is also a more gradual process. The shape of the pressure drop curves seems to be connected to the size of the scrubber. The liquid below the mesh pad in a large scrubber might be more unevenly distributed than in a smaller scrubber, and thereby some parts of the mesh pad become flooded at lower K-values, than other parts.

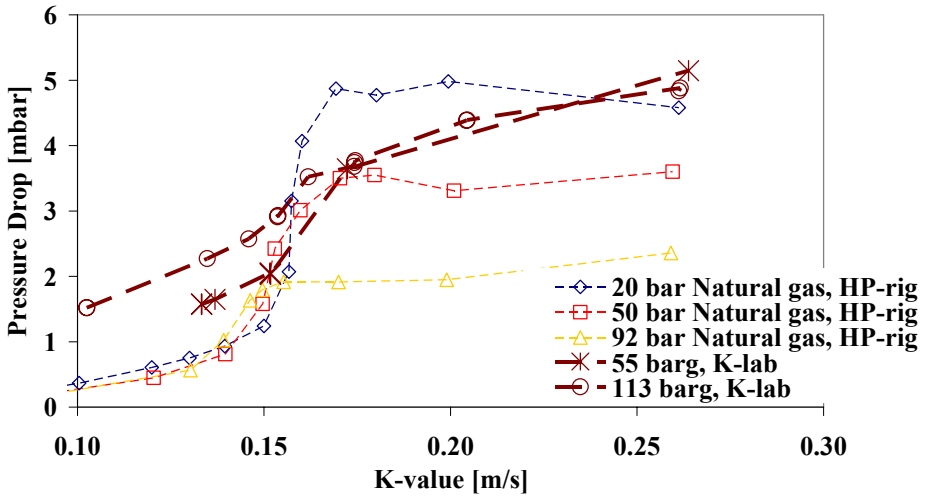

Figure 5.3 The pressure drop over the mesh pad in the HP-rig and the K-lab rig when natural gas was used as fluid. The tests are carried out with 0.2 vol% liquid injected in the inlet pipe.

The flooding point depends on, gas load, liquid load and some physical fluid properties as explained in Section 2.5.2. However, the K-value seems to be a suitable parameter for rougher design evaluations, since the flood point occurred at K-values in the range from 0.1 – 0.15 m/s in all experiments in the present study, where liquid concentrations up to 1 vol% were tested. The general tendency was that the flood point occurred at higher K-values at high-pressure than at low-pressure conditions. The velocity is much higher at low pressure than at high pressure when the K-value is kept constant and this might be a possible explanation for the difference. Also, since the comparison are made on basis of experiments with constant vol% liquid, the actual liquid load in the inlet pipe are higher in the low-pressure experiments than in the high-pressure experiments at the same K-value.

The actual liquid loading to the mesh pad in each case is not known, but by using the correlation for estimation of flooding in mesh pads given by Bürkholz (1989), the liquid loading to the mesh pad can be calculated for the flooding points. The

liquid load can be found from calculating the gas load parameter for the flooding point;

$$\frac{A_s u_{g,s}^2}{\varepsilon^3 g}\frac{\rho_g}{\rho_l}\mu_l^{0.2} \tag{5.1}$$

Then the corresponding dimensionless liquid load parameter can be found:

$$\frac{\dot{m}_l}{\dot{m}_g}\sqrt{\frac{\rho_g}{\rho_l}} \tag{5.2}$$

From the flooding curve given in Figure 2.8, the corresponding value for the expression in Equation (5.2) is found, and the liquid load can then be calculated. Further details are given in Section 2.5.2.

If the actual liquid loading to the mesh pad is known, the efficiency of the inlet vane can also be calculated for the flooding points. The efficiency based on these calculations is shown in Figure 5.4 for the HP-rig experiments. The calculated efficiency drops off with increasing pressure and the efficiency for the natural gas experiments is less than for the N2/Exxsol experiments as expected due to more critical fluid properties. However, the calculated efficiency is negative at 92 bara pressure and natural gas case. In other words, if the flood point prediction procedure given by Bürkholz is used to calculate the liquid load to the mesh pad, the liquid rate is larger than the liquid rate that was injected in the inlet pipe. Obviously, this is not possible and it can therefore be concluded that the correlation is not valid for the whole range of fluid properties examined in the HP-rig. The biggest difference is that Bürkholz based his correlation on data produced with water and Tri Ethylene Glycol (TEG), which have much higher viscosities than the Exxsol and natural gas condensate in the HP-rig. In addition, the tests were carried out under low-pressure conditions where the velocity is generally much higher than at the experiments in the HP-rig. Further tests are therefore needed in order to establish a correlation that can predict the flooding point at high-pressure conditions that are more relevant for natural gas scrubbers.

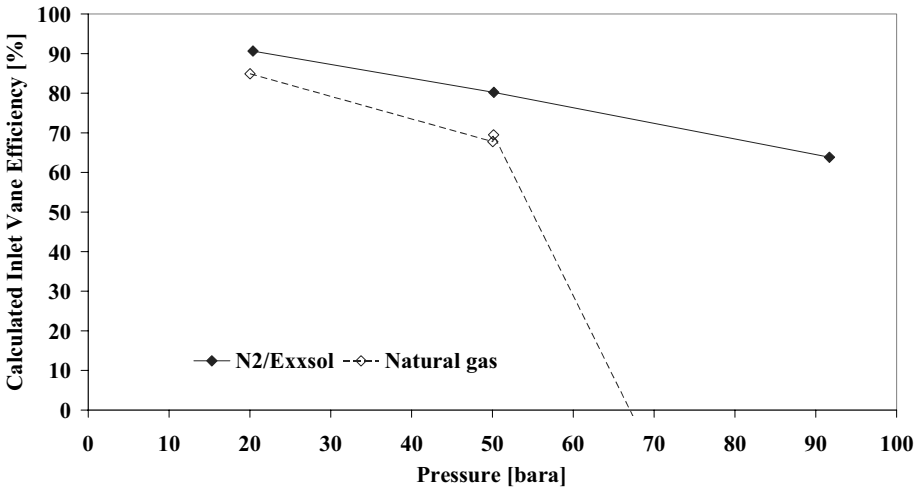

Figure 5.4 The calculated efficiency of the inlet vane in the HP-rig at the flooding points.

5.1.3 Primary Efficiency

In general, the primary efficiency increased with increasing liquid load in all three test rigs. In order to compare the primary efficiency in the three different rigs, the efficiency obtained with 0.2 vol% liquid in the inlet pipe has been compared on basis of the K-value in Figure 5.5. The comparison shows that the efficiency is lower in the LP-rig than in the two other rigs, despite the fact that the physical properties are more favourable in terms of separation in this rig. Further, it can be seen that the efficiency in the K-lab rig is better than in the HP-rig, even if the K-lab results are compared to the N2/Exxsol experiments in the HP-rig. The variations in efficiency from the three rigs must therefore be affected by more than just the physical fluid properties. Other conditions that might affect the primary efficiency are

- The dynamic gas pressure at the inlet i.e. the ratio of the diameter in the inlet pipe to the scrubber diameter.
- Distance between inlet vane and mesh pad
- The distribution of the gas and liquid in the inlet pipe and above the inlet vane.
- The ratio of the cross-sectional area of the inlet vane to the scrubber (blocked area of the inlet vane)

- The relevance of a comparison based on the liquid concentration in vol% since it implies the actual liquid load is lower at high pressure than at low pressure

A systematically comparison of the LP-rig compared to the two other rigs reveals the following differences:

- In the LP-rig the inlet dynamic pressure is much larger than in the two other rigs (see Figure 5.1).
- The distance between the inlet vane and mesh pad is only slightly smaller than in the HP-rig (350 mm in LP-rig and 410 mm in HP-rig).
- The pressure drop curves in Figure 5.2 and Figure 5.3 indicate that the liquid mal distribution becomes larger with larger scrubber diameter, but the results from the largest scrubber shows the highest efficiency.
- The blocked area of the inlet vane in the LP-rig is the same as in the HP-rig, but slightly larger than in the K-lab rig (LP- and HP-rig: ~40%, K-lab: ~36%)

Of the mentioned reasons above, only the relatively high dynamic gas pressure at the inlet is likely to explain the low efficiency in the LP-rig compared to the two other rigs. It is therefore concluded that the dimension of the inlet pipe has a significant impact on scrubber performance.

When it comes to the difference between results from the K-lab rig and the HP-rig, the explanations are less clear. However, the distance between the inlet vane and mesh are 80 % larger in the K-lab rig (see Section 3.4), and the inlet vane in the HP–rig occupies 4 % more of the scrubber cross sectional area. It might be that bulks of liquid easier separate out by gravity settling from the volume between the mesh and inlet vane due to these geometrical differences. Also, the liquid has shown signs of being highly uneven distributed in both the mesh pad and the cyclone deck in the K-lab rig. However, it is possible that this uneven liquid distribution is favourable in terms of gravity settling compared to a situation where the fluid is more evenly mixed.

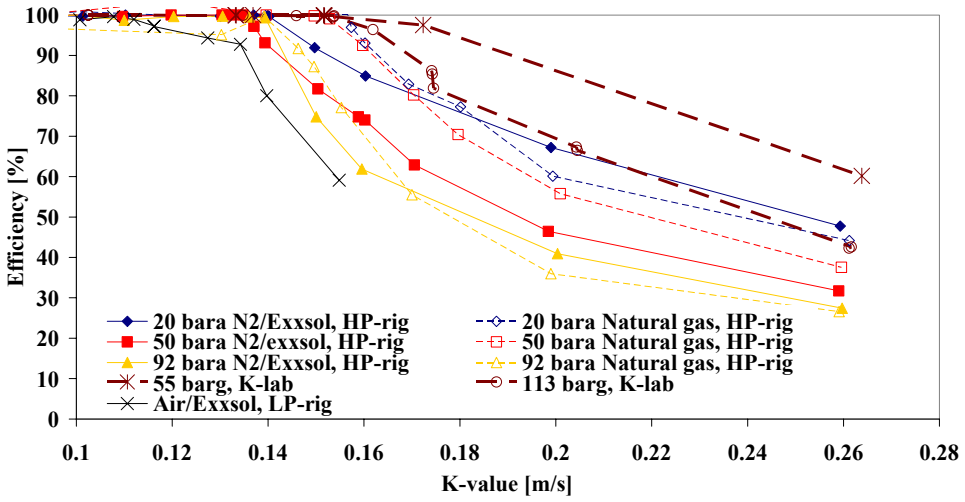

Figure 5.5 The primary efficiency in the three different test rigs when 0.2 vol % liquid was injected in the inlet pipe.

5.2 Demisting Axial Flow Cyclones

The separation efficiency of an axial flow cyclone is a combination of the ability to separate droplets and the ability to handle the separated liquid and prevent it from being swept along with the gas (re-entrainment). The most important parameter in terms of separation efficiency is the gas velocity. The gas velocity must be kept within certain a range in order to balance the requirements of separating small droplets and at the same time keep re-entrainment within acceptable limits. However, this gas velocity range becomes smaller as the pressure increases since the fluid properties become more critical as discussed earlier in Section 2.7. In Figure 5.6 the balance between droplet separation and re-entrainment is illustrated visually.

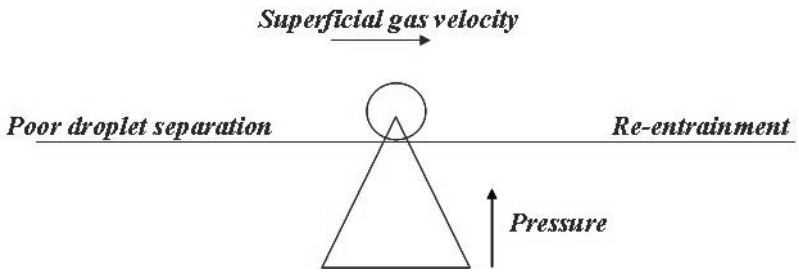

Figure 5.6 The efficiency of a cyclone is very dependent on the superficial gas velocity which is visually demonstrated in the figure. High velocity may result in excessive re-entrainment while low velocity may lead to poor droplet separation. The range of acceptable velocities is decreasing with increasing pressure.

In this section the cyclone results from the three different experimental rigs are analyzed in light of the dilemma sketched in Figure 5.6

5.2.1 Grade Efficiency at High-Pressure Conditions

In Section 2.6.1, different models for grade efficiency have been compared to experimental data found in literature. The different models gave different results, but it was not possible to determine whether one model was more accurate than the others. Therefore all models have been used here in order to roughly estimate the range of droplet sizes the cyclone deck could expect to handle at the different conditions. As the pressure increases, the gas velocity decreases provided that the K-value is kept constant. In addition, with increasing pressures the density difference decreases and the gas viscosity increases. All these mentioned effects of increasing pressure will have a negative effect on the grade efficiency of the cyclones. In Figure 5.7 the calculated grade efficiency for the cyclones in the HP-rig is shown for the natural gas system at 92 bara pressure and a K-value in the scrubber of 0.15 m/s. Depending on the model, the predicted cut sizes d_{50} is in the range 11- 23 micron

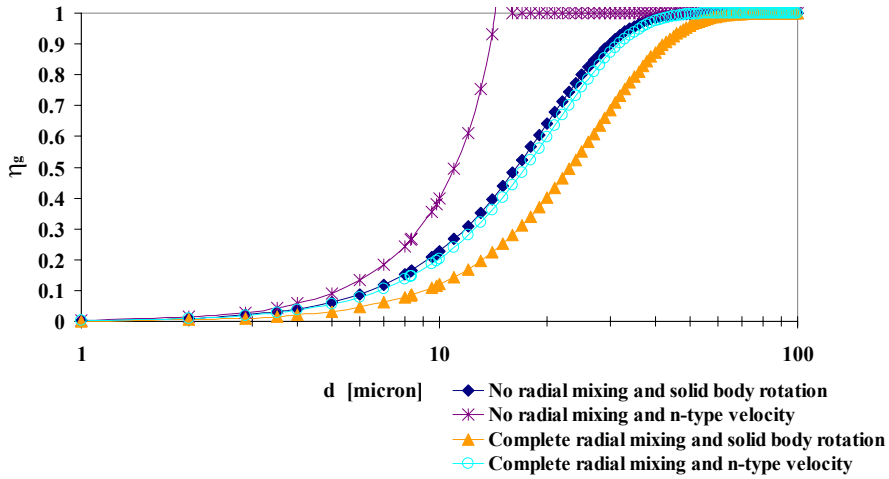

Figure 5.7 The curves show the calculated grade efficiency for the Verlaan cyclone in the HP-rig at 92 bara with natural gas when the K-value in the scrubber was 0.15 m/s ($u_{g,s}$ in cyclone = 1.3 m/s)

In Figure 5.8 the model assumption "No radial mixing and solid body rotation" was used to predict the cut sizes d_{50} and d_{95} for the three different pressures and the two different fluid systems used in the HP-rig. The calculations that were done for a K-value in the scrubber of 0.15 m/s, show that the cut sizes for the two different fluid systems is comparable except for the highest pressure, where the lower density difference and gas velocity of the natural gas system, suppress the influence of the gas viscosity which is higher for nitrogen than for the natural gas at the same pressure.

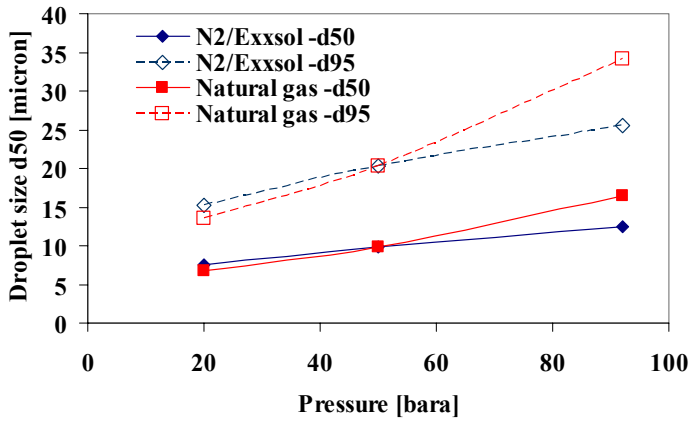

Figure 5.8 The cut size d_{50} or d_{95} increases with increasing pressure when the scrubber K-value is kept constant = 0.15 m/s. The basis for these predictions is the "No radial mixing and solid body rotation"-model

In Section 4.2.5 the droplet size distribution above a non-flooded mesh pad was measured. The volumetric median droplet size d_{v50} ranges from 30 microns at 20 bara to 70 microns at 92 bara, while the cut sizes of the cyclone is considerably lower as seen from Figure 5.8. This indicates that the cyclones in the HP-rig are capable of collecting the majority of the droplets formed in the N2/Exxsol system. However, at 92 bara a measurement was carried out on droplets that were created by condensation of the natural gas system. The majority of these droplets were smaller than 10 microns, and will not be separated in the present setup (see Figure 5.7). Therefore, wherever fine mist, created from upstream condensation at high-pressure natural gas conditions, is required separated out from the gas, other types of demisting devices capable of separating much smaller droplets than an AFC's should be considered.

If small droplets influenced the separation efficiency of the AFC's in the test carried out in this study, the efficiency should increase with increasing gas velocity, due to higher centrifugal force. Moreover, the efficiency should also increase with increasing liquid load for reasons discussed earlier in Section 2.6.1. The gas velocity was varied systematically in both the LP-rig (Figure 4.3, Figure 4.4 and Figure 4.7) and in the HP-rig (Figure 4.20), but no trends showing that the efficiency increased with increasing velocity were found. In the HP-rig, where the fluid properties were most critical, the gas velocity was varied systematically only when the liquid load to the cyclone was 45 l/hr. It is possible that a positive effect of gas velocity could be found if it was varied systematically at lower liquid loadings.

The effect of liquid loading was investigated in all three rigs. In the LP-rig the efficiency increased with increasing liquid load for very small amounts up to 7 l/hr liquid load per cyclone. Note that this trend was only seen when the liquid was introduced in the inlet piping at a gas load that was below the flood point of the mesh (see Figure 4.15). The liquid to the cyclone deck was, hence, small droplets that either penetrated the mesh pad or was re-entrained from the mesh pad. Whenever the liquid was introduced either through a nozzle below the cyclone deck or as entrained liquid from a mesh pad in flooded condition, the cyclone efficiency decreased with increasing liquid load.

In the HP-rig a weak tendency of increasing efficiency with increasing liquid loading was seen at low loadings at 50 and 92 bara pressure. Typically the loadings where this behaviour was seen were below 25 l/hr (see Figure 4.21).

Even though increasing liquid load was seen to have a positive effect in the present study at low loadings, the reason for the observed behaviour is not totally evident. In Section 2.6.1 the effect of droplets that shield one another from the drag of the gas were discussed. This effect has a positive impact on the grade efficiency. However, some other possible reasons for increasing efficiency with increasing liquid load are:

- It might be that droplets coalesce upstream of the cyclone so that the droplet size distribution in the cyclone inlet increases as the liquid load increases.
- There is some kind of coalescence mechanisms going on within the cyclone that increases as the cyclone increases.
- There is some kind of small slip stream, rivulet or similar mechanism that is quite constant and independent on liquid load (above a lower limit). When the liquid rates increases its contribution to the total liquid carry-over becomes smaller and the total efficiency, hence, increases.

In the K-lab experiments the cyclone efficiency increased with increasing average liquid load up to approximately 100 l/hr per cyclone before it started to decrease (see Figure 4.34). However, the cyclone performance at K-lab was heavily influenced by liquid mal distribution. As discussed in Section 5.1.2, it is observed by use of differential pressure measurements, that the mesh pad at K-lab flooded more gradually than in the HP-rig -possible due to uneven liquid loading. It is possible that while much of the bulk liquid travelled near the wall on its way up to the cyclone deck, it left a finer mist in the centre of the vessel. As the liquid concentration in the scrubber cross-section increased, the droplet size may have increased due to increasing coalescence such that the increasing liquid load had a positive effect on the efficiency of the cyclone deck.

The main conclusion from investigating the cyclone performance in the present tests is that small droplets have played a less important role in determining the overall efficiency for the large majority of the tests. The main trend in all results is that the overall efficiency is governed by some kind of re-entrainment mechanism rather than small droplets except for some few cases discussed here.

5.2.2 Re-entrainment in Cyclones

The results from the cyclone experiments in the HP-rig in Section 4.2.1 show that efficiency drops off with increasing gas velocity and liquid load. It also shows that the liquid carry-over is much larger when the pressure is increased and a natural gas fluid is used instead of a N_2/Exxsol fluid.

As discussed in Chapter 2, if the droplets are so small that the cyclone separation efficiency is determined by the droplet size, one would expect increasing efficiency with increasing volumetric gas flow and probably with increasing liquid loading (due to coalescence effects). However, if re-entrainment is the determining factor, the efficiency would be expected to drop off with higher volumetric gas flow and liquid loadings. Since the latter observation has been seen in the present results the main hypothesis is that the liquid carry-over from the cyclones are dominated by re-entrainment of liquid that has already settled on the cyclone wall.

Ishii and Grolmes (1975) assumed that liquid entrainment was possible when the drag forces of the gas exceeded the retaining forces of the interfacial tension i.e.

$$F_d \geq F_\sigma \tag{5.3}$$

Near the point of inception of droplet entrainment, the entrainment rate is increasing quite slowly with increasing gas velocity (Cousins et al., 1965; Steen and Wallis, 1964; Yablonik and Khaimov, 1972; Ueda and Tanaka, 1973), but at relatively high entrainment fraction the entrainment rate increases faster and appears to be linearly correlated with the superficial gas velocity. Since the droplets that are re-entrained inside a cyclone are exposed to a centrifugal force one can think of liquid carry-over as the amount of liquid that is entrained when equilibrium exists between the rate of droplets that are entrained and droplets that settles. With increasing shear forces, the amount of entrainment increases and therefore the efficiency of a cyclone can be investigated in terms of the force ratio rather than the determining the inception point i.e.:

$$\eta_{cycl} = f\left(\frac{F_d}{F_\sigma}\right) \tag{5.4}$$

Note that the expression in Equation (5.4) is only valid if the liquid carry-over is dominated by re-entrainment mechanisms. The work of Ishii and Grolmes are presented in Chapter 2.3.2. They found that inception of entrainment could be dependent on the Reynolds number for the liquid film, Re_l, and that different mechanisms of entrainment were dominant in different regions of Re_l. The definition of Re_l is:

$$Re_l = \frac{\rho_l v_l \delta_l}{\mu_l} = \frac{\Gamma \rho_l}{\mu_l} \tag{5.5}$$

Since neither the liquid film thickness nor the velocity is know, the product of the two quantities must be used. Γ is the volumetric liquid flow, $\dot{Q}_l$ per unit wetted perimeter, P_w. The wetted perimeter for a cyclone must take into account the direction of the liquid flow. If the cyclone body is rolled up it becomes a rectangle with short side length equal to the circumference of the inner cyclone wall as shown in Figure 5.9

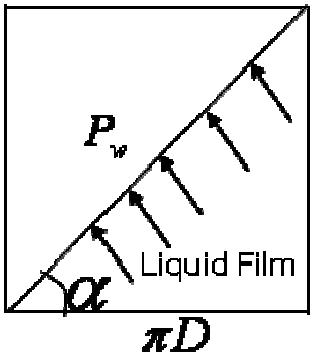

Figure 5.9 The lower part of the cyclone body when it is "rolled up". The wetted perimeter of the cyclone body is marked as the diagonal in the figure

The wetted perimeter is therefore:

$$P_w = \frac{\pi D}{\cos\alpha} \tag{5.6}$$

As an approximation the angle α is taken to indicate the direction of the gas flow i.e. 90^0 - β, where β is the exit angle (angle relative to the swirl vanes which is 45^0 for the Verlaan cyclone.

If we consider the liquid carry-over as a constant fraction of entrained liquid, the actual volumetric liquid flow on the cyclone wall must be corrected for this. We then get the following expression for the Reynolds number of the liquid film:

$$Re_l = \frac{\left(\dot{Q}_l \eta_{cycl}\right)\rho_l}{P_w \mu_l} \tag{5.7}$$

Ishii and Grolmes found that the transition from low Reynolds number entrainment to transition regime entrainment occurred at approximately Re_l = 160 for horizontal or vertical up flow and Re_l = 2 for vertical down flow. The transition to a rough turbulent regime occurred when Re_l exceeded 1500 – 1750. When Re_l is calculated for the experiments in the HP-rig, most of the N_2/Exxsol results are found to be in the low Reynolds number regime, while most of the natural gas experiments are found to be within the transition regime. If transition regime theory is used for experiments that are calculated to be within low Reynolds number regime, the results will become increasingly inaccurate as the velocity is decreased. However, on balance it was thought best to use the same theory for all the results avoiding an anomalous jump in prediction when changing from one theory to the other. All the results from the HP-rig are therefore treated as if they were within the transition regime in this analysis.

The theory of Ishii and Grolmes was discussed in Section 0. Here its adaptation to cyclone flow is considered, and, based on their theory, a re-entrainment number is derived to characterize the separation efficiency of cyclones for the case where this is dominated by re-entrainment.

The special feature in cyclones is that the flow is swirling, and that the force of gravity should therefore be replaced by the "centrifugal force".

The derivation of Ishii and Grolmes is based on a comparison of shear forces and surface tension forces acting on a wavelet on the film, and gravity in principle does not enter into this, except in one aspect, which will now be discussed.

Ishii and Grolmes' criterion for the onset of re-entrainment was:

$$\frac{\mu_l u_{g,s}}{\sigma}\sqrt{\frac{\rho_g}{\rho_l}} \geq \frac{Re_l^{-1/3}}{3C_w(N_\mu)} \tag{5.8}$$

In this expression, $C_w(N_\mu)$ is a coefficient that accounts for the modification due to surface tension of the shear stress acting on a liquid wavelet due to the flow of gas over it. Following earlier work of Hinze (1955), on droplet stability this coefficient was assumed to be a function of the viscosity number:

$$N_\mu = \frac{\mu_l}{\sqrt{\rho_l \sigma \sqrt{\frac{\sigma}{g\Delta\rho}}}} \tag{5.9}$$

The length scale chosen for N_μ by Ishii and Grolmes: $\sqrt{\sigma/g\Delta\rho}$ is the critical wavelength of a Taylor instability, and therefore characteristics for the length of waves on the film. This length scale involves the gravitational constant *g*. We replace this by the "centrifugal force" acting on the liquid film,

$$a_l = \frac{u_{l,tg}^2}{R} \tag{5.10}$$

To evaluate a_l, we need the tangential component of the liquid film velocity

$$u_{l,tg} = u_l \cdot \cos\alpha \tag{5.11}$$

We find this by evaluating the liquid film velocity, u_l in a similar way to Ishii and Grolmes as follows:

The tangential component of the liquid film velocity is not known but by looking at two different expressions for the shear force at the interface, an expression for the liquid film velocity can be found. If we call the tangential components of the shear stresses acting on the film due to the gas and on the wall due to the film $\tau_{i,tg}$ and the wall $\tau_{w,tg}$ respectively, we can say:

$$\tau_{i,tg} = f_{g,i} \frac{\rho_g u_{r,tg}^2}{2} \tag{5.12}$$

$$\tau_{w,tg} = f_{l,w} \frac{\rho_l u_{l,tg}^2}{2} = \tau_{i,tg} \tag{5.13}$$

The gas velocity is assumed to be much larger than the liquid film velocity so that

$$u_{g,tg} >> u_{l,tg} \Rightarrow u_{r,tg} \approx u_{g,tg} \tag{5.14}$$

By combining Equation (5.12), (5.13) and (5.14), an expression for the liquid film velocity can be found:

$$u_{l,tg} = \sqrt{\frac{f_{g,i} \cdot \rho_g u_{g,tg}^2}{f_{l,w} \cdot \rho_l}} \tag{5.15}$$

A correlation for the gas friction factor $f_{g,i}$ have not been measured for a liquid film on a cyclone wall, but there exists several investigations for annular flow in pipes and ducts. Wallis (1969) came up with a correlation for a rough wavy regime

$$f_{g,i} = 0.005\left[1 + 300\frac{\delta_l}{D}\right] \tag{5.16}$$

The same friction factor is here used for the cyclone, but due to the rotating gas flow, the diameter, D, of a duct is replaced by the radius, R, of the cyclone:

$$f_{g,i} = 0.005\left[1 + 300\frac{\delta_l}{R}\right] \tag{5.17}$$

The wall friction factor $f_{l,w}$ can be obtained from the correlation for a film thickness given by Hughmark (1973)

$$\sqrt{f_{l,w}} = K \cdot Re_l^m \tag{5.18}$$

Where:

$K = 3.73$ and $m = -0.47$ for $2 < Re_l < 100$
$K = 1.962$, $m = -1/3$ for $100 < Re_l < 1000$

Based on the experimental data from Hughmark, Ishii and Grolmes concluded that the latter expression seemed to be a good approximation for the transition regime.

The gas friction factor requires information about the liquid film thickness. From Equation (5.5) we can see that the product of the velocity and thickness is known i.e.

$$\Gamma = \frac{\dot{Q}_l}{P_w} = u_l \delta_l \Rightarrow \delta_l = \frac{\dot{Q}_l}{P_w \cdot u_l} \tag{5.19}$$

The tangential component of the liquid film velocity is given in Equation (5.15) and the relation between the absolute velocity and the tangential component is given in Equation (5.11). The expression for the liquid film thickness hence, becomes:

$$\delta_l = \frac{\dot{Q}_l}{P_w \cdot u_{l,tg}} \cos\alpha = \frac{\dot{Q}_l}{\pi D \cdot u_{l,tg}} \cos^2\alpha \tag{5.20}$$

We now have two expressions for the two unknown variables δ and $u_{l,tg}$ and the "centrifugal acceleration" for N_μ can be solved.

Tangential Gas Velocity

The tangential velocity profile within a cyclone could be regarded as something between a solid body rotation and a loss-free vortex (Hoffmann and Stein, 2002), and must be calculated based on the measured gas flow and the specific geometry. The tangential velocity varies with radial position, but the essential velocity for re-entrainment analyzes, will be the gas velocity at the gas-liquid interface on the inner wall of the cyclone. The wall velocity is sketched in Figure 5.10

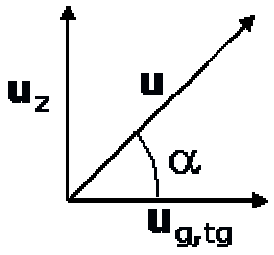

Figure 5.10 The flow coordinates at the cyclone wall

Tangential velocity can be expressed as:

$$u_{g,tg} = \frac{u_z}{\tan\alpha} \tag{5.21}$$

The tangential velocity of the 50 mm cyclone used in the current study and an 80mm scale-up of the same cyclone has been measured by use of a neutral helium bubble tracer technique. The velocity profile changes along the axial direction but he results reported in a Master Thesis on the Verlaan Cyclone (Jacobsson, 2004) show that the superficial gas velocity is approximately a factor 0.8 smaller than the axial gas velocity near the wall in the middle of the cyclone. This ratio will of course depend on the Reynolds number of the gas flow, but as an approximation the following expression has been used as a rough estimation of the velocity in the current set of data:

$$u_{g,tg} = \frac{u_{g,s}}{0.8 \cdot \tan\alpha} \tag{5.22}$$

The Re-entrainment Number

Based on the calculated Re_l number for the experiments in the HP-rig, most experiments seem to be within the transition regime where entrainment depends on Re_l as explained in Section 2.3.2. For all experiments the dimensionless viscosity number N_μ is less than 1/15. Assuming that transition regime is the dominant liquid film regime on the inner cyclone wall, the expressions in Equation (2.36) can be used in the force ratio in Equation (5.4) and, hence, we get the re-entrainment number:

$$\eta_{cycl}(a) = f\left(\frac{\frac{\mu_l u_{g,s}}{\sigma}\left(\frac{\rho_g}{\rho_l}\right)^{0.5}}{N_\mu^a Re_l^{-1/3}}\right) \tag{5.23}$$

Note that Ishii and Grolmes adjusted the power a of the viscosity number to fit their data for the inception of the entrainment rather than the entrained fraction as expressed in Equation (5.23). The power should therefore be adjusted to the cyclone experiments. The power of the viscosity number is important when experiments with different physical fluid properties like natural gas and N_2/Exxsol are scaled. The re-entrainment numbers for all experiments that have been carried out in the HP-rig (see Section 4.2) have been calculated in accordance with Equation (5.23) and are plotted in Figure 5.11. Since many of the experiments with low liquid loading showed increasing efficiency with increasing gas flow, it was assumed that droplet size played an essential role for the efficiency at these low loadings. Therefore only experiments were the liquid load exceeded 9 l/hr have been included in the plot.

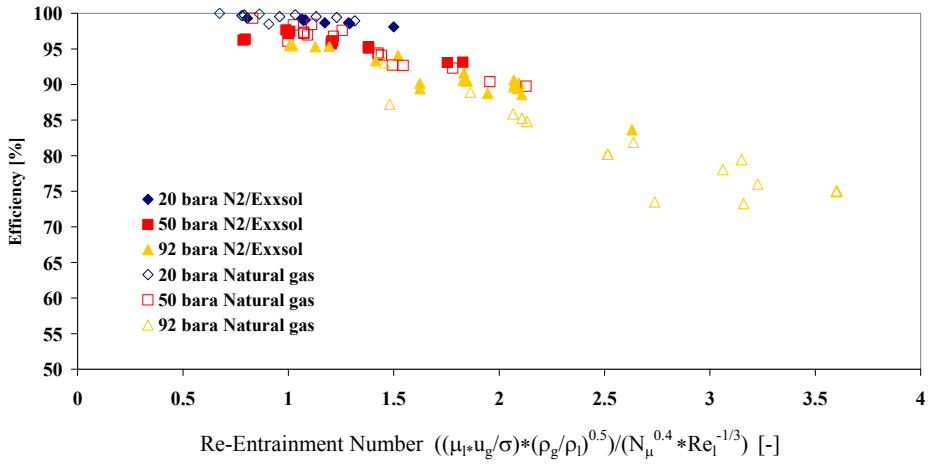

Figure 5.11 The cyclone efficiency in the HP-rig as function of the re-entrainment number. The plot includes liquid loads in the range 9 – 73 l/hr per cyclone

The power a = 0.4 results in a good fit between the natural gas and Exxsol as seen in Figure 5.11. However, the current form of the re-entrainment number seems not to fit the pressure scaling very well. Since the re-entrainment number manage to account for differences in physical fluid properties between the N_2/Exxsol and natural gas experiments but not for differences in operating pressure, it is likely that the gas and liquid densities are not correctly accounted for. For this reason, the power of the gas to liquid density ratio was subjected to regression and with a power of 0.8 a good fit was found as seen Figure 5.12.

The excellent correlation between the cyclone efficiency and the re-entrainment number indicates that the cyclone efficiency is dominated by liquid film re-entrainment rather than insufficient separation of small droplets. The plot in Figure 5.12 can be regarded as the maximum achievable efficiency due to limitations caused by re-entrainment for this particular geometry. However, if a significant amount of droplets comparable to the cut size of the cyclone are present in the inlet liquid loading, an extra contribution will be added to the liquid loss of the cyclone. Experiments with such contributions will have lower efficiency than predicted by the re-entrainment number solely.

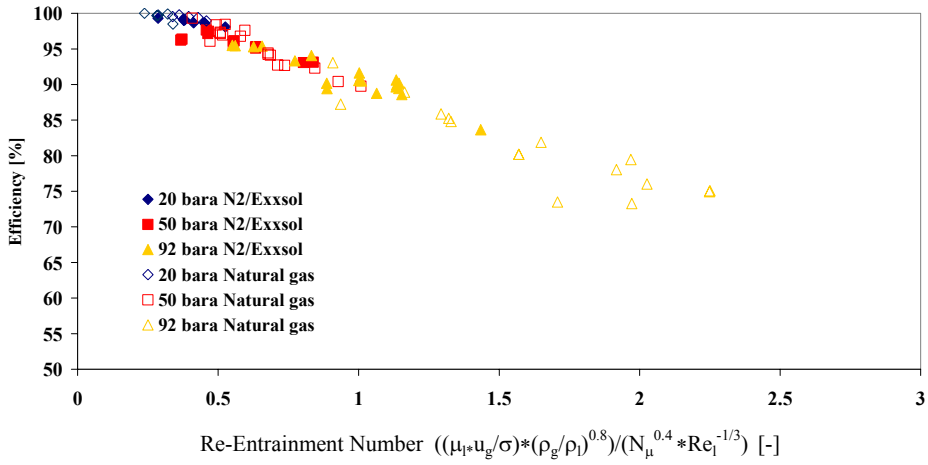

Figure 5.12 The cyclone efficiency in the HP-rig as function of the re-entrainment number with adjusted power of the gas to liquid density ratio. The plot includes liquid loads in the range 9 – 73 l/hr per cyclone

There is still some scatter in the results in Figure 5.12, but with all the simplifications done and the complex process of gas-liquid interactions involved, the correlation is still remarkably good. Some of the scatter might also be caused by small droplets, especially for the high-pressure natural gas case. Some of the most important simplifications are:

- Gradual drainage of liquid film through the slits in the cyclone wall has not been accounted for
- The film is assumed to be evenly distributed on the wall
- Transition regime entrainment is assumed even though some of the experiments appear to have a liquid Reynolds number smaller than the limit given by Ishii and Grolmes

Liquid Film Weber Number

The results with the modified Verlaan cyclone from the LP-rig show a general tendency of decreasing efficiency with increasing gas and liquid flow. This is consistent with re-entrainment behaviour. However, the calculated Re-liquid film number for the LP results indicates that the liquid film is below the transition regime as indicated in Figure 2.4. If these results are plotted against the re-entrainment number the decrease in performance appears to be faster in the LP-rig than in the HP-rig, although the re-entrainment number clearly brings also the LP rig results onto one curve.

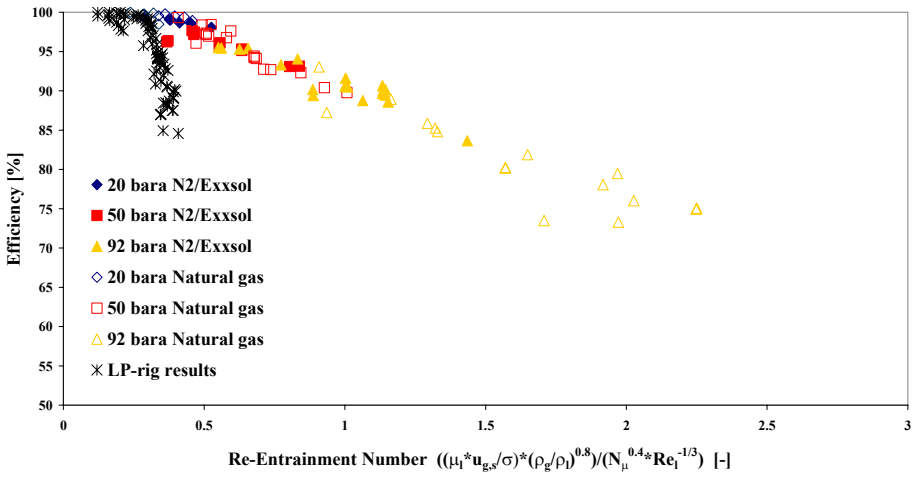

Figure 5.13 A comparison between the cyclone efficiency in the HP- and LP-rig in terms of the re-entrainment number.

Since the velocity is considerably higher at LP-conditions than at HP-conditions, re-entrainment still is possible as explained in Section 2.3.2. However, according to Ishii and Grolmes, the roll-wave entrainment mechanism used for the results in the HP-rig cannot be applied at these low values for Re_l. Instead, the liquid film Weber number that van Rossum (1959) used in a re-entrainment study can be applied i.e.

$$\eta = f\left(We_l\right) = f\left(\frac{\rho_g u_{g,s}^2 \delta}{\sigma}\right) \tag{5.24}$$

The result for the LP-rig then becomes:

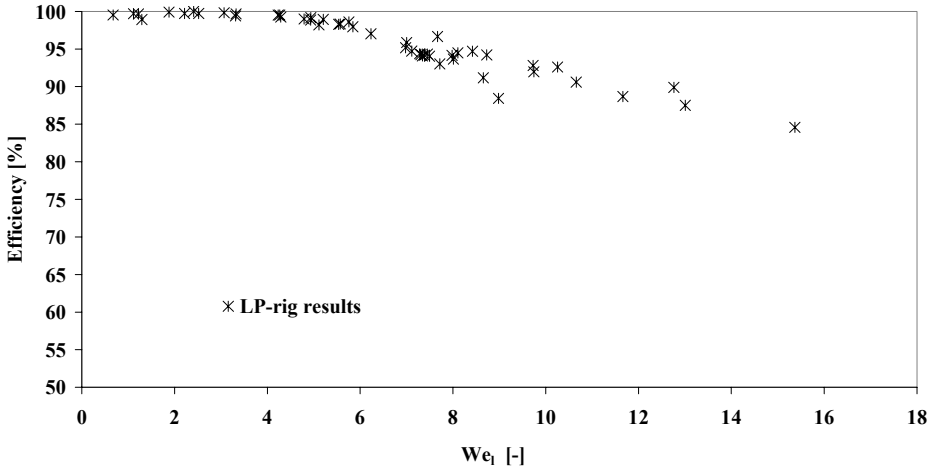

Figure 5.14 The results from the LP-rig as function of the Weber number for the liquid film

In the experiments with kerosine, a liquid that is comparable to Exxsol D60, van Rossum found that the critical Weber number for the onset of re-entrainment was in the range 6 – 10, depending on the correlation parameter S (Equation(2.42)). This result is in agreement with the plot in Figure 5.14 where re-entrainment appears to become significant around We_l = 6. Once again, the criterion was originally used to determine the onset of entrainment, and not the entrained fraction as plotted in Figure 5.14. However, also this criterion roughly seems to bring the efficiency results onto one curve.

The liquid film thickness has been calculated using Equation (5.20). The results show that there is a linear decrease in efficiency with increasing liquid film Weber number. Since the liquid density and the interfacial tension are approximately constant in the LP-rig, the variation in the liquid film number is near identical to the gas dynamic pressure times the liquid rate.

The experiments in the HP-rig have been plotted together with the LP-rig results as a function of the liquid film Weber number in Figure 5.15. We_l seems to roughly correlate the Exxsol results from the HP-rig onto the same curve as the LP-results. However, it can be seen that the trend of the measurements is not the same for the different pressures. The 20 bara measurements show better efficiency than the 50 bara, which again is better than the 92 bara measurements when they are compared on basis of We_l. Hence, it seems that re-entrainment scaling on basis of We_l is incapable of accounting for the changes in fluid properties at changing pressures. This assumption is strengthening by considering the results with the natural gas fluid, where the trends at the different pressures are even more different.

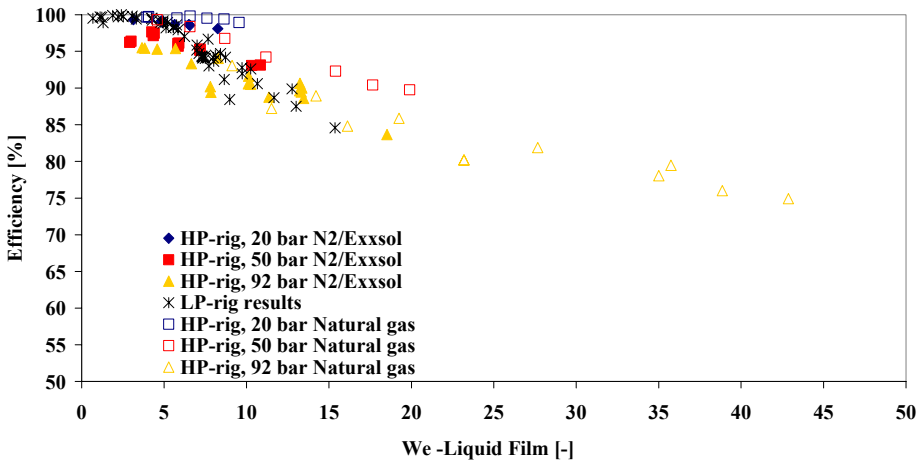

Figure 5.15 A comparison of the cyclone experiments in the HP- and LP-rig in terms of the liquid film Weber number

The differences between LP- and HP-results as seen in Figure 5.13 may have the same explanations as the differences seen in Figure 5.15. Since the experimental work in this project has been carried out within a certain range of K-values, the gas velocity is much higher in the LP-rig experiments than in the HP-rig experiments. This has been demonstrated graphically in Figure 2.20. In addition, the packing density of the cyclone deck was approximately twice as high in the HP-rig, thereby further reducing the gas velocity in the cyclones at high pressure. The calculated Re_l in the LP-rig experiments falls mainly within the region where no entrainment occurs as discussed in Section 2.3.2. However, due to the much higher gas velocity in the LP-rig, it is possible that re-entrainment still occurs due to a change in the basic re-entrainment mechanism. Ishii and Grolmes study the photographic study of van Rossum and concluded that the entrainment-mechanism in this study was similar to the wave-undercut mechanism rather than the roll-wave entrainment. It is therefore possible that the wave-undercut mechanism is dominating the re-entrainment at low pressure, while the roll-wave re-entrainment mechanism is the dominant at higher pressures where the gas velocity is lower.

Cyclone Efficiency in the K-lab Test Rig

The efficiency in the HP-rig is totally dominated by re-entrainment, at least for liquid loadings per cyclone above 9 l/hr. However, in the experiments at K-lab it was seen that outer cyclones in the cyclone deck handled up to 2.5 times the amount of liquid that the inner cyclones handled. Since the cyclone efficiency

generally drops off with increasing liquid load the outer cyclones might suffer from poorer efficiency. If, in addition, some of the cyclones in the middle of the cyclone deck receives a small amount of liquid but distributed as a fine mist, this might have a bad impact on the efficiency as seen for low liquid loadings in both the LP and HP-rig. In the small scale HP-rig only two cyclones where installed and obviously, no liquid mal distribution could have occurred. Therefore, the efficiency in the HP-rig can be regarded as the maximum efficiency limited by re-entrainment. If there, in addition, is a problem with liquid mal distribution, the efficiency will be lower than the maximum efficiency

In Figure 5.16 the measured cyclone efficiency at K-lab is compared to the maximum efficiency found in the HP-rig. The results are plotted as function of the re-entrainment number and the average liquid load per cyclone has been used as input in the calculations. The figure shows that the cyclone deck in the K-lab tests is very influenced by the poor liquid distribution. In fact, in one case the efficiency drops from an expected maximum efficiency of more than 80% down to an actual efficiency of approximately 40% i.e. the uneven distribution leads to 3 times as much liquid carry-over. This connection between large scale and low efficiency has never before been documented. The result is very important since it demonstrates how much the efficiency of a large scale scrubber can deviate from the efficiency found in a small scale lab –even when the gas velocity, liquid concentration and the fluid properties are identical. The re-entrainment number offers an analysis in order to quantify the impact of liquid mal-distribution.

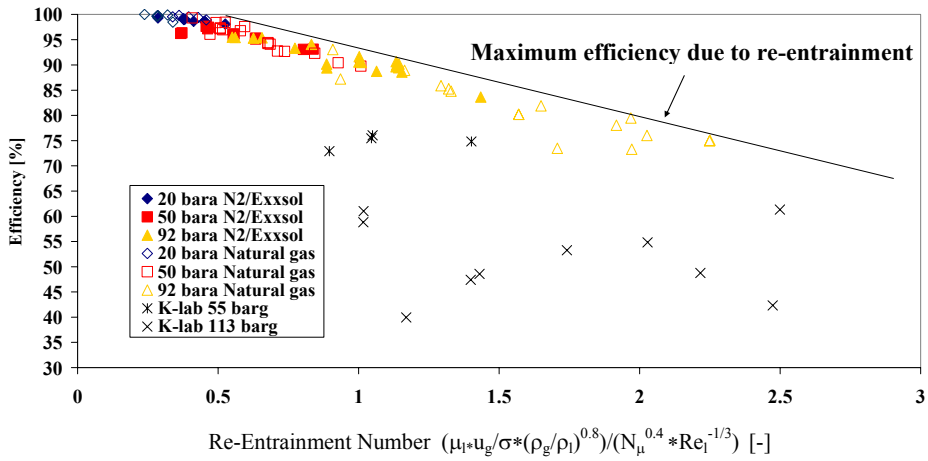

Figure 5.16 The cyclone results from the K-lab rig is suffering from lower efficiency than the results from the HP-rig. The maximum efficiency found in the HP-rig is extrapolated in order to cover the range of re-entrainment numbers tested at K-lab

5.3 Scaling/Extrapolating Low-Pressure Results

In Chapter 2, relevant theory for gas-liquid separation was presented. In this section some of the scaling rules are evaluated in light of the test results from the three different test rigs.

5.3.1 Gas Load Factor

The results from the three rigs show that the K-value is rather good in practise for deign of inlet vane and mesh pad, and confirm the design criterion of keeping $K \leq$ 0.15 m/s. However, the results do show significant impact on the physical fluid properties and also a significant influence of the pressure (Figure 4.22 and Figure 4.35). For more compact scrubbers i.e. $K > 0.15$ m/s, the K-value does not reflect the efficiency or liquid entrainment from neither the primary separation nor the total scrubber, as big variations are seen for varying fluids, pressures and liquid concentrations.

5.3.2 Scaling rules for cyclones

Different scaling rules that are often employed for cyclones at elevated pressures are discussed in Section 2.7. The issue of scaling is relevant when laboratory tests are used as a basis for prediction of cyclone efficiency at different conditions, typically at higher pressures and different fluids than used in the lab. The scaling rules include Stokesian scaling, constant dynamic gas pressure, constant velocity and constant K-value. Since the liquid carry-over from the cyclones in the present tests was dominated by a re-entrainment mechanism rather than small droplets that penetrated the cyclone, Stokesian scaling is not relevant, since it implies that the gas velocity should increase with increasing pressure. Further, if the gas velocity is kept unchanged at different pressures, this can heavily affect the cyclone efficiency with increasing pressure. In the HP-rig the efficiency dropped from more than 99% at 20 bara pressure down to ~75% at 92 bara pressure, when the volumetric gas and liquid rates were the same ($u_{g,s}$= 3m/s, $\dot{Q}_l$ = 45 l/hr).

The derivation of the K-value shows that it has no physical relevance for neither droplet separation nor re-entrainment in a cyclone. However, since it takes into account the density difference, using this criterion will ensure that the gas velocity decreases with increasing pressure. Scaling by keeping the dynamic gas pressure constant also ensures that the gas velocity decreases with pressure. This scaling rule keeps the shear force exerted from the gas phase on the liquid phase, approximately constant. It was shown that scaling by use of constant K-value and constant dynamic pressure was not very different. However, none of the mentioned scaling rules take into account the properties of the liquid film on the cyclone wall.

From the plot of the re-entrainment number in Figure 5.12 it can bee seen that the tests with N2/Exxsol at 20 bara in the HP-rig were carried out at re-entrainment numbers up to 0.55, at which the efficiency was found to be 98%. At this re-entrainment number the K-value in the vessel was 0.25 m/s and the dynamic gas pressure ($\rho_g u_{g,s}^2$) was 970 Pa. If a test at the same operating conditions had been used as a basis for scaling by use of either constant K-value or constant dynamic gas pressure, an efficiency of 98% could not be expected at higher pressures. If the same K-value and liquid load had been used as a scaling rule for the natural gas fluid at 92 bara in the HP-rig, the corresponding re-entrainment number would have been ~1.8 and hence the efficiency could not be expected to better than 75 – 80% i.e. more than 10 times as much liquid carry-over than found at 20 bar with N2/Exxsol. If constant dynamic pressure had been used instead, the deviation would have been even larger. The corresponding re-entrainment number for the same liquid load and a dynamic gas pressure of 970 Pa, is ~2.55. Under these operating conditions the separation efficiency would have been approximately 70%.

5.3.3 Separation Efficiency Specification

A typical general specification of maximum liquid entrainment in the cleaned gas has historically been 13 l/Sm^3 (0.1 US gallon/MSCF), but this seems to be a very unrealistic specification at high pressure. For example, within the range of gas and liquid loads tested in the HP-rig (K-values up to 0.26 m/s and liquid concentrations up to 1 vol%), this requirement implies that the separation efficiency must be better than 99.9% in all cases, and at the highest liquid loadings this requirement corresponds to an efficiency even better than 99.99%. In fact, this requirement is so strict that the corresponding liquid carry-over rate was below the accuracy of the measurement systems in the HP-rig.

This requirement was never met in any of the test rigs when the mesh pad was operated under flooded conditions. However, the scrubber internals in the present study are not optimized. The inlet vane is very simple, the mesh pad is not optimized for hydrocarbon service and the axial flow cyclones are very simple compared to the more sophisticated AFC's on the market today. It is therefore possible that some sophisticated and commercial available scrubber internals would be able to meet the strict requirement, especially at low pressure conditions. However, at higher pressures with natural gas fluids there will be a limit for any internals due to the dilemma between separating small droplets and preventing re-entrainment.

CHAPTER 6

Conclusions and Recommendations

Three different experimental rigs have been used in order to investigate the performance of a standard scrubber configuration. Unique results from tests with real fluids at high pressure have shown that the performance strongly depends on the fluids employed, the gas and liquid load, the operating pressure and the size of the scrubber.

6.1 Conclusions

The efficiency of an inlet vane with a mesh pad above was capable of separating near 100% of the liquid when the operating conditions are such that the mesh pad is in a non-flooded condition. The exception occurred at high pressure natural gas conditions where the interfacial tension is very low. At these conditions a significant amount of liquid carry-over was measured due to a combination of re-entrainment and small droplets that penetrated the mesh pad. Below flooding, efficiencies down to 95% were found at the most challenging conditions in this study.

Flooding of the mesh pad was found to occur at K-values in the range 0.11-0.15 m/s when the liquid concentration in the inlet pipe was 0.23 vol%. The results show that the K-value is rather good as an evaluation parameter and confirm the design criterion of $K \leq 0.15$ m/s normally handled as a rough design criterion for gas scrubbers. However, above this value the K-value is not a suitable design criterion or scaling parameter since it does not account for differences in interfacial tension and viscosities. Neither does it account for changing liquid loads, since all results show that the efficiency of the inlet vane and mesh pad increased with increasing liquid load. However, the absolute amount of liquid carry-over still

increased with increasing liquid load. The results also showed that the efficiency dropped off more rapidly at higher pressures when the results were compared in terms of the K-value. Further, the results showed that the efficiency was much lower when a live natural gas fluid system was used instead of a model system consisting of nitrogen as gas and paraffin (Exxsol D60) as liquid.

A method from literature for flooding point prediction which has been derived at low-pressure conditions for a mesh pad proved not to be consistent for high-pressure natural gas conditions. However, the method predicts that the flooding point occurs at decreasing gas load with increasing liquid load. This behaviour was in agreement with the experimental results.

The performance degradation of the axial flow cyclone used in this study was totally governed by a general re-entrainment process rather than insufficient separation of small droplets. A new approach to predict cyclone efficiency was therefore needed. By mathematically modelling cyclone geometry, flow and fluid properties a brand new relationship was derived that correlates extraordinary well with separation efficiency –the dimensionless re-entrainment number. The re-entrainment number does not only take into account changes in the drag force of the gas but it also accounts for the changes in the retaining forces of the interfacial tension and the formation of waves at the gas-liquid interface.

Cyclone efficiency at high-pressure conditions did not correlate well with results from low-pressure. When the differences in operating conditions between high and low pressure were examined, it was found that the basic re-entrainment mechanism might have been different at the two conditions. While the behaviour at high-pressure conditions seemed to be consistent with re-entrainment due to the shearing droplets off roll-wave crests, the re-entrainment at low pressure conditions might have been dominated more by a wave undercutting mechanism.

Some few droplets size distribution (DSD) measurements have for the first time been measured in a high-pressure scrubber. In most cases the largest droplets were larger than 400 microns which was the upper limit of the range of detectable droplet sizes. Therefore only measurements above a non-flooded mesh were carried out since the droplets at these conditions where small enough to be detected. The DSD measured with N2/Exxsol D60 at different pressures showed that the majority of the droplets were in the size range that could be separated by the cyclones. However, when droplets where formed from natural gas condensation in a heat exchanger rather than from nozzle injections at 92 bara pressure, some very small droplets were formed. These droplets where in the size range 1 – 10 microns –droplets that would generally not be separated at these pressures for common scrubber designs.

The tests revealed some important differences between the results from the small scale test rigs and the large scale K-lab rig. The pressure drop curves indicated that

the flooding of the mesh pad was a much more gradual process in the large scrubber than in the small scrubber. Gradual means that only parts of the mesh pad became flooded with increasing gas load until eventually the whole mesh pad was flooded. The transition from non-flooded to flooded condition at small scale on the other hand, was a more "sudden" process. The reason for this was probably uneven distribution of gas and liquid in the large scale scrubber cross section. This statement was supported by measurements of the liquid drained from the downstream cyclone deck in the large scale K-lab rig. The cyclones located closest to the wall drained out more than twice as much liquid as the inner cyclones, showing that the liquid concentration near the wall was much higher than in the centre of the scrubber. When the cyclone efficiency was analysed in terms of the re-entrainment number it was seen that the uneven liquid distribution caused up to 3 times as much liquid carry-over from the scrubber compared to what could be expected for a perfect distribution.

A commonly used efficiency specification for scrubbers of 13 l/MSm^3 of liquid in the gas leaving the scrubber seemed to be unrealistic for high-pressure natural gas services –at least for compact design (K > 0.15 m/s). But also for natural gas scrubbers of low compactness this requirement seems hard to meet as it is equivalent to a separation efficiency of > 99.9 % for most operational conditions.

6.2 Recommendations

Liquid carry-over from high-pressure scrubbers is in general more related to re-entrainment mechanisms rather than inefficient separation of small droplets. Re-entrainment will play an even more important role as more and more compact separation solutions are being developed for future process systems, especially for sub-sea solutions. For this reason more attention should be paid into the understanding and quantification of basic entrainment mechanisms –especially for live hydrocarbon fluids at high pressure.

In order to predict the performance of high-pressure natural gas scrubbers, tests at low-pressure conditions can only give limited information. For actual performance, high-pressure testing with live hydrocarbon fluids is needed. Since the distribution of gas and liquid in the scrubber cross-section varies significantly with the size of the scrubber, large scale testing should be carried out in order to get a good estimate of the real scrubber performance.

A scrubber configuration with a bank of axial flow cyclones (AFC) above a mesh pad should ideally not be designed at or just above the flood point of the mesh pad. The reason for this is that a large amount of liquid accumulates in the scrubber section between the mesh pad and the cyclones at these conditions. This leads to a transient behaviour of the liquid above the mesh pad which decreases the performance of the cyclones due to sudden pulses of liquid at the inlet.

Some few DSD measurements have for the first time been carried out in a high-pressure scrubber by use of an instrument based on laser scattering. However, the upper detectable droplet size where limited to 400 microns, which in most cases is below the largest droplets present in a scrubber. The droplet size range can be increased by using a lens with larger focal length. The focal length of the lens used in this study was 200 mm, but by replacing it with a 400 mm focal length lens the upper detectable droplet size can be increased to 850 microns. However, this requires better quality of the HP-windows since the larger lens is more susceptive to disturbances of the laser beam.

The primary efficiency of the scrubber was affected by the inlet conditions. If DSD measurements could be carried out at the inlet and downstream of the inlet arrangement, a better understanding of the droplet generation process and hence the efficiency, could be established. It is recommended to investigate the droplet size distribution at high pressure and how it varies with changing fluids, liquid loadings and different geometries.

References

Arnold, K. and Stewart, M. Designing oil and gas production systems. World Oil: Exploration, Drilling, Production. 1984; 199(6):73-78.

Arpandi I.; Joshi A.R; Shoham O.; Shirazi S., and Kouba G.E. Hydrodynamics of two-phase flow in gas-liquid cylindrical cyclone separators. Society of Petroleum Engineers.1995 Oct; SPE 30683:429-440.

Barker, R. and Schook, R. Multiphase separation and new technologies. Advances in multiphase separation and multiphase pumping technologies conference; Aberdeen. 2005

Bjornestad, S. O.; Ophaug, J.; Austrheim, T., and Vedvik, K. Resolving operating problems at Troll gas plant have also lead to a 40 % capacity increase. GPA annual conference; Barcelona. 2000.

Brenne, L.; Bjørge, T.; Gilarranz, J. L.; Koch, J. M., and Miller, H. Performance of a centrifugal compressor operating under wet gas conditions. 34th Turbomachinery Symposium; Houston, Texas. 2005.

Brunazzi, E. and Paglianti, A. Conventional and complex knitted mesh mist eliminators. Chem. Eng. Technol. 2001; 24(11):119-1204.

---. Design of complex wire-mesh mist eliminators. AIChE Journal. 2000; 46(6):1131-1137

---. Design of wire mesh mist eliminators. AIChE Journal. 1998; 44(3):505-512.

Brunazzi, E.; Paglianti, A., and Talamelli, A. Simplified design of axial-flow cyclone mist eliminators. AIChE Journal. 2003; 49(1):41-51.

Bürkholz, A. Droplet separation. VCH Publishers; 1989. ISBN:0-89573-879-1

Carpenter, C. L. and Othmer, D. F. Entrainment removal by a wire-mesh separator. AIChE Journal. 1955; 1(4).

Chandrasekhar, S. Hydrodynamic and hydromagnetic stability, Oxford Univ. Press, New York; 1961.

Chen, C. Y. Filtration of aerosols by fibrous media. Chemical Reviews. 1955; 55:595-623.

Chin, R. W.; Stanbridge, D., and Schook, R. Development and installation of an inline deliquidiser. SPE Annual Technical Conference and Exhibition; Denver, Colorado. 2003.

---. Increasing separation capacity with new and proven technologies. SPE Annual Technical conference and exhibition; San Antonio, Texas. 2002.

Clift, R.; Ghadiri, M., and Hoffmann, A. C. A critique of two models for cylone performance. AIChE Journal. 1991; 37(2):285-289.

Davies, C.N. Deposition from moving aerosols. Aerosol Science. Academic Press, London 1966; 393-446.

Diekmann, R.; Leppard, P., and Swanborn, R. Two and three phase separators with reliable flexibility for the oilfield industry. Society of Petroleums Engineers; 1994:720-736.

El-Dessouky, H. T.; Alatiqi, I. M.; Ettouney, H. M., and Al-Deffeeri, N. S. Performance of wire mesh mist eliminator. Chemical Engineering and Processing. 2000; 39(2):129-139.

Feord, D.; Wilcock, E., and Davies, G. A. A stochastic model to describe the operation of knitted mesh mist eliminators, computation of separation efficiency. Trans IChemE. 1993; 71(part A):282-294.

Gas Processsors Suppliers Association (GPSA). Engineering data book. 1998.

Gjertsen, L. H.; Lokken, K. V.; Marheim, N., and Ophaug, J. Separation efficiency of the Troll Kollsnes separators and the improvement in their performance. GPA, 82th Annual Convention Presentations; New Orleans. 2003.

Gomez L.E.; Mohan R.S.; Shoham O., and Kouba G.E. Enhanched mechanistic model and field application design of gas/liquid cylindrical cyclones. SPE Journal. 2000; 5(2):190-198

Gomez L.E.; Mohan R.S.; Shoham O.; Marrelli J.D., and Kouba G.E. Aspect Ratio Modeling and design procedure for GLCC compact separators. J. of Energy Resources Technology. 1999 Mar; 121.

Hinze, J. O. Fundamentals of the Hydrodynamic Mechanism of splitting in Dispersion Processes. AIChE Journal. 1955; 1(3):289.

Hoffmann, A. C. and Stein, L. E. Gas cyclones and swirl tubes. Berlin, Heidelberg, New York: Springer; 2002. ISBN: 3-540-43326-0

Holmes, T. L. and Chen, G. K. Design and selection of spray/mist elimination equipment. Chemical Engineering. 1984; 91(21):82-89.

Hughmark, G. A. Film thickness, entrainment and pressure drop in upward annular and dispersed flow. AIChE Journal. 1973; 19(5):1062-1065.

Ishii, M. and Grolmes, M. A. Inception criteria for droplet entrainment in two-phase concurrent film flow. AIChE Journal. 1975; 21(2):308-318.

Jacobsson, S. Single-phase characterization of the Verlaan cyclone: Department of Physics and Technology, University of Bergen, Norway; 2004. Notes: Master Thesis

Kvinnesland, E. Single-phase characterization of the inlet arrangement schoepentoeter: Department of Physics and Technology, University of Bergen, Norway; 2004. Notes: Master Thesis

Langmuir, I. and Blodgett, K.B., U.S. Army Air Forces Tech. Rept., 1946; 5418-

Leith, D. and Licht, W. The collection efficiency of cyclone type particle collectors: A new theoretical approach. " AIChE Symp. Ser. 1972; 126, (68) 196-

Cousins, L.B., W.H. Denton and Hewitt, G.F. Liquid mass transfer in annular two-phase flow" paper presented at Symp. On two-phase flow, 1965 Exeter, England

Licht, W. Air pollution control engineering. New York: Dekker; 1980.

Manynard, A. D. A simple model of axial flow cyclone performance under laminar flow conditions. Journal of Aerosol Science. 2000; 31(2):151-167.

Movafaghian S.; Jaua-Marturet J.A.; Mohan R.S.; Shoham O., and Kouba G.E. The effects of geometry, fluid properties and pressure on the hydrodynamics of gas-liquid cylindrical cyclone separators. Int. Journal of Multiphase Flow. 2000; 26(6):891-1061.

NG, S. Y. Gas-liquid separation using axial flow cyclones: University of Sheffield; 2004. Notes: PhD Thesis

Nieuwstadt, F. T. M. and Dirkzwager, M. A fluid mechanics model for an axial cyclone separator. Ind. Eng. Chem. Res. 1995; 34:3399-3404.

NORSOK. Process systems, P-100 Rev.2, Norwegian Technology Centre. 2001

OED, "Facts 2003, The Norwegian petroleum sector", Ministry of Petroleum and Energy, Norway. 2003 ISSN: 1502-5446

Oranje, L. Cyclone-type separators score high in comparative tests. Oil & Gas Journal. 1990;54-57.

Overcamp, T.J. and Scarlett, S.E. Effect of Reynolds number on the Stokes number of cyclones. Aerosol Sci. and Technol. 1993; 19:362-370

Pedersen, K. S. and Fredenslund, Aa. An improved corresponding states model for the prediction of oil and gas viscosities and thermal conductivities. Chemical Engineering Science. 1987; 42(1):182-186.

Peneloux, A. and Evelyne, R. A consistent correction for the Redlich-Kwong-Soave volumes. Fluid Phase Equilibria. 1982; 8:7-23.

Peng, W.; Hoffmann, A. C, and Dries, Huub W. A. Separation characteristics of swirl-tube dust separators. AIChE Journal. 2004; 50(1):87-96.

Perry, R. H.; Green, D. W., and Maloney, J. O. Perry's chemical engineers' handbook. 7 ed. McGraw-Hill; 1997.

Putnam, A. Integratable form of droplet drag coefficient. ARS Journal. 1961; 1467-1468.

Ramachandran, G and Raynor P.C. and Leith D. Collection efficiency and pressure drop for a rotary-flow cyclone. Filtration and Separation. 1994; 631-636.

Rawlins, H. and Ting, F. Testing of an in-line rotary separator (IRIS) at the Chevron F.Ramirez gas production facility. 52nd Annual Laurance Reid gas conditioning conference; Oklahoma. 2002.

Sarshar, S.; Beg, N., and Wordsworth, C. A review of the applications and operations of a novel compact separator, I-SEP. Advances in multiphase separation and multiphase pumping technologies conference; Aberdeen. 2005.

Sherwood, T. K.; Shipley, G. H., and Holloway, F. A. L. Flooding velocities in packed columns. Industrial and Engineering Chemistry. 1938; 30(7):765-769.

Shoham O. and Kouba G.E. State of the art of gas-liquid cylindrical cyclone compact-separator technology. SPE 39600. 1998.

Soave, G. Equilibrium constants form a modified Redlich-Kwong equation of state. Chemical Engineering Science. 1972; 27:1197-1203.

Souders, M. and Brown, G. G. Design of fractionating columns. Industrial and Engineering Chemistry. 1934; 26(1):98

Steen, D.A. and Wallis, G.B. The transition from annular to annular-mist cocurrent two-phase down flow", AEC Report NYO-3114-2 (1964)

Stenhouse, J. I. T. and Trow, M. The behaviour of uniflow cylcones. The second world filtration congress 1979; 151-155.

Sterner, A. J. Developments in gas/liquid separation technology. GPA 80th. Annual Convention Proceedings; San Antonio Texas. 2001GPA Annual Conference Proceedings, Annual Meetings.

Stewart, A. C.; Chamberlain, N. P., and Irshad, M. A new approach to gas-liquid separation. SPE European Petroleum Conference; The Hague, Netherlands. 1998: 481-490.

Svrcek, W. Y. and Monnery, W. D. Design two phase separators within the right limits. Chemical Engineering Progress. 1993:53-60

Swanborn, R.; Koene, F., and de Graauw, J. New separation internals cut revamping costs. SPE offshore technology conference; Houston, Texas. 1995.

Swanborn, R. A. A new approach to the design of gas-liquid separators for the oil industry: Delft University of Technology; 1988. Notes: PhD Thesis

Talavera, P. G. Selecting gas/liquid separators. Hydrocarbon Processing. 1990: 81-84

Ueda, T. and Tanaka, T. Studies of liquid film flow in two-phase annular and annular-mist flow regions, part 1 and 2. Trans. JSME, 1973; 39, 325, 2842-

van Rossum, J. J. Experimental investigation of horizontal liquid films. Chemical Engineering Science. 1959; 11:35-52.

Verlaan, C. J.; Olujic, Z., and Graauw, J. de. Performance evaluation of impignement gas-liquid separators. Proceedings of the 4th international conference on multi-phase flow; 1989: 103-115.

Verlaan, C. Performance of novel mist eliminators: Delft University of Technology; 1991. ISBN: 90-370-0054-1. Notes: PhD Thesis

Wallis, G.B. The onset of droplet entrainment in Annular gas-liquid flow", General Eletric report 62 GL 127, 1962

Wang S; Mohan R.S.; Kouba G.E, and Shoham O. Control System Simulators for Gas-Liquid Cylindrical Cyclone Separators. Journal of Energy Resources Technology. 2000; 122:177-184.

Wang S; Mohan R.S.; Shoham O.; Marrelli J.D., and Kouba G.E. Performance Improvement of gas-liquid cylindrical cyclone separators using integrated level and pressure control system. Journal of Energy Resources Technology, 2000; 122:185-191.

Weinaug, C. F. and Katz, D. L. Surface tension of Methane-Propane mixtures. Industrial and Engineering Chemistry. 1943; 35(2):239-246.

Yablonik, R. M. and Khaimov, V. A. Determination of the velocity of inception of droplet entrainment in two-phase flow. Fluid Mechanics-Soviet Research. 1972; 1(1):130-134.

York, O. H. Performance of wire-mesh demisters. Chemical Engineering Progress. 1954; 50(8):421-424.

Ziebold, S. A. Demystifiying mist eliminator selection. Chemical Engineering. 2000; 107:94-102.

APPENDIX A

Appendix A, K-lab Liquid Compositions

Three liquid samples and two gas samples were taken during the tests at K-lab. The 'stabilized condensate' is the liquid that was initially filled onto the Guard separator.

K-lab Liquid Composition, Stabilized Condensate

Component	Weight%	Mole%	Density	Mol.Wt
Nitrogen	0,00	0,00	0,8080	28,01
CO_2	0,00	0,00	0,8270	44,01
C1, (P)	0,00	0,00	0,3000	16,04
C2, (P)	0,00	0,01	0,3580	30,07
C3, (P)	0,01	0,02	0,5080	44,10
i-C4, (P)	0,30	0,58	0,5630	58,12
n-C4, (P)	2,84	5,41	0,5850	58,12
2,2-DM-C3 (P)	0,03	0,05	0,5970	72,15
Ic5 (P)	6,46	9,92	0,6250	72,15
nC5 (P)	6,44	9,90	0,6310	72,15
Hexanes Total	9,77	12,75	0,6673	84,95
Hexanes - P	9,15	11,77	0,6624	86,18
Hexanes - N	0,62	0,98	0,7500	70,13
Heptanes Total	13,97	17,10	0,7463	90,53

Component	Weight%	Mole%	Density	Mol.Wt
Heptanes - P	5,10	5,64	0,6875	100,20
Heptanes - N	7,22	9,12	0,7652	87,73
Heptanes - A	1,65	2,34	0,8840	78,11
Octanes Total	16,84	18,22	0,7741	102,45
Octanes - P	4,26	4,13	0,7064	114,23
Octanes - N	8,73	9,46	0,7723	102,34
Octanes - A	3,85	4,63	0,8710	92,14
Nonanes Total	9,41	9,12	0,8024	114,33
Nonanes - P	2,93	2,53	0,7211	128,26
Nonanes - N	1,94	1,85	0,7905	116,17
Nonanes - A	4,54	4,74	0,8713	106,17
Decanes Plus	33,93	16,92	0,8223	222,65
Totals	100.00	100.00	-	-
C10	6,66	4,97	0.730	134
C11	3,64	2,48	0.740	147
C12	2,48	1,54	0.804	161
C13	1,90	1,09	0.815	175
C14	1,32	0,693	0.826	190
C15+	17,93	6,15	0,8874	400,7

Detailed K-lab Liquid Composition @50.1 barg

Pressure:50.1 barg
Temperature: 30.4 ^{o}C
Density: 0.6889 g/cm^3

Component	Weight%	Mole%	Density [g/cm^3]	Mol.Wt [g/mol]
Nitrogen	0,01	0,03	0,8080	28,01
CO_2	0,32	0,62	0,8270	44,01
C1, (P)	3,53	18,66	0,3000	16,04
C2, (P)	1,90	5,37	0,3580	30,07
C3, (P)	0,58	1,11	0,5080	44,10

Component	Weight%	Mole%	Density [g/cm^3]	Mol.Wt [g/mol]
i-C4, (P)	0,32	0,46	0,5630	58,12
n-C4, (P)	2,91	4,25	0,5850	58,12
2,2-DM-C3 (P)	0,01	0,02	0,5970	72,15
Ic5 (P)	5,99	7,04	0,6250	72,15
nC5 (P)	6,39	7,50	0,6310	72,15
Hexanes Total	9,26	9,24	0,6675	84,90
Hexanes - P	8,65	8,51	0,6624	86,18
Hexanes - N	0,61	0,73	0,7500	70,13
Heptanes Total	13,29	12,48	0,7480	90,30
Heptanes - P	4,82	4,08	0,6875	100,20
Heptanes - N	6,70	6,48	0,7652	87,69
Heptanes - A	1,77	1,92	0,8840	78,11
Octanes Total	16,04	13,32	0,7764	102,11
Octanes - P	3,97	2,95	0,7064	114,23
Octanes - N	8,06	6,68	0,7723	102,27
Octanes - A	4,01	3,69	0,8710	92,14
Nonanes Total	8,84	6,57	0,8047	114,00
Nonanes - P	2,65	1,75	0,7211	128,26
Nonanes - N	1,76	1,28	0,7905	116,12
Nonanes - A	4,43	3,54	0,8713	106,17
Decanes Plus	30,61	13,33	0,8197	194,57
Totals	100,00	100,00	-	-
C10	5,96	4,45	0,730	134
C11	3,33	2,27	0,740	147
C12	2,18	1,36	0,804	161
C13	1,70	0,969	0,815	175
C14	1,10	0,579	0,826	190
C15+	16,34	3,70	0,8842	282,7

Detailed K-lab Liquid Composition, @111.6 barg

Pressure: 111.6 barg
Temperature: 31.1 ^{o}C
Density: 0.6551 g/cm^3

Component	Weight%	Mole%	Density [g/cm^3]	Mol.Wt [g/mol]
Nitrogen	0,02	0,06	0,8080	28,01
CO_2	0,65	1,04	0,8270	44,01
C1, (P)	7,24	31,94	0,3000	16,04
C2, (P)	3,31	7,79	0,3580	30,07
C3, (P)	1,00	1,60	0,5080	44,10
i-C4, (P)	0,29	0,35	0,5630	58,12
n-C4, (P)	2,33	2,84	0,5850	58,12
2,2-DM-C3 (P)	0,01	0,01	0,5970	72,15
Ic5 (P)	5,00	4,91	0,6250	72,15
nC5 (P)	5,44	5,34	0,6310	72,15
Hexanes Total	8,38	6,99	0,6676	84,87
Hexanes - P	7,81	6,42	0,6623	86,18
Hexanes - N	0,57	0,57	0,7500	70,13
Heptanes Total	13,05	10,17	0,7445	90,79
Heptanes - P	5,17	3,65	0,6876	100,20
Heptanes - N	6,23	5,03	0,7652	87,72
Heptanes - A	1,65	1,49	0,8840	78,11
Octanes Total	15,47	10,73	0,7759	102,18
Octanes - P	3,91	2,43	0,7064	114,23
Octanes - N	7,71	5,34	0,7724	102,27
Octanes - A	3,85	2,96	0,8710	92,14
Nonanes Total	7,93	4,89	0,7974	114,87
Nonanes - P	2,63	1,45	0,7211	128,26
Nonanes - N	1,72	1,05	0,7905	116,13
Nonanes - A	3,58	2,39	0,8685	106,17
Decanes Plus	29,88	11,34	0,8267	186,58
Totals	100,00	100,00	-	-

Component	Weight%	Mole%	Density [g/cm^3]	Mol.Wt [g/mol]
C10	6,02	4,49	0,730	134
C11	3,32	2,27	0,740	147
C12	2,18	1,35	0,804	161
C13	1,72	0,985	0,815	175
C14	1,12	0,589	0,826	190
C15+	15,52	1,66	0,9044	256,7